AWARD NUMBER: **W81XWH-14-1-0290**

TITLE: **Developing a novel therapeutic strategy targeting Kallikrein-4 to inhibit prostate cancer growth and metastasis**

PRINCIPAL INVESTIGATOR: **Dr. Brian Tse**

CONTRACTING ORGANIZATION: **Queensland University of Technology (QUT), Australia Brisbane 4102**

REPORT DATE: **August 2017**

TYPE OF REPORT: **Annual**

PREPARED FOR: U.S. Army Medical Research and Materiel Command

Fort Detrick, Maryland 21702-5012

REPORT DOCUMENTATION PAGE

Form Approved
OMB No. 0704-0188

1. REPORT DATE	**2. REPORT TYPE**	**3. DATES COVERED**
August 2017	Annual	31 Jul 2016 - 30 Jul 2017

4. TITLE AND SUBTITLE

Developing a novel therapeutic strategy targeting Kallikrein-4 to inhibit prostate cancer growth and **metastasis**

5a. CONTRACT NUMBER

5b. GRANT NUMBER
W81XWH-14-1-0290

5c. PROGRAM ELEMENT NUMBER

6. AUTHOR(S)

Dr. Brian Tse

email: thomas.kryza@qut.edu.au

5d. PROJECT NUMBER

5e. TASK NUMBER

5f. WORK UNIT NUMBER

7. PERFORMING ORGANIZATION NAME(S) AND ADDRESS(ES)

Queensland University of Technology. 2 George St, Brisbane 4000, Australia

8. PERFORMING ORGANIZATION REPORT NUMBER

9. SPONSORING / MONITORING AGENCY NAME(S) AND ADDRESS(ES)

U.S. Army Medical Research and Materiel Command
Fort Detrick, Maryland 21702-5012

10. SPONSOR/MONITOR'S ACRONYM(S)

11. SPONSOR/MONITOR'S REPORT NUMBER(S)

12. DISTRIBUTION / AVAILABILITY STATEMENT

Approved for Public Release; Distribution Unlimited

13. SUPPLEMENTARY NOTES

14. ABSTRACT

Kallikrein-related peptidase 4 (KLK4) is a rational therapeutic target for prostate cancer (PCa) as it is up-regulated in both localised and bone metastatic tissue, and has been reported to increase PCa cell proliferation, induce epithelial-to-mesenchymal (EMT)-like changes, and could have a role in PCa homing to bone. We therefore hypothesize that blockade of KLK4 activity will inhibit PCa growth and prevent metastasis to secondary sites like bone. This project aims to develop a novel therapeutic strategy targeting KLK4 specifically in PCa. KLK4 siRNA is incorporated into a novel polymeric-based drug-delivery platform currently in development by our laboratory (Queensland University of Technology)with collaborators from the Australian Institute of Bioengineering and Nanotechnology (AIBN), University of Queensland. In this drug-delivery system, the KLK4 siRNA is conjugated to a hyperbranched polymer (HBP) backbone, which is also attached at the periphery with a short peptide that binds to prostate specific membrane antigen (PSMA; expressed on 90% of PCa) for prostate-specific delivery of the therapeutic cargo.

15. SUBJECT TERMS

Kallikrein-related peptidase 4 (KLK4), therapy, nanotechnology, polymeric nanomedicine, PSMA targeting, siRNA

16. SECURITY CLASSIFICATION OF:			**17. LIMITATION OF ABSTRACT**	**18. NUMBER OF PAGES**	**19a. NAME OF RESPONSIBLE PERSON**
a. REPORT	**b. ABSTRACT**	**c. THIS PAGE**			USAMRMC
Unclassified	Unclassified	Unclassified	Unclassified	55	**19b. TELEPHONE NUMBER** *(include area code)*

Table of Contents

Page

1. INTRODUCTION:

The serine protease, Kallikrein-related peptidase 4 (KLK4), is a rational therapeutic target for prostate cancer (PCa) as it is up-regulated in both localised and bone metastatic cancerous tissue, and is an independent biomarker discriminating between benign and malignant prostate tissue [1,2]. KLK4 has been reported to increase PCa cell proliferation, induce an epithelial to mesenchymal transition (EMT)-like response in PC3 PCa cells [4], and could have a role in PCa "homing" to bone [5]. Recently, my co-mentor Distinguished Professor Judith Clement showed that KLK4 regulates the transforming growth factor (TGF)-β pathway in the tumor-stromal microenvironment by cleaving a number of TGF-β extracellular matrix binding partners; thus regulating the bioavailability of TGF-β (Fuhrman-Luck et al, *unpublished*), a cytokine that drives PCa growth, bone homing, EMT and immune suppression [6]. We therefore hypothesize that blockade of KLK4 activity will inhibit PCa growth and prevent metastasis to secondary sites like bone. This project aims to develop a novel therapeutic strategy targeting KLK4 specifically in PCa. KLK4 siRNA is incorporated into a novel drug-delivery platform currently in development by my mentor, Prof Pamela Russell with collaborators from the Australian Institute of Bioengineering and Nanotechnology (AIBN), University of Queensland. In this drug-delivery system, the KLK4 siRNA is conjugated to a hyperbranched polymer (HBP) backbone, which is also attached at the periphery with a short peptide that binds to prostate specific membrane antigen (PSMA; expressed on 90% of PCa) for prostate-specific delivery of the therapeutic cargo (Fig 1).

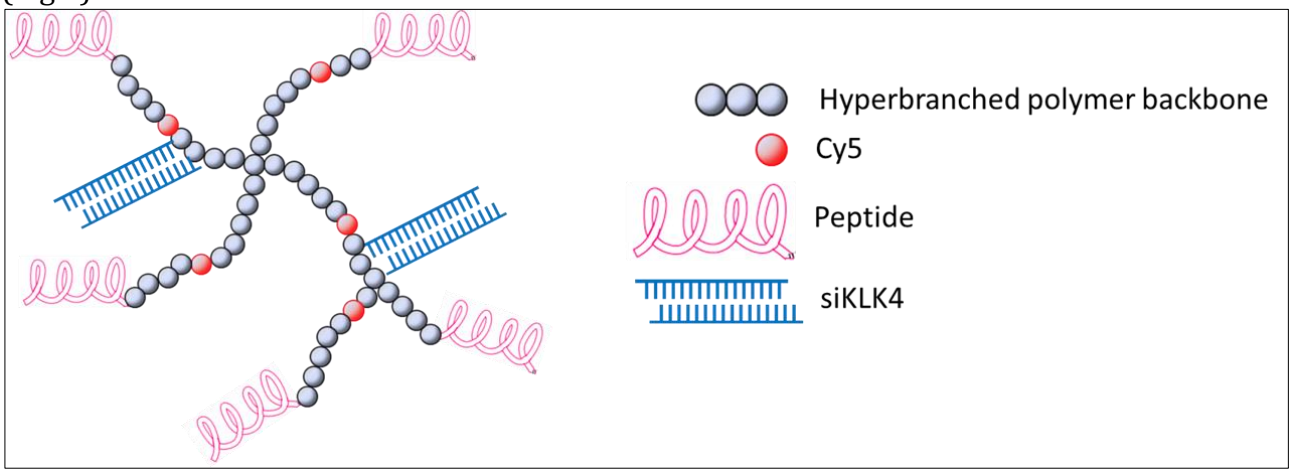

Fig 1. Schematic of our polymeric nanomedicine.

2. KEYWORDS:

Kallikrein-related peptidase 4 (KLK4), nanotechnology, polymeric nanomedicine, metastasis, prostate specific membrane antigen (PSMA)-targeting, siRNA, bone metastasis, imaging.

3. ACCOMPLISHMENTS:

- **What were the major goals of the project?**

Specific Aim 1: Synthesis of our KLK4-targeting agents and ethics applications
- Task 1: Synthesis of our KLK4-targeting conjugates (*in progress*)
- Task 2: Obtain animal ethics approval (*100% complete*)
- Task 3: Obtain human ethics approval (*100% complete*)

Specific Aim 2: Generation and characterisation of KLK4-expressing PCa cell lines
- Task 1: Transfection of PCa cell lines with KLK4 (*100% complete*)
- Task 2: Confirmation of KLK4 expression by transfectants (*100% complete*)

Specific Aim 3: *In vitro* studies to assess effect of KLK4-targeting conjugates

- Task 1: Determine effects of KLK4-inhibition on PCa cell behaviour and EMT (*50% complete)*
- Task 2: Study effects of KLK4-blockade on PCa homing and establishment in bone (*in progress*)

Specific Aim 4: *In vivo* studies to assess how KLK4-targeting affects PCa growth and bone metastasis

- Task 1: Effect of KLK4 antagonism on incidence and growth of orthotopic tumors and bone metastasis in mice (*50% complete*)
- Task 2: Studying the role of KLK4 in PCa homing using a novel human engineered model. (*50% complete*)

- **What was accomplished under these goals?**

Specific Aim 1: Synthesis of our –KLK4-targeting agents

- **Task 1: Synthesis of our KLK4-targeting conjugates**

In collaboration with chemists from AIBN, we have now successfully synthesised and characterized both *in vitro* and *in vivo* our PSMA-targeting hyperbranched polymer (HBP) basic structure (prior to KLK4 siRNA attachment). This work (Fuchs & Tse *et al*.) was recently published in the journal *Biomacromolecules* (impact factor 5.75). Since a high targeting efficiency towards PSMA by the HBPs is fundamental to our PCa-targeting therapeutic approach, a significant amount of my research activity was focused on optimising the system (hence caused some delay), but we have now successfully achieved this. HBPs were conjugated with one of three distinct ligands that bind to the extracellular domain of PSMA; 1) a short peptide (from Dr Warren Heston, Cleveland Clinic, USA), 2) the J591 antibody (from Dr Neil Bander, Weill Cornell Medical College, USA), and 3) urea glutamate (commercially available). We sought to determine which of these polymers ie HBP-peptide, HPB-J591, HBP-GlutUrea, or HBP-control (no ligand) has the best PSMA-targeting efficiency, and be subsequently attached with our KLK4 siRNAs. All HBPs were also labelled with the fluorophore Cy5. Flow cytometric analysis showed that HBP-peptide and HBP-J591 were internalised into PSMA-proficient PC3/PIP-DsRed^{+}luc^{+} cells (abbreviated as PC3/PIP hereafter) but not PSMA-deficient PC3/FLU-DsRed^{+}luc^{+} cells (abbreviated as PC3/FLU) via binding to PSMA in a time dose-dependent and time-dependent manner (please see Appendices section for full manuscript for all figures and methodology). No PSMA-mediated cell internalisation of HBP-GlutUrea or HBP-control was observed. These findings were confirmed by confocal microscopy (*see manuscript*). Since the HBP-peptide showed high specificity for PSMA, and as a smaller molecule as compared to HBP-J591, it is likely to have better pharmacokinetics *in vivo*; hence, we performed additional experiments with this polymer. *In vitro* competitive binding and internalisation assays further confirmed that endocytosis of HBP-peptide is PSMA-mediated (*see manuscript*). This was demonstrated using five PCa cell lines; PC3/PIP, LNCaP, C42b cells (all PSMA-proficient) and PC3/FLU and DU145 cells (both PSMA-deficient) (*see manuscript*). *In vivo*, HBP-peptide injected intravenously strongly targeted towards pre-established subcutaneous PC3/PIP tumors but minimally to PC3/FLU tumors, as assessed by *in vivo* fluorescence imaging (*see manuscript*). **These results strongly indicate that the HBP-peptide is an excellent therapeutic delivery vehicle to PCa cells (see Figs 2 to 4 for selected experiments from the manuscript involving HBP-peptide), and has been selected to be attached with KLK4 siRNA (see page 7).**

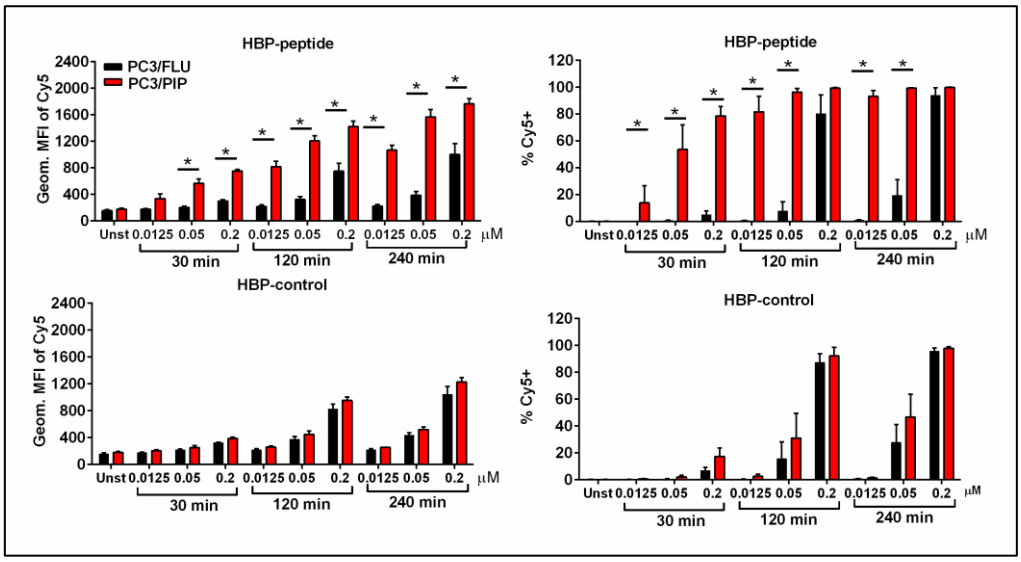

Fig 2. Flow cytometric analysis of PC3-FLU cells (PSMA-deficient; black bars) and PC3-PIP cells (PSMA-proficient; red bars) incubated with HBP-peptide or HBP-control across multiple concentrations and time points. Analysis was performed to assess Cy5 signal in cells given as the geometric mean fluorescence intensity (MFI) of Cy5 of the entire cell population, and the percentage of cells positively stained. n=3.

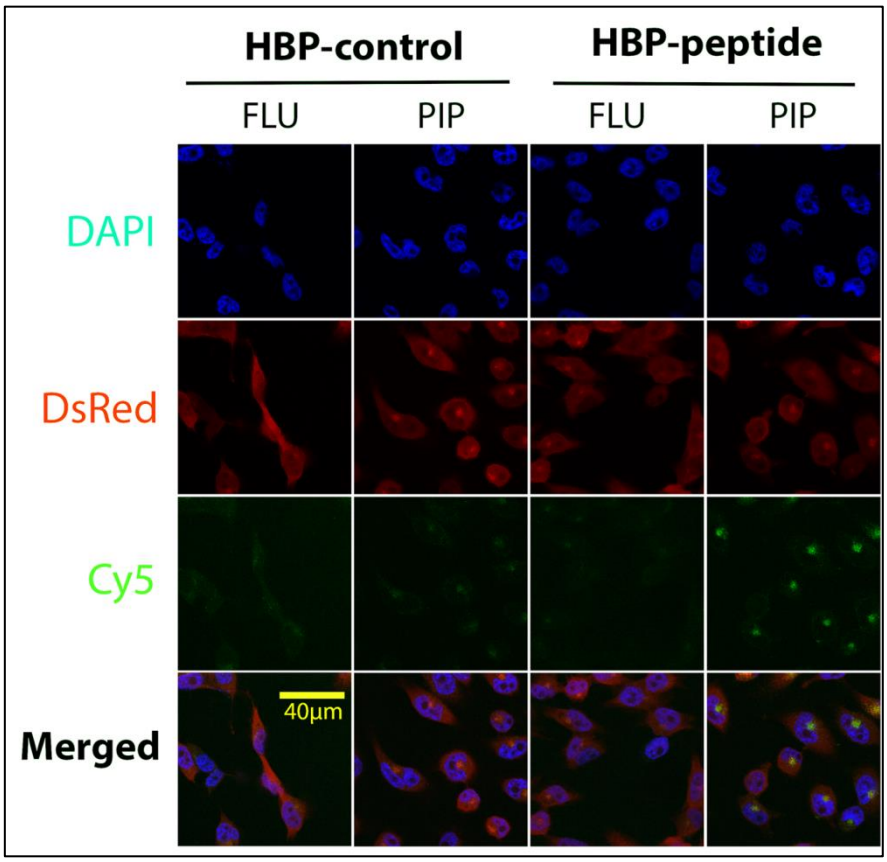

Fig 3. PSMA-mediated endocytosis of HBP-peptide and was confirmed by confocal microscopy. PC3-FLU and PC3-PIP cells were incubated with HBP-control or HBP-peptide at 0.2µM for 120mins. Confocal microscopy was performed to assess Cy5 signal in cells; DAPI (nuclear), DsRed (cytosolic) and Cy5 staining is shown.

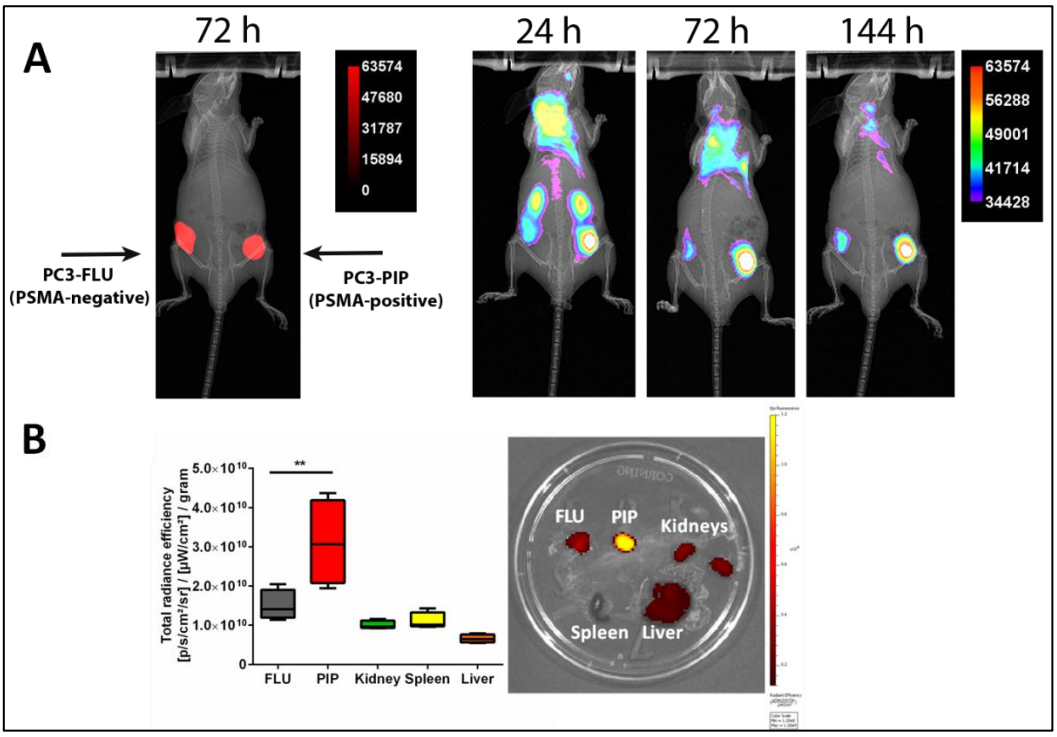

Fig 4. **(A)** A representative BALB/c nude mouse bearing subcutaneous PC3-FLU (left flank) and PC3-PIP (right flank) tumors injected intravenously with HBP-peptide and Cy5 localization imaged using the In-Vivo Xtreme instrument at 1, 3, and 6 days post injection. **(B)** Box and Whiskers plot (mean; min to max) of average radiance efficiency (Cy5) of various tissues/organs following excision 48 h post-injection with HBP-peptide (n = 4) with an accompanying representative fluorescence image.

The overall goal of this project is to develop a novel therapeutic system in which KLK4 siRNA can be delivered specifically to PCa cells, by virtue of their expression of PSMA, to inhibit KLK4-mediated pro-tumor mechanisms. Two siRNA sequences targeting KLK4, siKLK4(A) and siKLK4(B), were purchased from Ambion, Life Technologies. Transfection of KLK4-overexpressing PC3/PIP cells (*see page 9 for details regarding the generation of this cell line*) with siKLK4(A) or siKLK4(B) significantly reduced KLK4 mRNA levels by 75-80% relative to siControl treatment (Fig 5A and B). From experience, this level of knock-down is typical from siRNA treatment, and could be sufficient to induce changes in cellular function. **siKLK4(A), siKLK4(B) and siControl are currently being conjugated onto HBP-peptide by collaborators from AIBN.** siRNA sequences are shown in Table 1, and KLK4 qRT-PCR primers in Table 2.

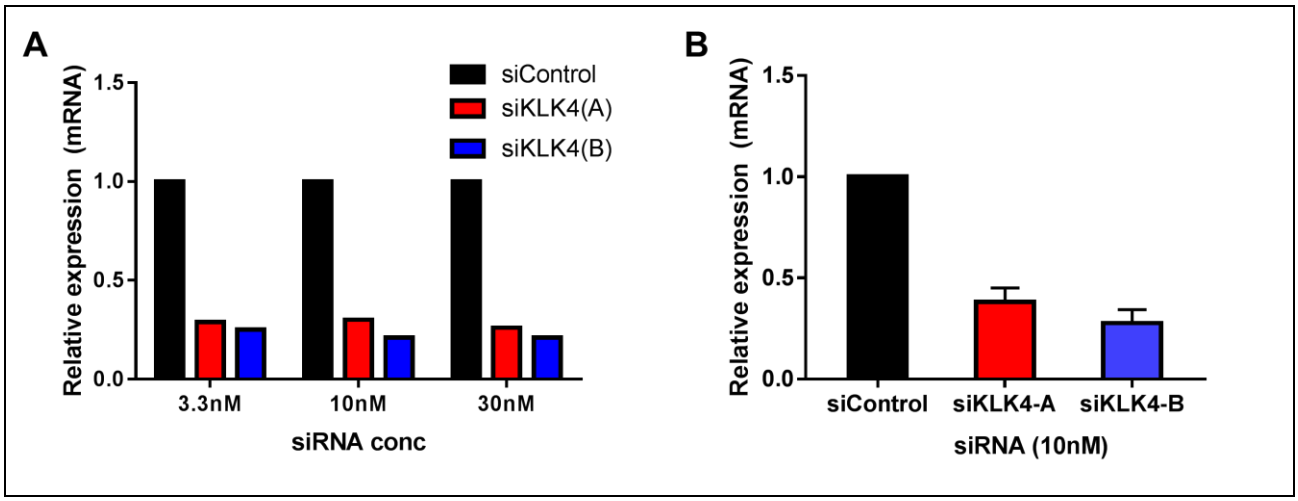

Fig 5A). Demonstration of KLK4 mRNA knock-down following transfection of PC3/PIP-KLK4 cells with siKLK4(A) or siKLK4(B) constructs using RNAiMAX reagent (Life Technologies) across a range of concentrations for 48 hours (n=1), as determined by qRT-PCR. **B)** Confirmation that both siRNA constructs when used at 10nM inhibit KLK4 mRNA expression (n=3).

Table 1. siRNA information.

	Sense (5'=>3')	Antisense (5'=>3')
siControl #1 (Cat# AM4611, Ambion)	Sequence not available	Sequence not available
siKLK4(A)	GAAGGACUCCUGCAACGGUtt	ACCGUUGCAGGAGUCCUUtg
siKLK4(B)	GUGGAUAGAGAAAACCGUCtt	GACGGUUUUCUCAUCCACtc

Table 2. KLK4 primer sequences for qRT-PCR.

	Sense (5'=>3')	Antisense (5'=>3')
KLK4	GAGGGCAAGACCAGAAGGACT	TTTCCGAAAGACACAAGGCC
RPL32 (reference)	GCACCAGTCAGACCGATATG	ACTGGGCAGCATGTGCTTTG

- **<u>Task 2</u>: Obtain animal ethics approval**

Animal ethics approval has been granted, and *in vivo* experiments are underway (see Specific Aim 4 section). The animal ethics approval number is: QUT/TRI/542/15/DOD/APCRC-Q. The study title is: *"Targeting KLK4 to inhibit prostate cancer growth and metastasis".*

- **<u>Task 3:</u> Obtain human ethics approval**

Human ethics for using bone tissue from patient donors have been obtained. The QUT human ethics approval number is: 1400001024. The study title is *"Investigating the biology of human join tissue"*.

Specific Aim 2: Generation and characterisation of KLK4-expressing PCa cell lines

- **<u>Task 1</u>: Transfection of PCa cell lines with KLK4.**

PC3/PIP (PSMA+), PC3/FLU (PSMA-) and C42b (PSMA+) cells (all negative for KLK4 protein) were stably transfected with the pRc/RSV-full length KLK4 plasmid (full length KLK4) or the pRc/RSV plasmid (empty vector), provided by Prof Viktor Magdolen (Technical University of Munich, Germany). Briefly, $3x10^5$ cells seeded in 6-well plates were transfected with 500ng of plasmid DNA using Lipofectamine reagent (Life Technologies), and selection for transfectants began 72 hours post-transfection with G418 antibiotic at 1mg/mL.

- **<u>Task 2</u>: Confirmation of KLK4 expression by transfectants**

Stable over-expression of KLK4 mRNA by PC3/PIP-KLK4 cells and C42b-KLK4 was demonstrated by qRT-PCR (Fig 6A). PC3/PIP-KLK4 cells have ~120,000-fold higher expression of KLK4 mRNA as compared to PC3/PIP-Vec cells. In contrast, C42b-KLK4 cells have ~3-fold greater KLK4 transcript levels than C42b-Vec cells. KLK4 protein was detected by western blot in the conditioned media (CM) of PC3/PIP-KLK4 cells but not C42b-KLK4 (Fig 6B). Confocal microscopy further confirmed expression of KLK4 protein by transfectants (Fig 6C). Since KLK4 protein was detectable only in PC3/PIP-KLK4, the PC3/PIP model was primarily used in subsequent functional assays.

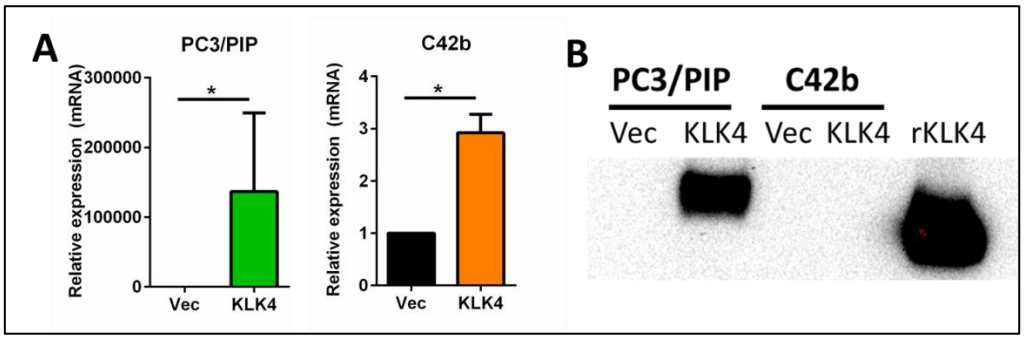

Fig 6. A) Over-expression of KLK4 mRNA levels by PC3/PIP-KLK4 and C42b-KLK4 cells was confirmed by qRT-pCR, but KLK4 protein was only detectable in CM of PC3/PIP-KLK4. **B)** The CM was prepared culturing 3 million tranfectant cells in serum-free media in T75 flasks for 48 hours. 100 ng of rKLK4 was positive control. (n=4).

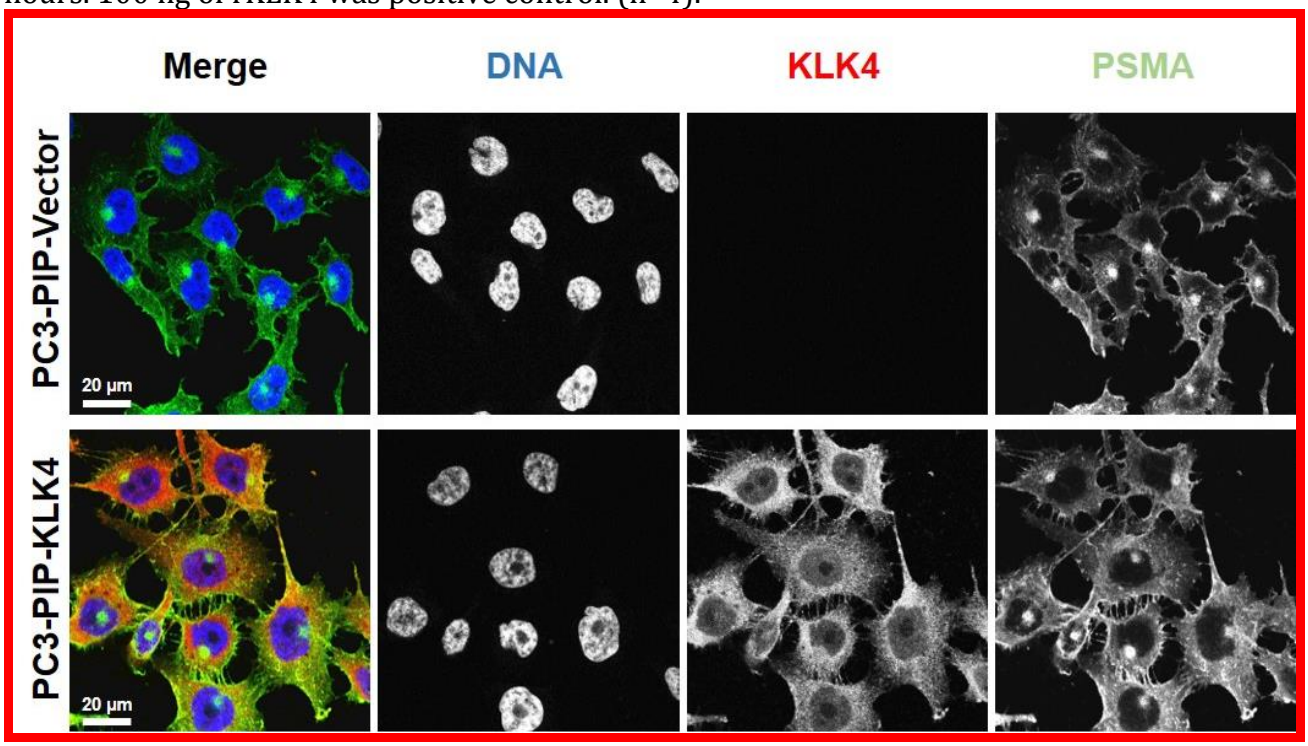

Fig 6.C) Confocal fluorescence microscopy images confirming cytoplasmic expression of KLK4 by PC3-PIP-KLK4 cells but no expression by control cells.

<u>Specific Aim 3</u>: *In vitro* studies to assess effect of KLK4-targeting conjugates

- **<u>Task 1:</u> Determine effects of KLK4-inhibition on PCa cell behaviour and EMT**
  - *Subtask 1 and 2): Cell proliferation, migration and invasion assays.*

Since KLK4 siRNA is currently being conjugated onto HBP-peptide by our collaborators, the experiments done to date have mainly involved comparing the *in vitro* characteristics of KLK4-transfectants with vector-transfectants, to identify cellular functions of KLK4 which we aim to inhibit with HBP-peptide/KLK4siRNA. PC3/PIP-KLK4 showed a trend towards having a faster rate of cell proliferation when compared to PC3/PIP-Vec cells, as assessed by Prestoblue reagent (Life Technologies) (Fig 7A). Treatment of PC3/PIP-KLK4 cells with siKLK4(A) and siKLK4(B) also reduced cell proliferation as assessed by cell counting in a preliminary experiment (Fig 7B). Since KLK4 protein was not detectable in CM of C42b-KLK4 or C42b-Vec cells, proliferation assays were not performed on those cells.

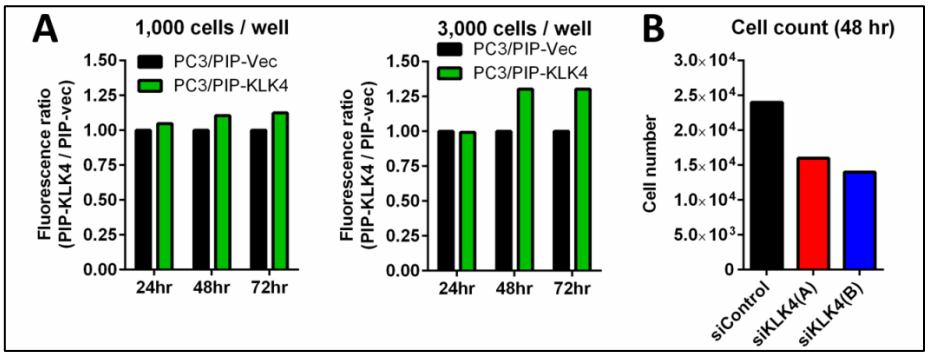

Fig 7. Effect of KLK4 on proliferation of PC3/PIP cells. **A)** Proliferation rate of PC3/PIP-Vec and PC3/PIP-KLK4 cells seeded at 2 different cell densities in 96-well plates was assessed by incubation with Prestoblue reagent**. B)** Cell counting using a haemcytometer was performed on cells 48 hours after siRNA treatment (10nM). (n=1).

The effect of KLK4 over-expression on cell migration was assessed using the Incucyte time-lapse microscopy system. PC3/PIP-KLK4 cells showed a trend towards a faster rate of wound closure in the wound-scratch assay as compared to PC3/PIP-Vec cells (Fig 8A). The correlation between KLK4 with a faster migration rate is unlikely to be due to cell proliferation as differential migration rate is apparent after 4-6 hours. These findings will be validated by transwell migration assays. Another preliminary experiment was performed to assess the migration of PCa cells towards CM containing KLK4. Parental PC3/PIP cells migrated more rapidly towards CM of PC3/PIP-KLK4 cells than to those from PC3/PIP-Vec cells in a transwell assay (Fig 8B). The ability of HBP-peptide/KLK4siRNA to inhibit the effects of KLK4 on cell motility will be assessed.

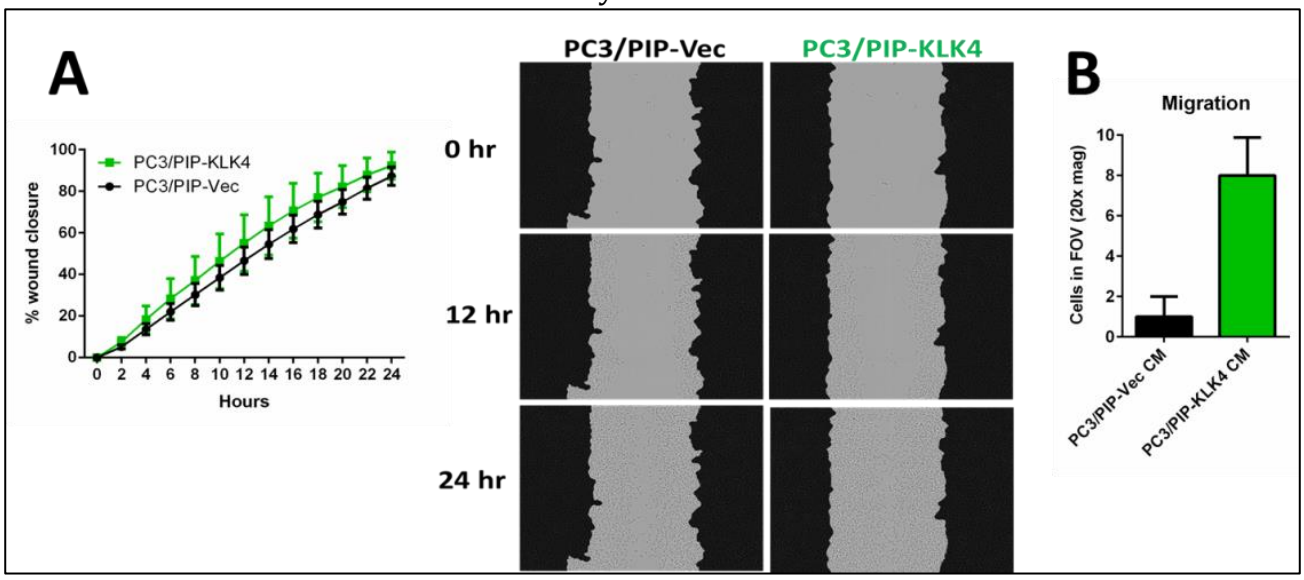

Fig 8. A) Preliminary evidence of faster migration rate by PC3/PIP-KLK4 cells than PC3/PIP-Vec (n=2 biological replicates, each with 40 technical replicates) based on the Incucyte time-lapse microscopy system. **B**) Parental PC3/PIP cells appear to move more rapidly towards CM containing KLK4. (n=2 biological rep, each with 3 technical reps).

The next question addressed was, whether or not the apparent faster cell migration rate of PC3/PIP-KLK4 was mediated by KLK4 over-expression, and if so, could this be inhibited by KLK4 siRNA treatment? PC3/PIP-KLK4 cells were seeded in a 96-well plate at 70% confluence, treated with either siControl, siKLK4(A) or siKLK4(B) (all at 10nM) for 48 hours (to allow sufficient time for protein expression inhibition), then setup in a wound-scratch assay in the

Incucyte system. Treatment with either siKLK4 constructs correlated with a slower rate of wound closure as compared to siControl, suggesting that KLK4 plays a role in the apparent enhanced-migratory rate of PC3/PIP-KLK4 cells (Fig 9). The results also suggest that these specific siKLK4 sequences have potential therapeutic activity.

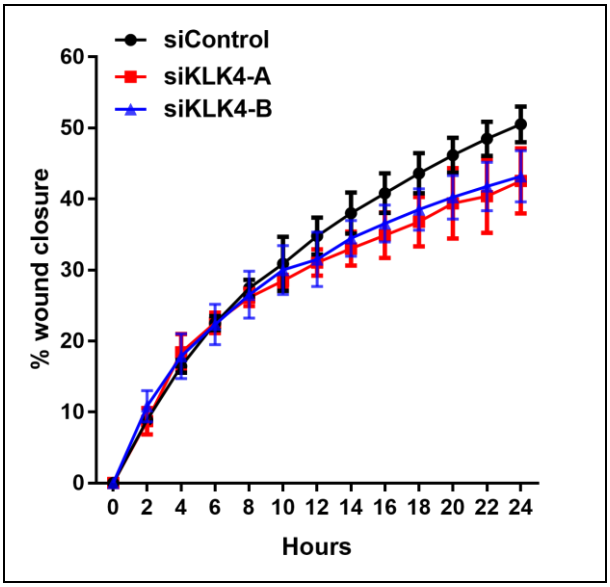

Fig 9. Pre-treatment of PC3/PIP-KLK4 cells with siKLK4(A) or siKLK4(B) correlated with slower cell migration in the Incucyte scratch-wound assay (n=3 biological reps, each with 30 technical reps).

The effect of KLK4 over-expression on the invasive capabilities of PC3/PIP cells was assessed cells using a modified 3D Matrigel™ assay. The culture of PC3/PIP-KLK4 cells over a period of 7 days resulted in the majority of colonies growing with an invasive stellate morphology (Fig 10A). In contrast, PC3/PIP-Vec cells grew as more rounded and less-invasive colonies over the same period. This effect was highly reproducible (n=3). Mechanistically, KLK4 could be mediating an invasive phenotype by acting intracellularly, or through extracellular activities. To explore the latter possibility, parental PC3/PIP cells were again grown on matrigel but incubated with 100% CM from PC3/PIP-KLK4 or PC3/PIP-Vec cells for up to 5 days (Fig 10B). Cells treated with PC3/PIP-KLK4 CM exhibited a more invasive phenotype, suggesting that the extracellular function of KLK4 mediates this effect. The cells failed to grow further beyond 5-7 days. The ability of HBP-peptide/KLK4siRNA to inhibit the pro-invasive effects of KLK4 will be assessed using the same assays.

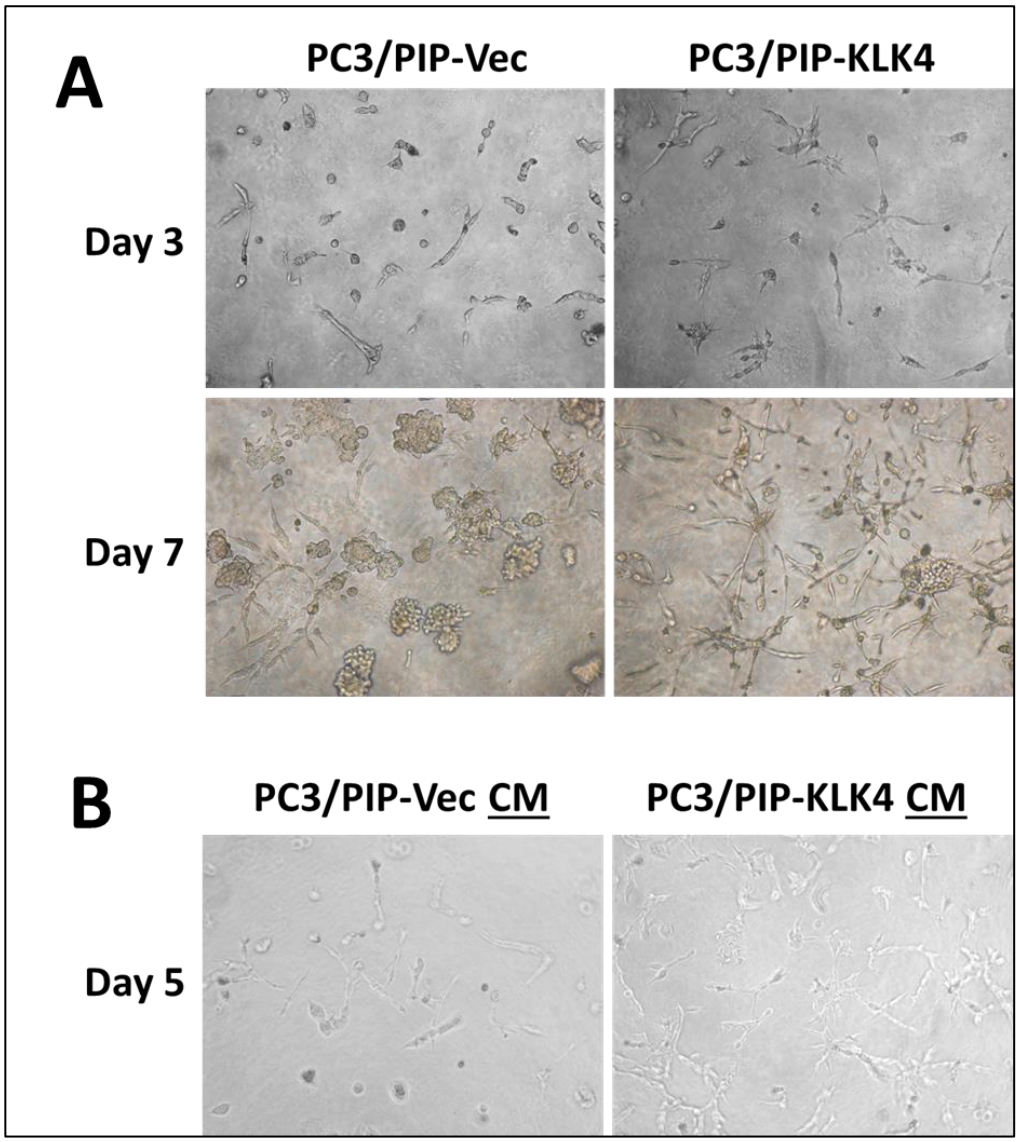

Fig 10. A) Growth of PC3/PIP-Vec and PC3/PIP-KLK4 on matrigel in media containing 5% FBS for up to 7 days to assess their invasive morphology. **B)** Growth of parental PC3/PIP cells on matrigel and incubated in 100% CM from PC3/PIP-Vec or PC3/PIP-KLK4. n=3.

Although C42b-KLK4 and C42B-Vec cells did not secrete detectable amounts of KLK4 protein, I performed the matrigel experiments as described above as well. As expected, there is no evidence of KLK4 altering the phenotype of the C42b model (Fig 10).

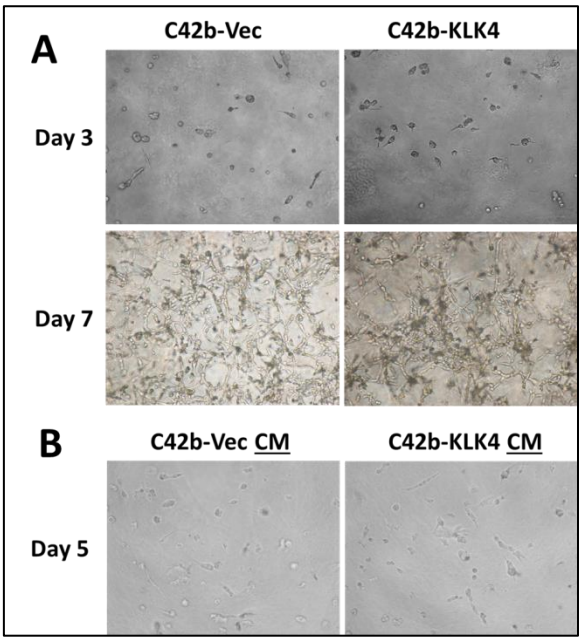

Fig 11. Growth of C42b-Vec and C42b-KLK4 on matrigel in media containing 5% FBS (A) or CM from KLK4- or Vec-transfectants (B).

- *Subtask 3): RT-qPCR and western blot for markers of EMT*

To study the potential effect of KLK4 over-expression in inducing EMT-like changes in PCa cells, qRT-PCR was performed on a number of EMT-associated markers on RNA of KLK4-transfected or Vec-transfected cells (Fig 11). Over-expression of KLK4 in the PC3/PIP model positively correlated with higher mRNA level of Snail, a potent EMT-inducing transcription factor. However, no overt changes in the expression of other EMT-related genes were observed. To test if the increase in Snail expression in PC3-PIP/KLK4 cells was mediated by KLK4, we examined Snail mRNA levels in cells treated with the siRNA constructs. Treatment with siKLK4(A) did not influence Snail mRNA levels (Fig 13). However, to our surprise, siKLK4(B) treatment appeared to correlate with higher Snail mRNA levels. The reason for this is not clear, and further investigations are warranted. As expected, no differences between KLK4 and EMT markers were seen in the C42b model (Fig 12). Currently, the link between KLK4 and EMT in these cells is not clear. The primer sequences for these genes are listed in Table 3 below.

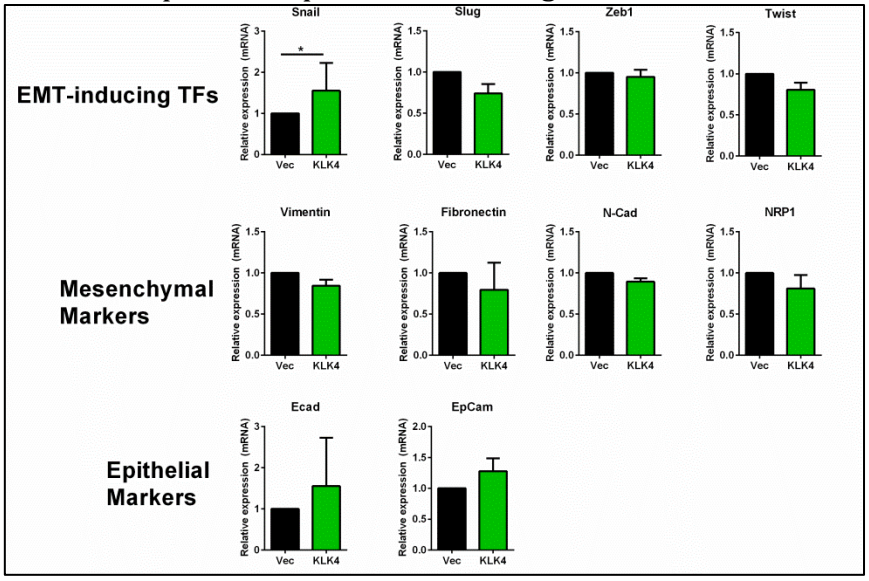

Fig 12. qRT-PCR for EMT markers in the PC3/PIP model. (n=5).

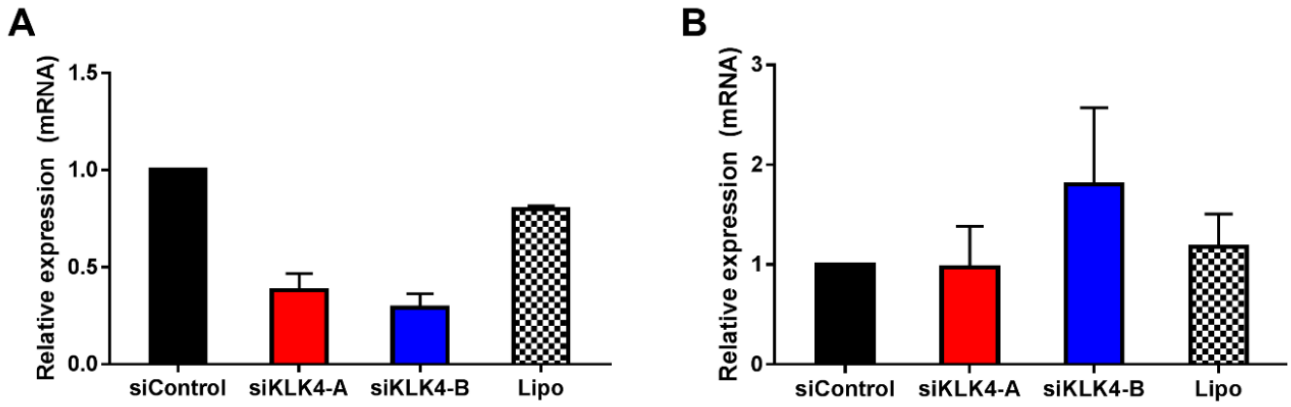

Fig 13. Relative expression of KLK4 (**A**) or Snail (**B**) in PC3-PIP/KLK4 cells treated with siControl, siKLK4(A), siKLK4(B) or lipofectamine (control). (n=3 biological reps, each with 2 technical reps).

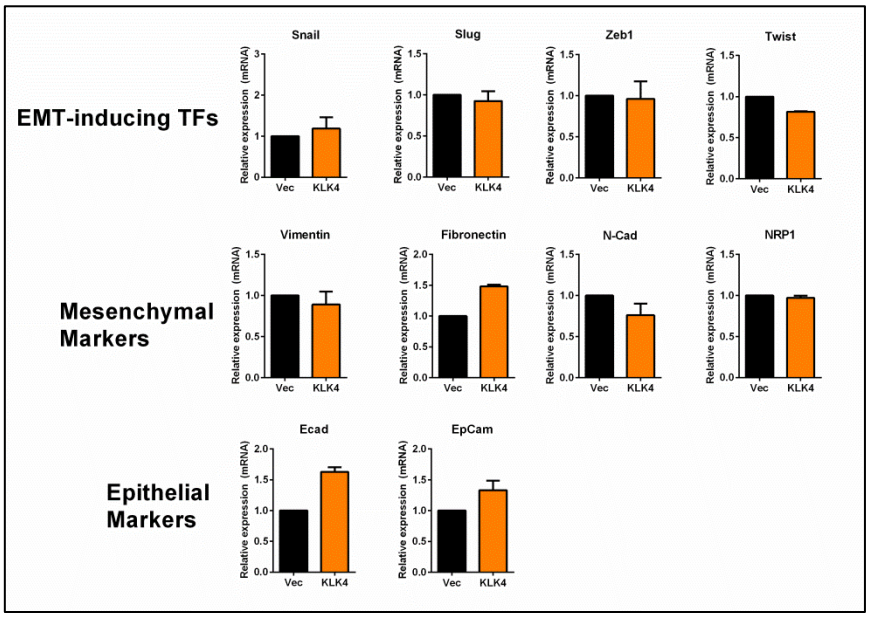

Fig 14. qRT-PCR for EMT markers in the C42b model. (n=3).

Table 3. Primers for EMT markers.

	Sense (5'=>3')	Antisense (5'=>3')
Snail	CCTCCCTGTCAGATGAGGAC	CCAGGCTGAGGTATTCCTTG
Slug	GGGGAGAAGCCTTTTTCTTG	TCCTCATGTTTGTGCAGGAG
Zeb1	CAACTACGGTCAGCCCT	GCGGTGTAGAATCAGAGTC
Twist	GGAGTCCGCAGTCTTACGAG	TCTGGAGGACCTGGTAGAGG
Vimentin	GAGAACTTTGCCGTTGAAGC	GCTTCCTGTAGGTGGCAATC
Fibronectin	CAGTGGGAGACCTCGAGAAG	TCCCTCGGAACATCAGAAAC
N-Cadherin	ACAGTGGCCACCTACAAAGG	CCGAGATGGGGTTGATAATG
Neuropilin-1(NRP1)	AGGACAGAGACTGCAAGTATGAC	AACATTCAGGACCTCTCTTGA
E-Cadherin	TGCCCAGAAAATGAAAAAGG	GTGTATGTGGCAATGCGTTC
EpCam	TGCTCAAAGCTGGCTGCCAAATG	GTGCCGTTGCACTGCTTGGC
RPL32 (reference)	GCACCAGTCAGACCGATATG	ACTGGGCAGCATGTGCTTTG

- **<u>Task 2</u>: Study effects of KLK4-blockade on PCa homing and establishment in bone**
  - *Subtask 1): Migration assays using CM from human osteoblasts – in progress*

- *Subtask 2): Cell adhesion assay – in progress*
- *Subtask 3):Co-culture of PCa cells with osteoblasts within a novel tissue engineered bone. Yet to commence – this is because fresh patient material/osteoblasts are very precious and expensive to transformed into tissue engineered bone, hence these experiments will be performed with HBP-peptide/siKLK4 is successfully conjugated.*

<u>Specific Aim 4</u>: *In vivo* studies to assess effect of KLK4-targeting conjugates

Two *in vivo* experiments designed to optimise the cell dose for injection via the intraprostatic (modelling primary prostatic tumours) and intracardiac (modelling metastasis) routes, and thereby, reveal potential effects of KLK4 expression on tumour growth and metastasis, are complete. In the orthotopic model, tumour expression of KLK4 correlated with significantly smaller tumours based on ex vivo tumour weight and in vivo bioluminescence (Fig 15A-C). In vivo expression of KLK4 was confirmed by immunohistochemistry of resected tumours (Fig 16). Tumours were also stained for Numa (human marker), ki67 (proliferation) and cleaved caspase 3 (apoptosis).

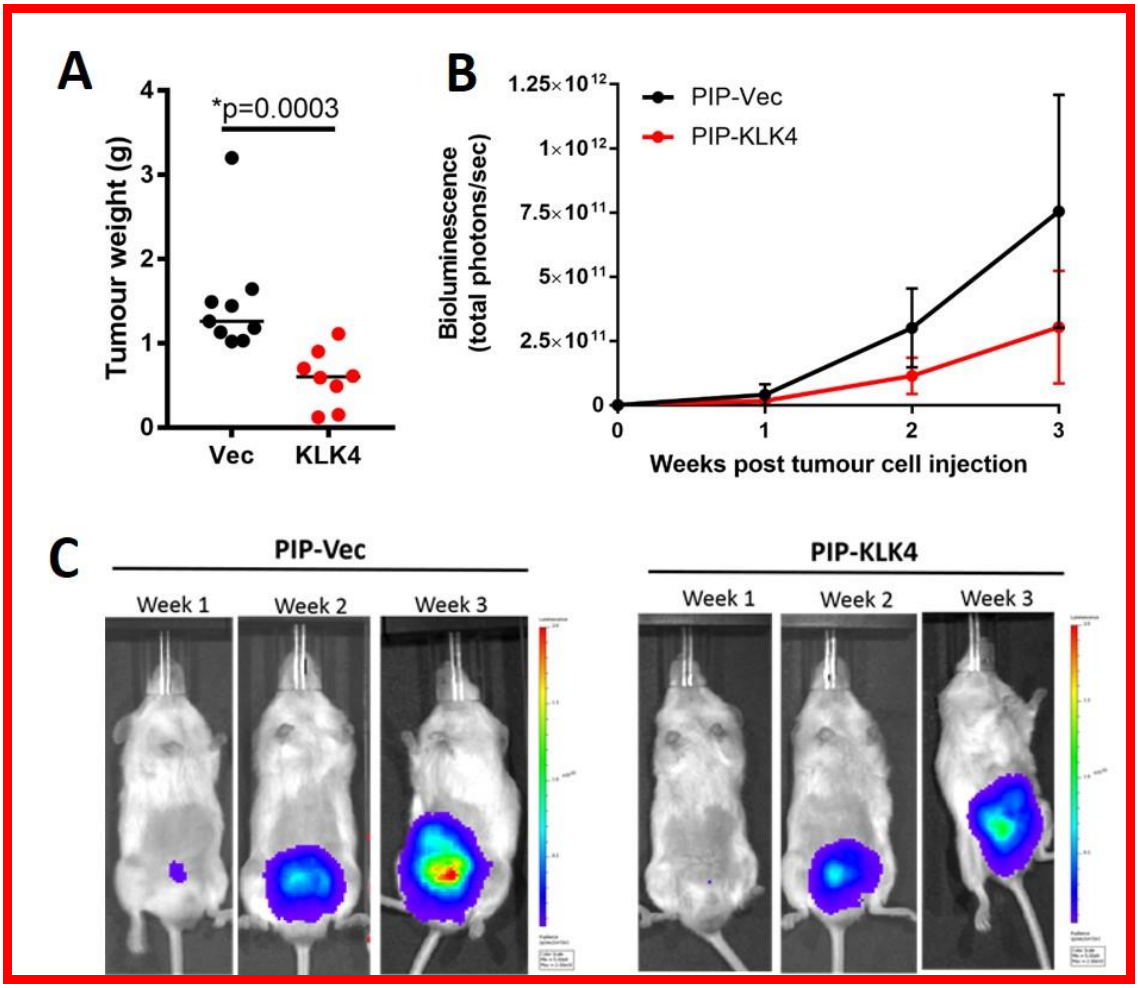

Fig 15. ***KLK4 production by prostate cancer cells is associated with tumour growth inhibition in an orthotopic tumour model.*** **A**) Post-necropsy tumour weight of PIP-Vec was significantly higher than that of PIP-KLK4. **B)** Lesser tumour bioluminescence by PIP-KLK4 cells throughout the experiment. C) Tumour bioluminescence images of representative mice from PIP-Vec and PIP-KLK4 groups.

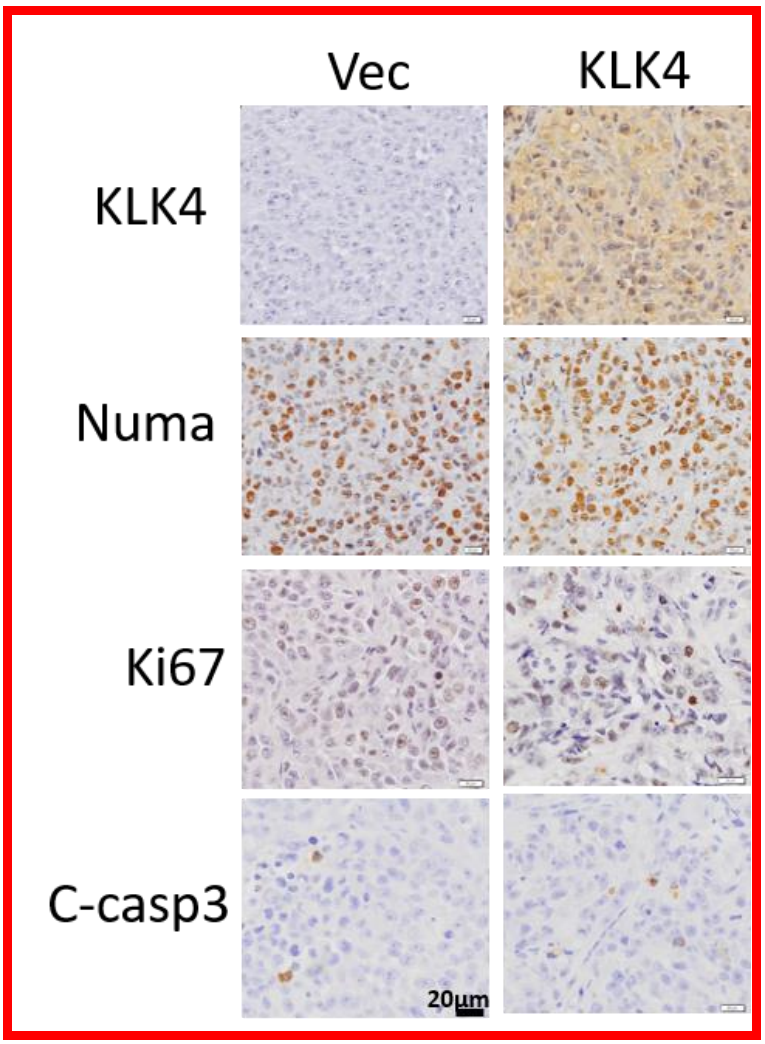

Fig 16. Immunohistochemical analysis of resected orthotopic PIP-KLK4 tumours confirms expression of KLK4 protein. Staining for human cell origin (Numa), Ki67 and cleaved caspase-3 also performed.

In the metastatic model where tumour cells were injected intracardiac, mice injected with PC3-PIP/KLK4 cells consistently had lesser tumour burden based on bioluminescence imaging throughout the course of the experiment as compared to the PC3-PIP/Vec group (Fig 17). These results are consistent with the orthotopic model, and overall suggest that KLK4 may exhibit an anti-tumour effect when expressed at large amounts. This is a surprising observation given that our hypothesis was that KLK4 expression would render tumour cells more aggressive. The mechanisms underpinning the apparent anti-tumour effect of KLK4 is not clear, and will be investigated. Analysis of the effects KLK4 on bone (osteolysis vs osteogenesis) by ultra-high resolution microCT (computed tomography) and histology is currently underway.

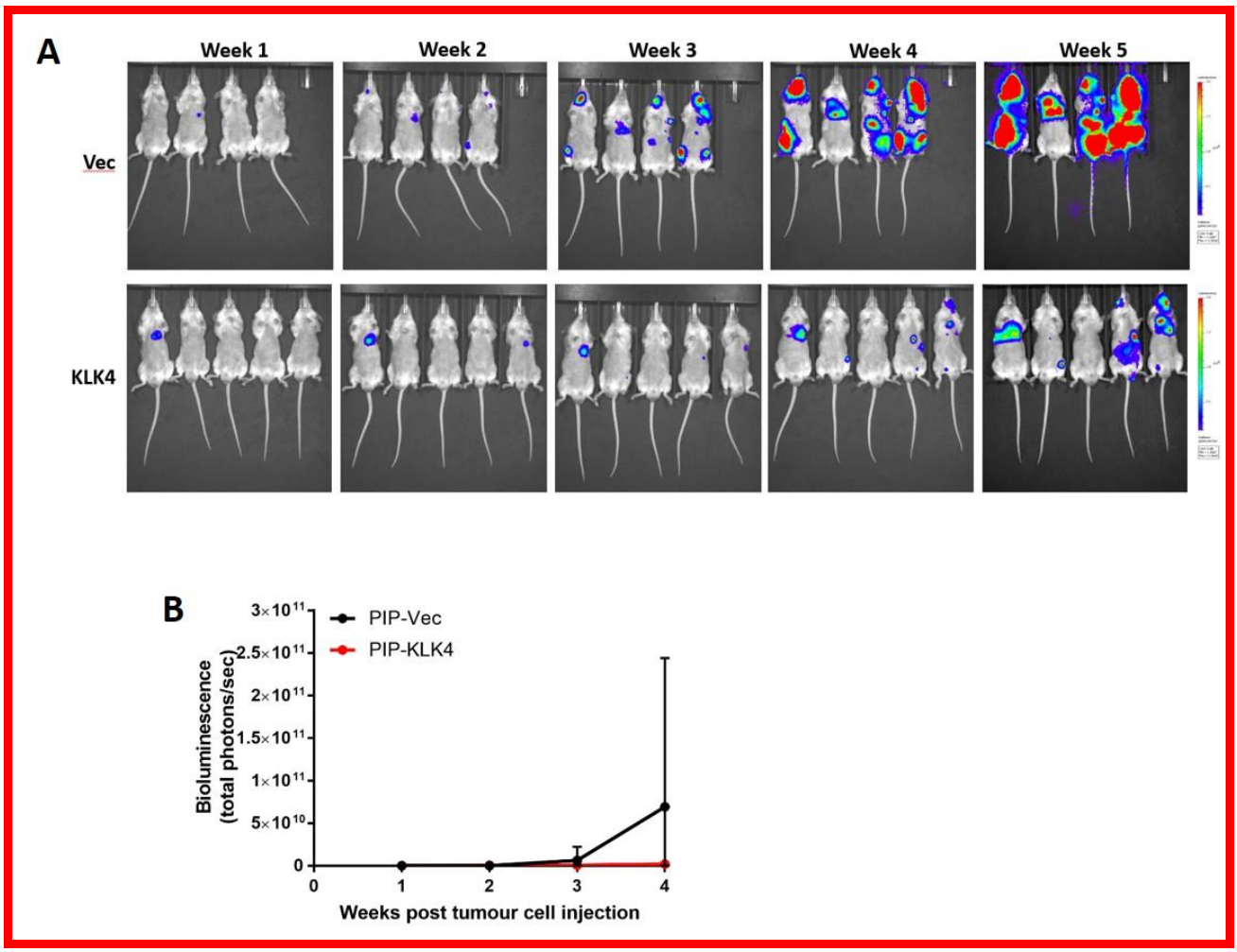

Fig 17. ***KLK4 production by prostate cancer cells is associated with tumour inhibition in a metastasis model.*** A) Tumour bioluminescence images showing lesser tumour burden in mice injected intracardiac with PIP-KLK4 cells. B) PIP-KLK4 mice had significantly lower total tumour bioluminescence signals throughout experiment.

- **What opportunities for training and professional development has the project provided?**
  My laboratory, the Australian Prostate Cancer Research Centre-Queensland (APCRC-Q), Queensland University of Technology, has provided me with excellent training opportunities in PCa research. Led by world renowned PCa researchers in Prof Colleen Nelson (Executive Director), Prof Judith Clements (Scientific Director; my co-mentor) and Prof Pamela Russell (Head of Biomedical Imaging and Prostate Cancer Models; my mentor), I have been working alongside and learning from experts in varied specialties. I have had significant exposure to biomarker discovery, hormonal regulation of gene expression, epithelial to mesenchymal transition (EMT), animal models, cancer imaging, cancer stem cells, circulating tumor cells (CTCs), metabolomics, targeted therapeutics and bioinformatics. In addition, I have been regularly discussing research ideas with clinician-scientists from the Princess Alexandra Hospital, which has been invaluable in my development into a truly translational PCa research scientist.

  My individualised training program involves regular meetings with my mentor, co-mentor and collaborators to discuss results and brainstorm new ideas:
  - I have one-on-one meetings with my mentor, Prof Pamela Russell, at least three times a week. She has >30 years of experience in PCa research with an international reputation

for development of *in vitro* and *in vivo* urological cancers, including the RM1(BM) model of bone metastasis in an immunocompetent mouse model, gene therapy (to proceed to Phase I clinical trial; NCT00625430; http://clinicaltrials.gov) and more recently, on PCa theranostics using nanotechnology. She has >200 publications (H-index 53, Google Scholar), procured >$35million in grants, and received the inaugural award for Prostate Cancer Researcher of the year in 2010 from the Prostate Cancer Foundation of Australia which she helped to establish, and was a member of the scientific committee for Movember's Global Action Plan (2010-2014), amongst other honours. I also receive guidance from her in relation to writing manuscripts, grant/fellowship applications, and for networking with potential collaborators.

- I have regular meetings with my co-mentor, Distinguished Professor Judith Clements, fortnightly to discuss the progress of my project. I also attend the lab meetings of her group fortnightly. Prof Clements is a world leading researcher in the kallikrein family of proteases. She has >240 publications (H-index 57, Google Scholar), and has made many seminal findings including the identification of 12 new PSA-related enzymes, extending the Kallirekin family of genes to 15. In 2007 she was awarded the prestigious international Frey-Werle Foundation Gold Medal for her significant contributions to the kallikrein protease field on their roles in hormone dependent cancers. I have received a tremendous amount of support from her.
- I meet with my polymer chemistry collaborators, Professor Andrew Whittaker and Dr Kris Thurecht from AIBN, every two months to discuss about the project. Both are experts in the fields of biomaterials science, nanotechnology and imaging. Working with them has given me invaluable insight into the chemistry/nanotechnology discipline.

The table lists other professional development opportunities I have, or will, participate in:

Prostate cancer-focused seminars/meetings/conferences		
APCRC-Q laboratory meetings	Tuesdays	Weekly
Endocrine, Metabolism & Plasticity (EMP) group meetings	Thursdays	Fortnightly
Prostate Cancer World Congress	August 17-20, 2015	Annually
International Symposium on Kallikreins and Kallikrein-Related Peptidases	Sept 28-Oct 1, 2015	Biannually
2015 Prostate Cancer Collaborative Research Symposium	Nov 25-28, 2015	Biannually
Institute seminars		
TRI Symposium	Tuesdays	Fortnightly
TRI Early Career Researcher (ECR) Seminars	Fridays	Weekly
Workshops		
Research Methods Group (RMG) - Biostats	Thursdays	Fortnightly

- **How were the results disseminated to communities of interest?**
  Our first manuscript (Fuchs and Tse *et al*.) which describes the design, synthesis and initial *in vitro* and *in vivo* characterisation of our hyperbranched polymer system used in this project was published in the journal *Biomacromolecules.* This is a cross-disciplinary journal that covers the fields of chemistry, nanotechnology, bioengineering and medicine (impact factor 5.75). Based on this work, the original awardee, Brian Tse, gave oral and poster presentations at the Prostate Cancer World Congress held at Cairns, Australia (Aug 17-20, 2015). The conference was attended by world leading clinicians (urologists, surgeons, medical oncologists, radiation oncologists etc…) as well as high profile translational research scientists. He also presented data at two other international conferences, both held in Australia: 1) the 6th annual International Symposium on Kallikreins and Kallikrein-

Related Peptidases (Sept 28-Oct 1, 2015), and 2) the 2015 Prostate Cancer Collaborative Research Symposium (Nov 25-28, 2015). I gave a lecture on prostate cancer imaging and therapy to third year science students at the Queensland University of Technology (QUT) on September 22nd, 2015. I have also presented my work at the Australian Prostate Cancer Research Centre-Queensland (APCRC-Q) weekly seminars, as well as the group meetings of my co-mentor Prof Judith Clements, and collaborators at Australian Institute of Bioengineering and Nanotechnology (AIBN), University of Queensland. Dr Thomas Kryza has only been working on this project for the past 4 months and there have been no external presentations on this topic by him during this time except internally to the mentoring team and Dr Brian Tse who is acting as an advisor on the project and the Clements lab group.

- **What do you plan to do during the next reporting period to accomplish the goals?**All in remaining in vitro and in vivo work will be completed by Dr Thomas Kryza.

4. IMPACT:

- **What was the impact on the development of the principal discipline(s) of the project?**
  Whilst this project has yet to result in translational outcomes, it has the potential to significantly improve clinical management of PCa. Despite the development of next generation anti-androgen drugs and chemotherapies, castrate-resistant PCa remains incurable. Thus, new therapies that target other PCa-promoting pathways need to be developed. Our therapy aims to prevent PCa progression by inhibiting KLK4, which promotes EMT and homing to bone, in order to prolong patient survival and improve their quality of life. Experiments are designed to not only perform preclinical testing of our therapy, but to also study how KLK4 promotes PCa progression. This knowledge is invaluable in its own right, and will help us refine our therapies in the future.

- **What was the impact on other disciplines?**
  Nothing to report.

- **What was the impact on technology transfer?**
  Nothing to report.

- **What was the impact on society beyond science and technology?**
  Nothing to report.

5. CHANGES/PROBLEMS:

- **Changes in approach and reasons for change AND actual or anticipated problems or delays and actions or plans to resolve them**
  Please see below the revised SOW for Dr Kryza upon acceptance of the award.

Site 1:	**APCRC-Q, QUT** Level 3, TRI, 20 Cornwall Street, Woolloongabba, Brisbane, 4102 Australia *Investigators*: Dr Thomas Kryza (PI) Prof Pamela Russell (Mentor) Prof Judith Clements (Co-Mentor)	**Site 2**:	**AIBN** Level 4, Building 75, University of Queensland, St Lucia, Corner of College and Cooper road, Brisbane 4072, Australia *Investigators*: Prof Andrew Whittaker (Collaborator) Dr Kris Thurecht (Collaborator)
Site 3:	**IHBI, QUT** Level 6, IHBI, 60 Musk Avenue, Kelvin Grove, Brisbane, 4059 Australia *Investigators*: A/Prof Jonathan Harris		

	Time	Site
Specific Aim 1: Synthesis of KLK4-targeting agent, and Ethics Application		
Task 1: Synthesis of our KLK4-targeting conjugates (siRNA and antibody conjugated to hyperbranched polymers). Collaborators from AIBN are still in the process of performing the conjugation of KLK4-targeting siRNA (siKLK4) to the hyperbranched polymer (HBP) linked with a PSMA-targeting peptide. As described in detail in the progress report, the conjugation of the PSMA-targeting peptide to the HBP (the first step) had been optimized, and we clearly showed in vitro and in vivo that these polymers are taken up by PSMA+ prostate cancer cells specifically, and with high efficiency; these exciting data were recently published: Fuchs & Tse et al. (2015) *Biomacromolecules* 16 (10), pp 3235–3247. The conjugation of KLK4 siRNA to this polymer (second step) has required more optimization than initially anticipated; hence the delay. Our collaborators continue to work diligently to finalise the chemistry procedure. To ensure the completion of Task 1, we have now enlisted Dr Jon Harris at the Institute of Health and Biomedical Innovation (IHBI), Queensland University of Technology (QUT), who has extensive experience in synthetic peptide chemistry to attempt an alternative conjugation strategy for attaching the siKLK4 to a synthetic polymer base. We acknowledge that design and synthesis of these polymers may take some time, and final products are likely to be available to test in the second half of the remaining 6 months of the award. As such, during months 1-6, we will primarily focus on the biological function of KLK4 in prostate cancer both *in vitro* and *in vivo*, as additional evidence toward its role in driving the disease, and supporting the efficacy of inhibiting KLK4 as an anti-cancer strategy. Particularly, to date there have been no *in vivo* studies analyzing the role for KLK4 in prostate cancer metastasis, despite strong supporting evidence from *in vitro* studies [1,2], its elevated expressing during EMT [3] and in clinical metastases [2], and its established functional role in other clinical pathologies involving bone remodelling [4]. Thus, the proposed remaining *in vivo* work is an important final step in validating the role for KLK4 as a driver of prostate cancer metastasis. Completing the remaining proposed *in vitro* and *in vivo* experimentation will also provide optimised platforms for testing the utility of the above novel conjugate KLK4 inhibitors, once they become available.	18-24 months	AIBN (AW, KT) IHBI (JH) APCRCQ (TK)
Task 2: Write animal ethics application, and obtain regulatory approval from local animal ethics committees (QUT & UQ), and DoD Animal Care and Use Review Office. Animal ethics conditionally approved.		

[1] Veveris-Lowe et al, Endo-Rel Can; 2005;12(3):631; [2] Gao et al, Prostate; 2007; 67(4):348; [3] Hollier et al, unpublished data; [4] Wright et al, Cells Tissues Organs; 2009; 189(1-4):224.

Task 3: Write human ethics application, and obtain regulatory approval from local ethics committees (QUT & UQ), and DoD Human Research Protection Office. 100% complete.		
Specific Aim 2: Generation and characterisation of KLK4-expressing PCa cell lines		
Task 1: Transfection of PCa cell lines with KLK4. 100% complete.		
Task 2: Confirmation of KLK4 expression by transfectants. 100% complete.		
Specific Aim 3: *In vitro* studies to assess the anti-tumor efficacy of KLK4-targeting conjugates.		
Task 1: Determine effects of KLK4-inhibition on PCa cell behaviour and EMT Some tasks complete; remaining tasks outlined below. Subtask 1) *Cell migration and invasion assays*. Preliminary results showed that parental PC3-PIP/KLK4 cells exhibited increased migration toward conditioned media (CM) from PC3-PIP/KLK4 cells, compared to /mock cells. This result will be replicated, as per below, +/- siKLK4 to confirm the specific involvement of KLK4 in this process. Transwell: Parental PC3-PIP cells will be serum starved for 24hr and the rate of cell migration through an 8um pore transwell insert towards conditioned media from PC3-PIP/KLK4 and /mock cells (or media containing 10% FBS, as a positive control) will be assessed (24hr). For experiments involving siRNA treatment, cells will be pre-incubated with siKLK4 (or siControl) for 24hr, to allow sufficient time for KLK4 knock-down, before proceeding with the protocol. Given the promising results demonstrating the invasive phenotype of PC3-PIP/KLK4, but not mock, cells when grown in Matrigel, Transwell invasion assays will further be performed with these cells, similar to migration assays above, but with inserts pre-coated with Matrigel (incubation time 48-72hr). All experiments will be performed in triplicate, with 3 biological replicates. *Subtask 2) 3D growth assay (Matrigel) and proliferation assays*. 3D growth assays (Matrigel) are 100% complete. Preliminary proliferation assays demonstrated that siKLK4-treatment of PC3-PIP/KLK4 cells decreased cell number, in accordance with an increased proliferation of PC3-PIP/KLK4 versus /mock cells. These results will be repeated in triplicate using PrestoBlue reagent, a measure of cell metabolism, as well as CyQuant reagent (Life Technologies), to assess total DNA content, concomitant with total cell number. *Subtask 3) RT-qPCR and western blot for markers of EMT.* 100% complete.	18-20 months	APCRC-Q (TK)
Task 2: Study effects of KLK4-blockade on PCa homing and establishment in bone *Subtask 1) Migration assays using CM from human osteoblasts*; *Subtask 3) Co-culture of PCa cells with hOBs within a novel tissue engineered bone (TEB) construct and performance of Scanning Electron Microscopy (SEM).*	20-22 months	APCRC-Q (TK)

Given the limited timeframe for completion of remaining aims, we believe the ability for KLK4 to influence prostate cancer bone metastasis will be better assessed using the *in vivo* animal models outlined in Task 3. Coupled with the expense of acquiring patient-derived human osteoblasts and culturing these cells in synthetic scaffolds, these sub-aims have been discontinued, with a greater focus instead on Aim 4. *Subtask 2) Cell adhesion assay*. As Matrigel is a complex mix of basement membrane proteins, the invasive phenotype of PC3-PIP/KLK4 cells in Matrigel may be due to KLK4-mediated changes to cell adhesion or the remodeling of specific matrix proteins. Thus, The ability for PC3-PIP/KLK4 and /mock cells to adhere to collagen I, IV, fibronectin, vitronectin and laminin will be assessed, using a Cytomatrix kit from Millipore that has already been purchased. Should differences in cell adhesion be observed, adhesion of the above cells pre-treated with siKLK4 or siControl will be assessed.		
Specific Aim 4: *In vivo* studies to assess how KLK4-targeting affects PCa growth and bone metastasis		
Task 1: Effect of KLK4 antagonism on incidence and growth of orthotopic tumors and pseudo-metastases. To generate primary tumors, or bone pseudo-metastases, immunodeficient NOD/SCID mice will be injected orthotopically or intracardiac, respectively, with 10^5 cells of either PC3-PIP/KLK4 or /mock (10 mice/group). Each group will be divided into 2 subgroups, one receiving the KLK4-targeting conjugate, and the other with the relevant control (5 mice each). These agents will be administrated intravenously on the same day as tumor cell injection. Mice will be sacrificed when they lose >20% of weight loss or become lethargic, in accordance with approved animal ethics guidelines. The impact of KLK4 over-expression and KLK4 blockade on tumor incidence, size and growth rate will be assessed by tumor bioluminescence (all cell lines express already luciferase) using the IVIS Spectrum, and will be correlated with immunohistochemical (IHC) analysis (*ex vivo*) for markers of apoptosis (caspase3) and proliferation (Ki-67). Effects on bone homing and/or metabolism will be assessed by skeletal tumor incidence (by bioluminescence, and post-euthanasia microCT; Siemens Inveon), IHC (ex vivo) for osteoblast/clastic activity (Tartrate-resistant acid phosphatase staining), and measuring surrogate markers of bone metabolism in serum (osteopontin, osteonectin) by ELISA. **Task 2: Studying the role of KLK4 in PCa homing using a novel hu**For similar reasons as described in Aim 3, task 2 (above), this task has been discontinued.	19-24 months	APCRC-Q (TK) AIBN (AW, KT) IHBI (JH)
Training & Mentoring Plans		
Meet mentor Prof Russell and co-mentor Prof Clements every 1-2 weeks to discuss project progress, manuscript preparation, grant/fellowship applications and forming collaborations, in addition to attending Clements group lab meetings. Visit the laboratories of collaborators every 2 months and to discuss the project. Attend and present data at APCRC-Q weekly meetings, journal club and at conferences (national & international).	18-24 months	APCRC-Q, AIBN & IHBI

A number of minor but rational changes in approach were made, causing slight delay in some cases.

- In the original fellowship application, the PSMA-targeting ligand to be attached to HBPs was the J591 antibody, with the alternative ligand being urea glutamate. However, since that time, the peptide ligand became available to us from Dr Warren Heston. As described in the accomplishment section above, we generated HBPs linked with each of the three PSMA ligands, and performed a large body of optimisation and characterisation experiments to determine which polymer has the highest PSMA-targeting efficiency and specificity, and most rational to attach our KLK4 siRNA onto. This process caused some delays; however, the HBP-peptide has now been determined as the best one to use. At the moment, HBP-peptide/siKLK4(A), /siKLK4(B) and /siControl are being synthesised, and we anticipate them to be ready in approximately two months.
- In the original application, two KLK4-inhibiting strategies were proposed: siRNA and antibody. However, after careful re-evaluation of the strategy, it was decided that the siRNA approach would be by far more effective than antibody, given the surprisingly high amount of KLK4 protein secreted by PC3/PIP-KLK4 cells. The amount of antibody required for attachment to HBP-peptide, and the dosage of the resultant polymer needed to reverse KLK4-induced cellular changes are not feasible – certainly not *in vivo*. In addition to having greater KLK4 silencing potential compared to an antibody approach, siRNA is also more feasible cost-wise. For these reasons, siRNA has been selected as the KLK4-silencing mechanism for our HBP-peptide system. This modification did not result in delays.
- The original plan was to over-express KLK4 using the plasmids that Prof Clements used in her previous study [4, 5]. However, the data described in this report involved the use of cells transfected with plasmids from Prof Viktor Magdolen. Although full length KLK4 is encoded on plasmids from both sources, a key difference was the vector backbone (pcDNA3.1 versus pRVS). KLK4 protein production was much greater in cells transfected with Prof Magdolen's constructs; hence the switch. In addition, preliminary data generated from these cells provide good evidence of KLK4-mediated effects.
- An unexpected research finding was that KLK4-over expression did not induce overt EMT-like changes, which has been reported in the literature. Only the Snail transcription factor was differentially expressed between KLK4 transfectants and control PC3/PIP cells. However, there is evidence that KLK4 alters cell invasiveness and motility, which are related to but not exclusive to EMT processes. The approach now is to treat parental PC3/PIP cells with CM from PC3/PIP-KLK4 or PC3/PIP-Vec cells to determine whether or not under those circumstances EMT-like changes are induced. If so, we would test whether or not HBP-peptide/siRNA can inhibit this.
- A minor problem encountered which caused some delay was that during the plasmid transfection stage, our laboratory/institute experienced a one-off widespread mycoplasma contamination. The exact cause was not determined, possibly related to incubators or shared pipette guns, but the problem has now been fully resolved. Unfortunately due to mycoplasma infection, I had to perform cell line transfection an extra two times, which caused delays of weeks to months.
- The proposed experiments involving the use of human tissue engineered bone have been slightly delayed. I am waiting for the HBP-peptide/siRNA to be ready before proceeding with those experiments, as they are very precious and expensive to perform. I anticipate the experiments will commence in 2-3 months.

- **Changes that had a significant impact on expenditures**
  Nothing to report.

- **Significant changes in use or care of human subjects, vertebrate animals, biohazards, and/or select agents**
  Nothing to report.

- **Significant changes in use or care of human subjects**
  Nothing to report.

- **Significant changes in use or care of vertebrate animals.**
  Nothing to report.

- **Significant changes in use of biohazards and/or select agents**
  Nothing to report.

6. PRODUCTS

- **Publications, conference papers, and presentations**
  - **Journal publications**

  Two manuscripts related to this DOD project have been published or accepted (please see full manuscripts/publications at Appendices section).

  1. Fuchs AV*, **Tse BW-C***, Pearce AK, Yeh MC, Fletcher N, Huang SS, Heston WD, Whittaker AK, Russell PJ, Thurecht KJ. Evaluation of polymeric nanomedicines targeted to PSMA: Effect of ligand on targeting efficiency. *Biomacromolecules* (accepted for publication on 25-Aug 2015). **Equal first.*

  2. Pearce AK, Rolfe B, Russell PJ, **Tse BW-C**, Whittaker AK, Fuchs AV, Thurecht KJ. Development of a polymer theranostic for prostate cancer. *Polymer Chemistry.* 2014. doi:10.1039/C4PY00999A.
  Another paper related the synthesis and characterisation of polymeric nanoparticles for prostate cancer imaging and treatment (not the same polymer system as in my DOD project). I contributed to experimental setup and wrote parts of the paper. Polymer Chemistry has an impact factor of 5.52.

  - **Books or other non-periodical, one-time publications**
    Nothing to report.

  - **Other publications, conference papers, and presentations**

  I recently attended the Prostate Cancer World Congress (Aug 17-20, 2015) at Cairns, Australia, and gave an oral presentation based on our preliminary hyperbranched polymer work. The abstract was entitled **"**Multimodal hyperbranched polymers targeting Prostate Specific Membrane Antigen (PSMA) for imaging of prostate cancer**"** (please see full abstract at Appendices section). I have also submitted an abstract based on my preliminary KLK4 work to the upcoming 6th annual International Symposium on Kallikreins and Kallikrein-Related Peptidases (ISK 2015) in Brisbane, Australia (Sept 28-Oct 1, 2015), of which my co-mentor Prof Judith Clements is Chair of the organising committee. The abstract is entitled "Targeting KLK4 to inhibit prostate cancer epithelial to mesenchymal transition (EMT) and homing to bone" (please see full abstract at Appendices section).

- **Website(s) or other Internet site(s)**

The awarding of my DOD Postdoctoral Training Award for Prostate Cancer Research was announced on the website of our institute, the Australia Prostate Cancer Research Centre-Queensland (APCRC-Q). URL below:
<http://www.australianprostatecentre.org/news/funding-flows-for-dr-brett-hollier-and-dr-brian-tse>

- **Technologies or techniques**
  Nothing to report.

- **Inventions, patent applications, and/or licenses**
  Nothing to report.

- **Other Products**
  Nothing to report.

7. PARTICIPANTS & OTHER COLLABORATING ORGANIZATIONS

- **What individuals have worked on the project?**

Name:	*Brian Tse*
Project Role:	*Post-doctoral Training Award recipient (PI)*
Researcher Identifier	*N/A*
Nearest month person worked	*18*
Contribution	*Lead project and perform experiments*

Name:	*Thomas Kryza*
Project Role:	*Post-doctoral Training Award recipient (PI)*
Researcher Identifier	*N/A*
Nearest month person worked	*18-*
Contribution	*Lead project and perform experiments*

- **Has there been a change in the active other support of the PD/PI(s) or senior/key personnel since the last reporting period?**
  Nothing to report.

- **What other organizations were involved as partners?**

Organisation Name:	Australian Institute of Bioengineering and Nanotechnology (AIBN), University of Queensland
Location of Organisation:	Brisbane, Australia
Partner's contribution to the project:	• Collaboration (staff to perform polymer synthesis including attachment of siKLK4) • In-kind support • Facilities

8. SPECIAL REPORTING REQUIREMENTS
Nothing to report.

9. APPENDICES (continues in next pages)

1. Fuch & Tse et al. Manuscript accepted for publication in *Biomacromolecules*
2. Pearce et al. *Polymer Chemistry.* 2014, 5:6932-6942.
3. Thomas Kryza biosketch

References:

1. Klokk et al,Cancer Res 2007;67:5221; **2**.Avgeris et al,Prostate 2011;71:1789; **3**.Beaufort et al; Biol Chem 2006;387:217; **4.**Veveris-Lowe et al, Endo-Rel Can; 2005;12:631; **5**.Gao et al; Prostate 2007;67:348; **6**.Jones et al; Exp Opin The Targ 2009;(2):227.

Article

pubs.acs.org/Biomac

Evaluation of Polymeric Nanomedicines Targeted to PSMA: Effect of Ligand on Targeting Efficiency

Adrian V. Fuchs,[†,●] Brian W.C. Tse,[‡,●] Amanda K. Pearce,[†] Mei-Chun Yeh,[‡] Nicholas L. Fletcher,[†] Steve S. Huang,[§] Warren D. Heston,[∥] Andrew K. Whittaker,[†,⊥] Pamela J. Russell,[*,‡] and Kristofer J. Thurecht[*,†,⊥]

[⊥]ARC Centre of Excellence in Convergent Bio-Nano Science and Technology and [†]Australian Institute of Bioengineering and Nanotechnology and Centre for Advanced Imaging, University of Queensland, Brisbane 4072, Australia

[‡]Australian Prostate Cancer Research Centre − Queensland, Institute of Health and Biomedical Innovation, Queensland University of Technology at Translational Research Institute, Brisbane 4102, Australia

[§]Department of Nuclear Medicine, Cleveland Clinic, Cleveland, Ohio 44195, United States

[∥]Department of Cancer Biology, Cleveland Clinic, Cleveland, Ohio 44195, United States

Supporting Information

ABSTRACT: Targeted nanomedicines offer a strategy for greatly enhancing accumulation of a therapeutic within a specific tissue in animals. In this study, we report on the comparative targeting efficiency toward prostate-specific membrane antigen (PSMA) of a number of different ligands that are covalently attached by the same chemistry to a polymeric nanocarrier. The targeting ligands included a small molecule (glutamate urea), a peptide ligand, and a monoclonal antibody (J591). A hyperbranched polymer (HBP) was utilized as the nanocarrier and contained a fluorophore for tracking/analysis, whereas the pendant functional chain-ends provided a handle for ligand conjugation. Targeting efficiency of each ligand was assessed in vitro using flow cytometry and confocal microscopy to compare degree of binding and internalization of the HBPs by human prostate cancer (PCa) cell lines with different PSMA expression status (PC3-PIP (PSMA+) and PC3-FLU (PSMA−). The peptide ligand was further investigated in vivo, in which BALB/c nude mice bearing subcutaneous PC3-PIP and PC3-FLU PCa tumors were injected intravenously with the HBP-peptide conjugate and assessed by fluorescence imaging. Enhanced accumulation in the tumor tissue of PC3-PIP compared to PC3-FLU highlighted the applicability of this system as a future imaging and therapeutic delivery vehicle.

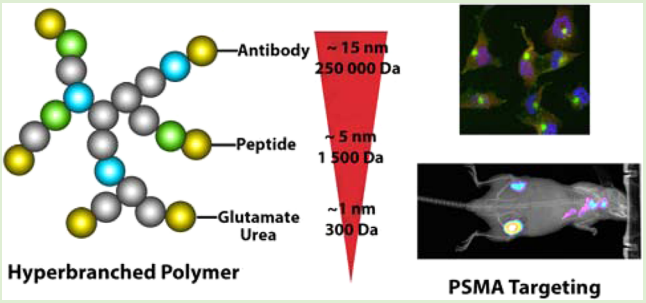

INTRODUCTION

Prostate cancer (PCa) is the most frequently diagnosed cancer in men and the sixth leading cause of cancer-related deaths of men worldwide. In 2008, an estimated 903 000 men were newly diagnosed, and 258 000 died from PCa.[1] In clinical management of PCa, common uncertainties include the inability to discriminate clinically significant PCa from more aggressive disease and the precision of loco-regional staging (lymph node involvement) in advanced disease states. This unreliability exists despite improvements in imaging, the most notable being the recent implementation of a Ga68-PSMA agent for positron emission tomography (PET) that is showing good discrimination of PCa in humans.[2−4] However, there still exists the need to better treat PCa building on advances in targeted systems.

PSMA, a 750-amino acid, type 2 transmembrane glycoprotein with folate hydrolase (FOLH1) and carboxy peptidase II activity,[5] is an attractive surface protein for prostate-cancer targeting.[6,7] Also known as glutamate carboxypeptidase II (GCPII), PSMA is highly expressed on the surface of over 90% of PCas, including lymph node and bone metastases, and its level increases progressively in higher grade tumors, metastatic and hormone-refractory disease.[8−10] Thus, PSMA serves as a biomarker that is both specific and sensitive for tumor volume. In addition, the cytoplasmic domain of PSMA contains a MXXXL motif, which mediates its internalization and endosomal cycling.[11,12] Various targets/ligands have been identified for PSMA, ranging from antibodies (and their fragments)[13,14] to aptamers,[15,16] peptides,[17,18] and small molecules.[19,20] The pharmacokinetic and biodistribution profile of these targeting moieties differ greatly due to their variations in size, structure, and functionality.

Glutamate ureas have shown great success in the targeting of PSMA.[21,22] This is due to the ability of PSMA (or GCPII) to

Received: July 9, 2015
Revised: August 23, 2015
Published: September 3, 2015

DOI: 10.1021/acs.biomac.5b00913
Biomacromolecules 2015, 16, 3235−3247

Scheme 1. Synthetic Pathway Used in the Generation of the Core Polymer Platform (4) from Which Various PSMA-Targeting Materials Was Generated

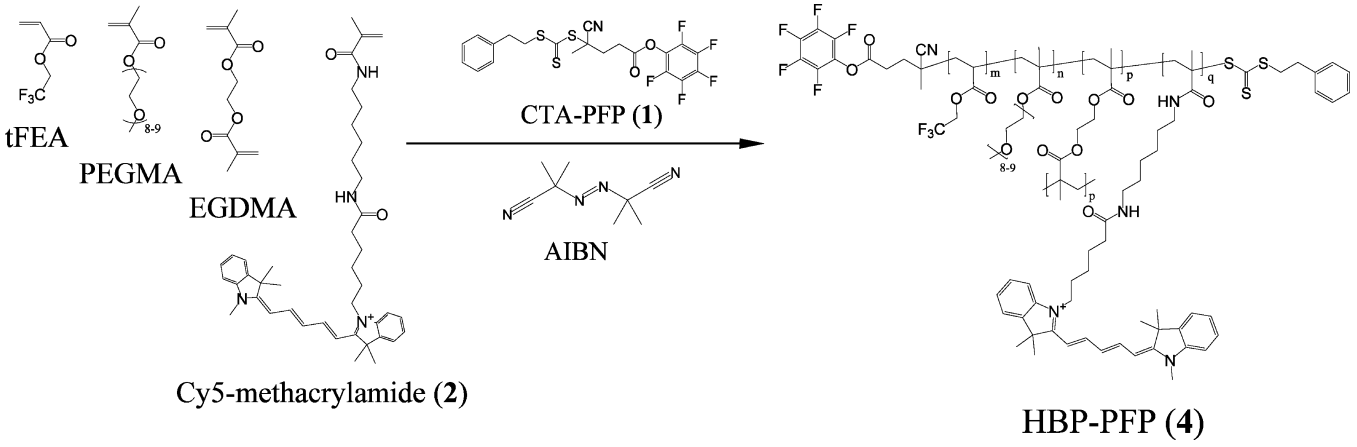

hydrolyze *N*-acetyl-aspartyl glutamate to glutamate plus *N*-acetyl-aspartamate (NAALADase).[9] As a consequence, inhibitors of NAALADases also show high affinity toward PSMA. Variants of the 2-[3-(1,3-dicarboxypropyl)-ureido]pentanedioic acid family modified through the C2 position have been particularly investigated.[19,23] Heston et al.[18,24] have investigated peptides carrying the urea-based moiety. These peptides contain the negatively charged glutamate urea at the N-terminus. The glutamate urea headgroup was thus extended, by the trailing peptide segment, into the 20 Å pocket of the GCPII.[25] This provided effective access to the glutamate binding region, and Huang et al. have shown through SPECT/CT imaging that when radiolabeled with ^{99m}Tc, good targeting of PSMA expressing tumors in mice was observed.[18] The glutamate−urea group attached to polymeric, docetaxel-loaded micelles "BIND-014" has also recently made the clinical transition as a targeted nanoparticle and is under phase 2 clinical trials.[26] Antibodies have also been utilized to bind PSMA. PSMA was first identified as the antigen binding the 7E11-C5.3 monoclonal antibody (mAb), raised vs human LNCaP cells.[27] This mAb forms the basis of "ProstaScint" imaging for PCa,[28] but binds to an internal epitope of PSMA. Recent testing uses the J591 mAb, which, after binding to an external domain of PSMA,[29] is internalized by endocytosis via clathrin-coated pits.[30]

In order to exploit this high level of specificity toward the PSMA receptor, nanomedicines have been developed that allow delivery of a wide range of therapeutic cargos to PCa. Nanomedicines provide an expansive platform for both imaging and treating prostate cancer, facilitating longer circulation times, higher accumulation of therapeutics/imaging agents at the site of disease as well as the potential to deliver a range of therapeutic agents.[31] However, there are no reports that directly assess and compare the targeting ability of different ligands toward PSMA on a particular nanomedicine. Therefore, in this report, the objective was to assess the targeting efficiency of polymeric nanomedicines (as a pseudodrug carrier) toward PSMA using a small molecule (glutamate urea), peptide, and whole antibody (J591). By keeping the polymeric nanomaterial the same in each case, the ability to target PSMA-expressing tumor cells could be monitored experimentally. To achieve this aim, we have chosen to use hyperbranched polymers as a model nanomaterial, because these materials exhibit versatility in design, function, and have previously been shown to be effective as therapeutic and imaging agents *in vivo*.[32−36]

The synthesis and characterization of a HBP platform which effectively targets PSMA via postpolymerization conjugation of either glutamate urea (HBP-GluUrea), a glutamate urea-carrying peptide (HBP-peptide), or the J591 monoclonal antibody (HBP-J591) has been achieved. The HBP contains activated ester chain-ends from which post-polymerization conjugation strategies were employed. Cyanine5 (Cy5) and a fluorinated monomer were also polymerized into the HBP construct to provide imaging and diagnostic capabilities to the materials while poly(ethylene glycol) monomethyl ether methacrylate 475 (PEGMA) was incorporated to provide water solubility and biocompatibility. The materials were extensively characterized, and their comparative ability to be endocytosed via PSMA into prostate cancer cells with varying PSMA expression level was assessed.

MATERIALS AND METHODS

Materials. Ethylbenzyl thiol, carbon disulfide, potassium *tert*-butoxide, iodine, azobis(cyanovaleric acid) (ACVA), pentafluorophenol (PFP), methacrylic acid, dicyclohexylcarbodiimide (DCC), dimethylamino pyridine (DMAP), triethylamine (TEA), phosphate-buffered saline (PBS), trifluoroacetic acid, 1-ethyl-3-(3-(dimethylamino)propyl) carbodiimide hydrochloride (EDC·HCl), azobis(isobutyronitrile) (AIBN), and *N*-(2-aminoethyl)maleimide·TFA were all used as received from Sigma-Aldrich. *N*-hexane, ethyl acetate, dichloromethane, dimethylformamide, diethyl ether, pyridine, tetrahydrofuran, acetonitrile, and methanol were used dry where applicable and of reagent grade quality. Milli-Q water (18.2 mΩ/cm) was used throughout. Cy5amine was purchased from Lumiprobe. Monomers, poly(ethylene glycol) monomethyl ether methacrylate 475 (PEGMA475), ethylene glycol dimethacrylate (EGDMA), and trifluoroethyl acrylate (TFEA) were filtered through basic alumina to remove radical inhibitors before use.

The human PCa cell lines PC3-PIP and PC3-FLU, which were previously modified to express DsRed and luciferase,[22] LNCaP, DU145, (both sourced from American Type Culture Collection (ATCC), U.S.A.), and LNCaP-C42B (abbreviated as "C42B") (from Dr Leland Chung, Cedars-Sinai Medical Center, U.S.A.) were maintained in RPMI media containing 5% fetal bovine serum (Gibco, Life Technologies). All cell lines were incubated at 37 °C in a humidified atmosphere of 5% CO_2/air.

Synthesis of Hyperbranched Polymers. The synthetic pathway for the production of hyperbranched polymers (HBPs) **5**, **6**, **8**, and **9** required the synthesis of several precursors **1**, **2**, **3**, and **7**, including the

DOI: 10.1021/acs.biomac.5b00913
Biomacromolecules 2015, 16, 3235−3247

Scheme 2. Post-Polymerization Conjugation Pathways Used in the Generation of the Various PSMA-Targeting Materials

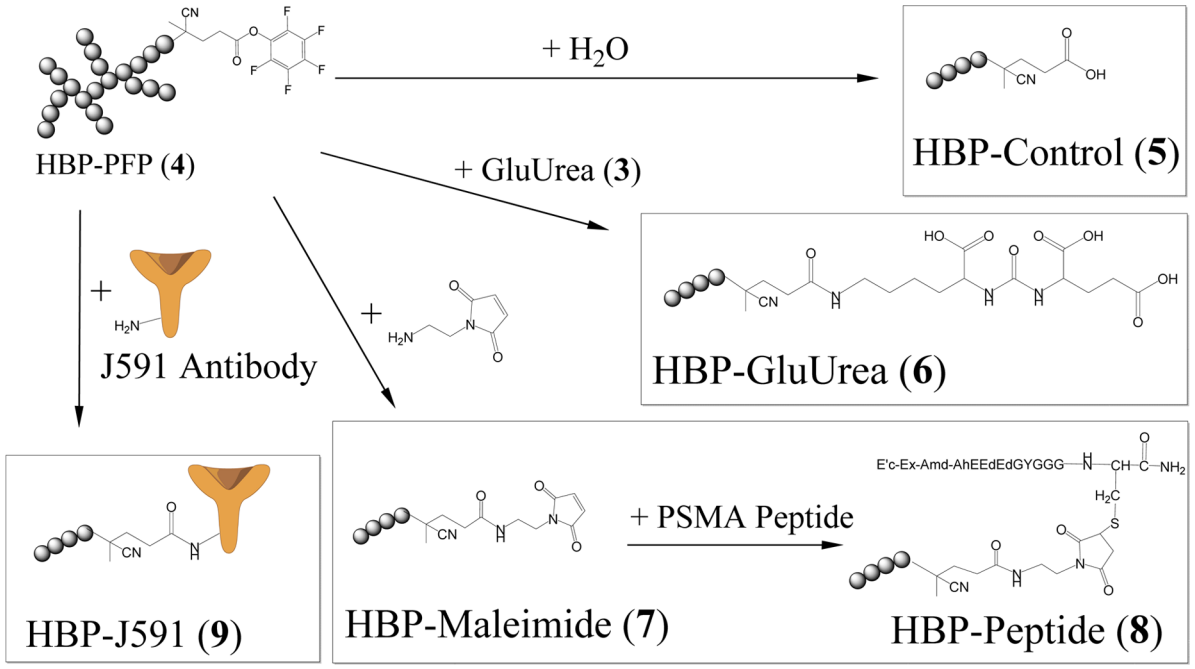

core HBP platform (**4**) (Scheme 1), from which the postpolymerization conjugations were performed (Scheme 2).

*Synthesis of Pentafluorophenyl-(4-cyano-4-phenylethylsulfanylthiocarbonyl)sulfanyl Pentanoate (**1**).* The synthesis of the RAFT chain transfer agent (CTA-PFP) was adapted from that previously published.[37−39] Briefly, 2-phenylethanethiol (25 g, 181 mmol) was added dropwise to a stirred suspension of NaH (7.6 g, 60% in mineral oil, 190 mmol) in 350 mL of diethyl ether over 10 min at 5 °C. The reaction was left to stir for a further 30 min after which carbon disulfide (14.5 g, 190 mmol) was added dropwise over 10 min and left to stir for an additional hour. The solid was then filtered and redispersed in diethyl ether (400 mL). To this, iodine (23 g, 90.5 mmol) was added portion-wise and stirred for 3 h at room temperature. The reaction mixture was filtered, and the filtrate was washed three times with sodium thiosulfate (0.25 M) brine and dried over anhydrous magnesium sulfate. After solvent removal, a yellow solid resulted (Bis(phenylethylsulfanylthiocarbonyl) disulfide). Yield: 27.4 g (71%).

^{1}H NMR (300 MHz, $CDCl_3$) δ (ppm): 7.40−7.18 (m, 5H, Ar−H), 3.56 (m, 2H, CH_2), 2.98 (m, 2H, CH_2).

To a 250 mL round-bottom flask was added DCC (3.64 g, 17.6 mmol) and ACVA (2.06 g, 7.35 mmol) in 100 mL of THF under stirring in an ice bath at 0 °C. The solution was degassed with N_2 for 20 min before the addition of pentafluorophenol (3.00 g, 16.3 mmol) dissolved in 10 mL of cold THF. This was directly followed by the dropwise addition of DMAP (0.361 g, 2.96 mmol) in a further 10 mL of cold THF. The reaction was sealed and left to warm to room temperature with stirring overnight. The solid was filtered off and the solvent removed under reduced pressure at room temperature on a rotary evaporator. (CAUTION: Explosion risk. A protective shield should be used when subjecting azo-initiators to reduced pressures and increased temperatures. The crude product was then twice dissolved in cold acetonitrile and filtered to remove any further by products. This was purified by silica gel column chromatography using DCM as eluent. The first fraction resulted in a viscous yellow oil (ACVA-PFP). Yield: 2.1 g (45%).

^{1}H NMR (700 MHz, DMSO-d_6) δ (ppm): 3.06−2.87 (m, 2H, CH_2), 3.06−2.87 (m, 2H, CH_2), 1.76, 1.72 (2 s (cis, trans), 3H, CH_3).

^{19}F NMR (659 MHz, DMSO-d_6) δ (ppm): −152.97 (m, 2F, *o*-Ar), −157.85 (m, 1F, *p*-Ar), −162.62 (m, 2F, *m*-Ar).

The ACVA-PFP (1.0 g, 1.6 mmol) and the above bis-(phenylethylsulfanylthiocarbonyl) disulfide (0.582 g, 1.36 mmol) were dissolved in ethyl acetate and heated to reflux under an inert atmosphere overnight. The solvent was removed, and the crude product was purified by silica gel column chromatography using *n*-hexane:ethyl acetate (85:15) as eluent. The second fraction afforded a viscous yellow oil (CTA-PFP **1**). Yield: 0.98 g (74%).

^{1}H NMR (700 MHz, DMSO-d_6) δ (ppm): 7.33−7.21 (m, 5H, Ar−H), 3.65 (m, 2H, CH_2), 3.13−3.01 (m, 2H, CH_2), 2.96 (m, 2H, CH_2), 2.70−2.54 (m, 2H, CH_2), 1.90 (s, 3H, CH_3).

^{19}F NMR (659 MHz, DMSO-d_6) δ (ppm): −152.97 (d, 2F, J = 20.8 Hz, *o*-Ar), −157.78 (t, 1F, J = 23.3 Hz, *p*-Ar), −162.53 (t, 2F, J = 22.1 Hz, *m*-Ar).

*Synthesis of Cy5-Methacrylamide (**2**).* Methacrylic acid (2.2 g, 25.6 mmol), EDC·HCl (8.4 g, 43.8 mmol), and DMAP (61 mg, 0.50 mmol) were combined and dissolved in 45 mL of DCM. This was stirred in an ice bath for 20 min to which was then added dropwise a solution of PFP (7.9 g, 43.0 mmol) in DCM (5 mL) and left to stir overnight. After the reaction, the solvent was removed and the crude product was purified by silica gel column chromatography using hexane:ethyl acetate (90:10) as eluent yielding a slightly yellow liquid (4.62 g, 72% yield).

^{1}H NMR (500 MHz, $CDCl_3$) δ (ppm): 6.45 (s, 1H, C<u>H</u>H), 5.90 (s, 1H, CH<u>H</u>), 2.08 (s, 3H, CH_3).

^{19}F NMR (471 MHz, $CDCl_3$) δ (ppm): −152.9 (d, 2F, J = 18.2 Hz, *o*-Ar), −158.23 (t, 1F, J = 21.8 Hz, *p*-Ar), −162.62 (dd, 2F, J = 21.3, 18.0 Hz, *m*-Ar).

Cy5-amine.2Cl (9.6 mg, 0.0147 mmol) was dissolved in DMF (0.5 mL) to which was slowly added triethylamine (1.55 mg, 0.0153 mmol). Then the pentafluorophenol-activated methacrylate ester (4.5 mg, 0.0178 mmol) was added dropwise to the solution and left to stir overnight. The product was purified by silica gel column chromatography using first hexane:ethyl acetate (10:90) to remove the pentafluorophenol, TEA and DMF. Then the column was flushed with DCM:ethyl acetate:MeOH (80:10:10) resulting in 10.8 mg (>95% yield) of a blue waxy solid (Cy5-MA, **2**).

^{1}H NMR (500 MHz, $CDCl_3$) δ (ppm): 7.85 (dd, 2H, J = 25.7, 12.7 Hz), 7.79 (m, 1H), 7.36 (dt, 4H, J = 22.0, 6.9 Hz), 7.22 (m, 2H), 7.14 (d, 2H, J = 7.9 Hz), 7.08 (d, 2H, J = 7.9 Hz), 6.84 (t, 1H, J = 12.6 Hz), 6.68 (m, 1H), 6.48 (d, 1H, J = 13.9 Hz), 6.24 (d, 1H, J = 13.5 Hz), 5.74 (s, 1H), 5.26 (s, 1H), 4.08 (t, 2H, J = 7.6 Hz), 3.59 (s, 3H), 3.28 (m, 2H), 3.21 (m, 2H), 2.35 (t, 2H, J = 7.1 Hz), 1.95 (s, 3H), 1.82 (m, 2H), 1.74 (m, 2H), 1.69 (m, 12H), 1.53 (m, 6H), 1.35 (m, 4H).

No signal was detected in the ^{19}F spectrum.

DOI: 10.1021/acs.biomac.5b00913
Biomacromolecules 2015, 16, 3235−3247

ESI-MS (positive mode, methanol): Calculated $[M]^+$ - 649.45 g/mol; measured $[M]^+$ - 649.82 m/z.

Synthesis of 2-(3-(5-Amino-1-carboxypentyl)ureido)pentanedioic Acid (3). (*S*)-Di-*tert*-butyl 2-(3-((S)-6-amino-1-tert-butoxy-1-oxohexan-2-yl)ureido)pentanedioate (glutamate urea PSMA targeting ligand) was synthesized in two steps on the basis of the method previously described.[22,40] This was then deprotected through the addition of TFA (0.1 mL) in DCM (0.4 mL) to the above product (0.080 g, 0.164 mmol) with vigorous stirring. This was left overnight whereupon the product (**3**) was extracted three times with water and lyophilized. A sticky yellow solid was isolated in near quantitative yield (GluUrea, **3**).

^{1}H NMR (500 MHz, DMSO-d_6) δ (ppm): 7.70 (s, 2H, NH_2), 6.33 (m, 2H, CHNHCO), 4.11−4.00 (m, 2H, CH), 2.83−2.71 (m, 2H, CH_2NH_2), 2.29−2.15 (m, 2H, CH_2COOH), 1.90 (m, 1H, CHCHH CH_2COOH), 1.74−1.61 (m, 2H, CHCHH CH_2COOH and CH_2CH_2CHHCH), 1.52 (m, 3H, CH_2CH_2CHHCH and $CH_2CH_2CH_2NH_2$), 1.31 (m, 2H, $CH_2CH_2CH_2CH$).

Synthesis of PSMA-Targeting Peptide. The PSMA peptide (E′E-Amc-Ahx-dEdEdEGYGGGC-NH_2) was used as received from the Department of Cancer Biology, Cleveland Clinic, Cleveland, Ohio. The peptide was assembled using standard Fmoc peptide synthesis. Detailed synthesis is described elsewhere.[18]

Synthesis of Hyperbranched Polymers (4−9). The HBP-PFP (**4**) was synthesized by adding; PEGMA (2.0 g, 4.21 mmol), TFEA (0.278 g, 1.86 mmol), EGDMA (0.0776 g, 0.391 mmol), Cy5-MA (0.009 g in 200 μL DCM, 0.014 mmol), CTA-PFP (0.1978 g, 0.391 mmol), and AIBN (12.85g, 0.0783 mmol) to a Schlenk tube. The reagents were dissolved in THF (3.8 mL) and the solution was degassed with N_2 for 20 min, sealed and submerged in an oil bath at 75 °C for 24 h. The resultant THF solution was triturated three times in excess hexane:ether (70:30). The product was a highly viscous blue oil that rapidly settled to the bottom of the beaker whereupon the supernatant was decanted off and the product redissolved in THF and the precipitation repeated. Note that dialysis was not performed as to avoid hydrolysis of the PFP-activated esters. Yield: 2.22 g, 84%.

Molar ratio of RAFT:PEGMA:TFEA was measured from ^{1}H NMR to be 1:40:15.8 respectively. This equates to a mole percentage of 28% TFEA from a feed ratio of 30%. This was measured through the integration of the phenyl moiety of the CTA-PFP (7.15−7.35 ppm) with respect to the methylene of both the PEGMA ($COOCH_2CH_2$−) and TFEA ($COOCH_2CF_3$) at 3.8−4.4 and 4.4−4.9 ppm, respectively. The length of a single chain was also measured in this way.

GPC − MALLS - 70 200 g/mol; M_w/M_n = 1.83.

The HBP-control (**5**) was produced through the hydrolysis of the PFP-activating group contained on the HBP-PFP. This was achieved by dialysis against Milli-Q water using 10k MWCO snakeskin tubing. Dialysis was performed for 3 days with replacement of the dialysis solution twice daily. Removal of PFP-activating groups was confirmed via ^{19}F NMR.

The end-group conjugation of **4** to form the HBP-GluUrea (**6**) was achieved by dissolution of the HBP-PFP (200 mg, 0.0085 mmol equivalents of PFP-activated end-groups) in 0.6 mL of pyridine. To this was added **3** (6.0 mg, 0.019 mmol) dissolved in a further 0.2 mL of pyridine. This was left to stir at room temperature for 18 h whereupon the crude product was triturated three times in excess hexane:ether (70:30). This was further purified by dialysis against Milli-Q water using 10k MWCO snakeskin tubing. Yield: 184 mg.

HBP-peptide (**8**) was produced through the initial conjugation of *N*-(2-aminoethyl)maleimide·TFA to the HBP-PFP which facilitated the Michael addition of the C-terminal sulfhydryl from the cysteine to the HBP. Briefly, **4** (406 mg, 0.017 mmol equivalents of PFP-activated end-groups) was dissolved in DCM to which a solution of *N*-(2-aminoethyl)maleimide·TFA salt (9.3 mg, 0.037 mmol), TEA (7.3 mg, 0.072 mmol) in DMF (0.1 mL) was added dropwise. This was left to stir at room temperature for 15 h and subsequently triturated three times resulting in a blue viscous oil (HBP-Maleimide, **7**). Yield: 396 mg. Two hundred milligrams of **7** was then dissolved in a 1 mM EDTA solution of 0.1 M PBS (pH 7.4, 1.6 mL). The PSMA-targeting peptide (17.0 mg, 0.012 mmol) was then added and left to stir at room temperature for 20 h. The crude product was triturated three times in excess hexane:ether (70:30) and further purified by dialysis against Milli-Q water using 10k MWCO snakeskin tubing resulting in a sticky blue solid (**8**). Yield: 178 mg.

HBP-J591 (**9**) was conjugated to the HBP-PFP by the dissolution of **4** (2.4 mg, 1.04×10^{-4} mmol equivalents of PFP-activated end-groups) in 1 mM EDTA solution of J591antibody (1.45 mL, 2.3 mg/mL, 2.22×10^{-5} mmol containing 0.5 μL of TEA. The reaction was left to stir at room temperature for 21 h. The conjugate (**9**) was purified through successive filtration cycles using a 100k MWCO Amicon Ultra Centrifugal Filter spin membrane until the filtrate gave no absorbance at 647 nm (from the Cy5 incorporated in the unconjugated HBP-PFP) (Nanodrop, Thermo Scientific).

Nuclear Magnetic Resonance Studies. All NMR spectra were recorded on either a Bruker Avance 500 or 700 MHz spectrometer at ambient temperature and 128 scans. All ^{1}H diffusion spectra were recorded at 500 MHz at 95% gradient, ambient temperature, and 256 scans. Diffusion ordered spectroscopy (DOSY) was used to measure the diffusion coefficient of the HBPs in $(CD_3)_2SO$. Fifteen milligrams of HBP was dissolved in 600 μL of $(CD_3)_2SO$ where a series of 16 spectra were collected at 256 scans each using a linear gradient ramp from 2−98% of the maximum gradient strength. A gradient duration (d) of 4.4 ms and diffusion time (D) of 343.5 ms was used in all cases. The Stokes−Einstein equation was then used to calculate hydrodynamic diameter (D_h).

Gel Permeation Chromatography − Multiangle Laser Light Scattering Studies. GPC-MALLS chromatographic system consisted of a 1515 isocratic pump (Waters), a 717 auto sampler (Waters), Styragel HT 6E and Styragel HT 3 columns (Waters), 2414 differential refractive index detector (Waters) and a Dawn Heleos laser light scattering detector (Wyatt). THF was used as the mobile phase with a flow rate of 1 mL/min. In order to minimize the absorption of the light scattering laser (658 nm) by the Cy5-labeled polymers (λ_{max}= 637 nm) and thus providing false scattering signals, the Cy5 was degraded by bubbling the HBP in THF with oxygen for 1 h and left overnight. Number-average molecular weight was then determined using the dn/dc of the HBP as was measured in solutions of THF using a Pocket Refractometer (Atago, Tokyo).

UV−vis Spectroscopy. Samples were measured on a NanoDrop 2000c (Thermo Scientific). HBPs were analyzed to obtain chain size with respect to CTA end-group in acetonitrile calibrated against CTA-PFP standards ($\varepsilon_{309\ nm}$ = 10 566 M^{-1} cm^{-1}). Similarly, Cy5 content in the HBPs was calibrated against Cy5-methacrylamide standards ($\varepsilon_{637\ nm}$ = 177 207 M^{-1} cm^{-1}) and J591 using $\varepsilon_{280\ nm}$ = 210 000 M^{-1} cm^{-1}.

Flow Cytometric Analysis of HBP Internalization. Cells were seeded at 10^5 per well in 24-well plates in growth media overnight. The monolayers were then incubated with fresh growth media (500 μL) containing HBP-control, HBP-peptide, HBP-J591, or HBP-GluUrea at 0.0125, 0.05, or 0.2 μM for 30, 120, or 240 min at 37 °C. Cells were washed twice in PBS, lifted using trypsin and washed twice in PBS containing 5% FBS (FACSWASH). Cells were then run on a FACS Canto (BD Bioscience, U.S.A.), and data were analyzed using Flowjo software (Tree Star Inc, U.S.A.). The geometric mean fluorescence intensity (MFI) of Cy5 of the entire cell population and the percentage of cells positively stained with Cy5 after polymer incubation, were used to assess PSMA-mediated endocytosis. In the competitive binding and internalization assays, cells were incubated with a mixture of HBP-peptide (0.0125, 0.05, or 0.2 μM) and free peptide (2 μM) for 30 or 120 min in the incubation step.

Confocal Microscopy Studies. A total of 10^5 cells were grown overnight on 12 mm diameter glass coverslips (Menzel-Glaser, Germany) placed inside the wells of 24-well plates. Cell monolayers were then incubated with fresh growth media (500 μL) containing HBP-control, HBP-peptide, HBP-J591 or HBP-GluUrea at 0.2 μM for 120 min at 37 °C. Cells were fixed with 4% paraformaldehyde in PBS for 15 min, permeabilized with 0.5% Triton X100 in PBS for 10 min, and nuclear stained with 4′,6-diamidino-2-phenylindole (DAPI) (Life Technologies, U.S.A.) in PBS for 20 min. The cells were washed thrice in PBS after each of the aforementioned steps. The coverslips were then mounted onto microscope slides using Mowiol 4-88 (Sigma-

DOI: 10.1021/acs.biomac.5b00913
Biomacromolecules 2015, 16, 3235−3247

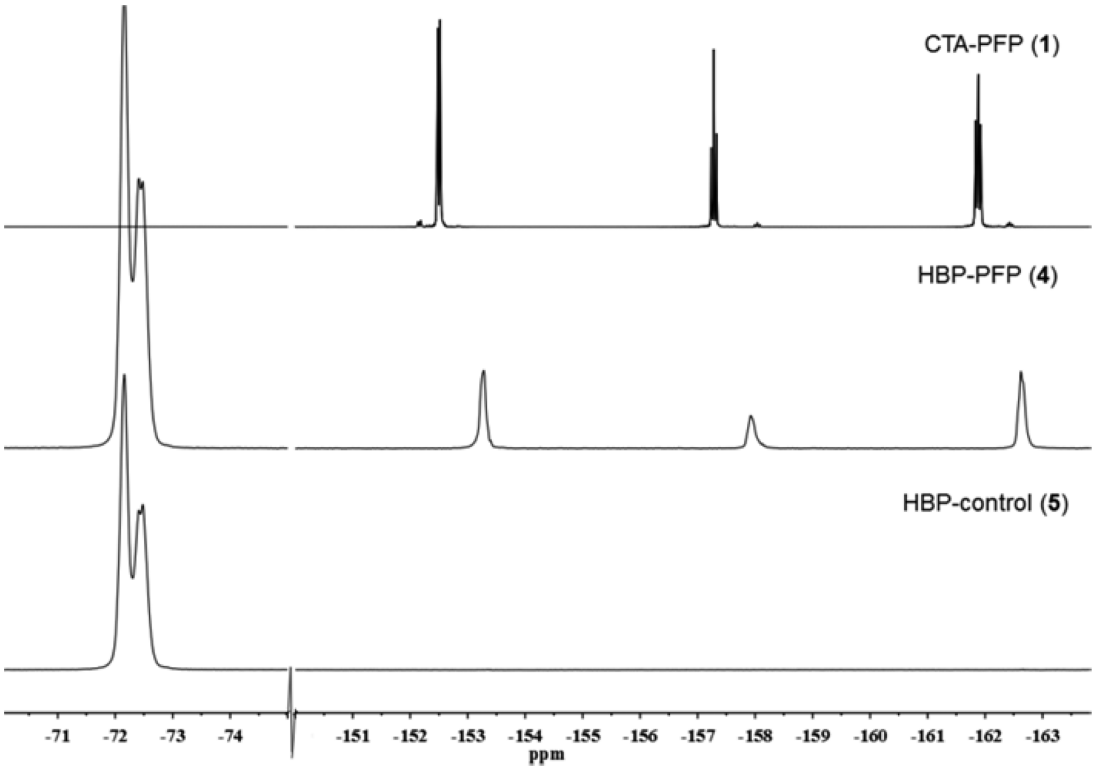

Figure 1. ^{19}F NMR spectra of CTA-PFP, HBP-PFP, and HBP-control.

Aldrich, U.S.A.), and fluorescence images were acquired with an Olympus FV1200 confocal microscope.

Animal Studies. All studies were in accordance with guidelines of the Animal Ethics Committees of Queensland University of Technology (QUT) and The University of Queensland (UQ), and Australian Code for the Care and Use of Animals for Scientific Purposes. PC3-PIP and PC3-FLU cells were lifted from culture flasks with trypsin, washed twice with FACSWASH, and resuspended at 10^7 cells/mL in serum-free media. Male BALB/c nude mice (Australian Resources Centre, Australia) were anaesthetized by isoflurane inhalation then implanted subcutaneously with 10^6 PC3-PIP cells and 10^6 PC3-FLU cells on opposite flanks. Tumor size was monitored by caliper measurements twice per week, and in vivo fluorescence imaging using an In-Vivo Xtreme (Bruker, Germany) imaging station weekly through excitation of the DSRed fluorophore. Three weeks after tumor cell implantation, 100 μL of HBP-peptide at 10 mg/mL was injected into the tail vein of each mouse, and live animal fluorescence imaging was performed 1, 3, and 6 days postinjection. Images were acquired using an excitation filter of 630 nm and an emission filter of 700 nm for Cy-5, whereas DsRed acquisitions used an excitation filter of 540 nm and an emission filter of 600 nm. Mice were anaesthetized with 2% isofluorane during the experiments. Ex vivo imaging of harvested organs was performed on the IVIS Spectrum (Xenogen, U.S.A.) following the same protocols as above. One hundred microliters of HBP-peptide (n = 4) or HBP-control (n = 1) at 5 mg/mL was injected into the tail vein of a mouse. Mice were then euthanized after 48 h, and relative fluorescence of harvested organs was measured.

Statistical Analysis. In all cases, data analysis was performed using multiple t-tests using GraphPad Prism v6 software. Differences of $p < 0.05$ were considered to be statistically significant. All data was obtained from biological experiments performed a minimum of three times.

RESULTS AND DISCUSSION

This report aims to investigate the targeting efficiency of three different targeting ligands toward PSMA following conjugation to a polymeric nanomaterial. An HBP was used as a model nanomedicine and was designed to allow for direct comparison of the targeting ability and uptake efficacies between a small molecule glutamate urea ligand, a peptide ligand, and monoclonal antibody-decorated HBP. Although these and similar moieties have been investigated previously, as described in the Introduction section, direct comparison between the different systems is difficult due to the various constructs used to deliver the targeting ligand. Thus, to address this issue a core nanomaterial was developed from which all postpolymerization ligation could be achieved using a single conjugation strategy. Consequently, all subsequent HBP bioconjugates inherited the same core HPB properties of chemical functionality, size, and chromogenic properties. The core platform was synthesized as outlined in Scheme 1. The advantage of such a synthetic route allows for the PFP-activated end groups to be directly conjugated to the targeting ligand to form HBP-GluUrea (**6**), HBP-J591 (**9**), or HBP-peptide (**8**). Hydrolysis of the HBP-PFP (**4**) generated the acid-terminated control (HBP-control (**5**)). These facile strategies were performed under mild conditions thus minimizing any deleterious effects to the integrity of the polymer, Cy5 dye, or other functional chain end-groups in the polymer.

Synthesis of Hyperbranched Polymers. The HBP core nanomaterial (HBP-PFP) was synthesized using PEGMA, TFEA, Cy5-methacrylamide, CTA-PFP, and EGDMA as a branching agent using a facile methodology that utilizes well-established RAFT chemistry.[22,32,34,41] As such, HBPs **4**, **5**, **6**, **7**, and **8** (Scheme 2) were characterized using ^{1}H, ^{13}C, and ^{19}F NMR, GPC-MALLS, and UV−vis spectroscopy in order to fully elucidate the number of branches per polymer, the integrity of chain-ends following modification strategies, as well as the coupling efficiency of each targeting ligand. Owing to the complexity of large protein−polymer conjugates, HBP-J591

DOI: 10.1021/acs.biomac.5b00913
Biomacromolecules 2015, 16, 3235−3247

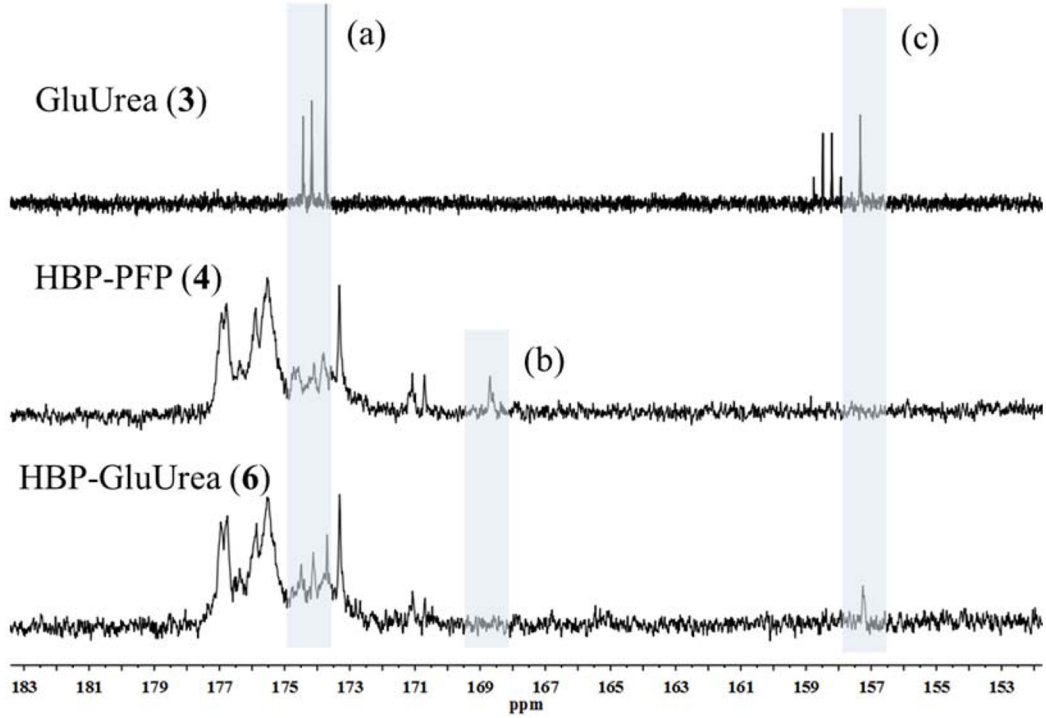

Figure 2. ^{13}C NMR spectra of the HBP-PFP, HBP-GluUrea and the GluUrea. Highlighted regions show (a) the glutamate carbonyl signal in (**6**), (b) the PFP-ester carbonyl end-group, and (c) the urea carbonyl peak.

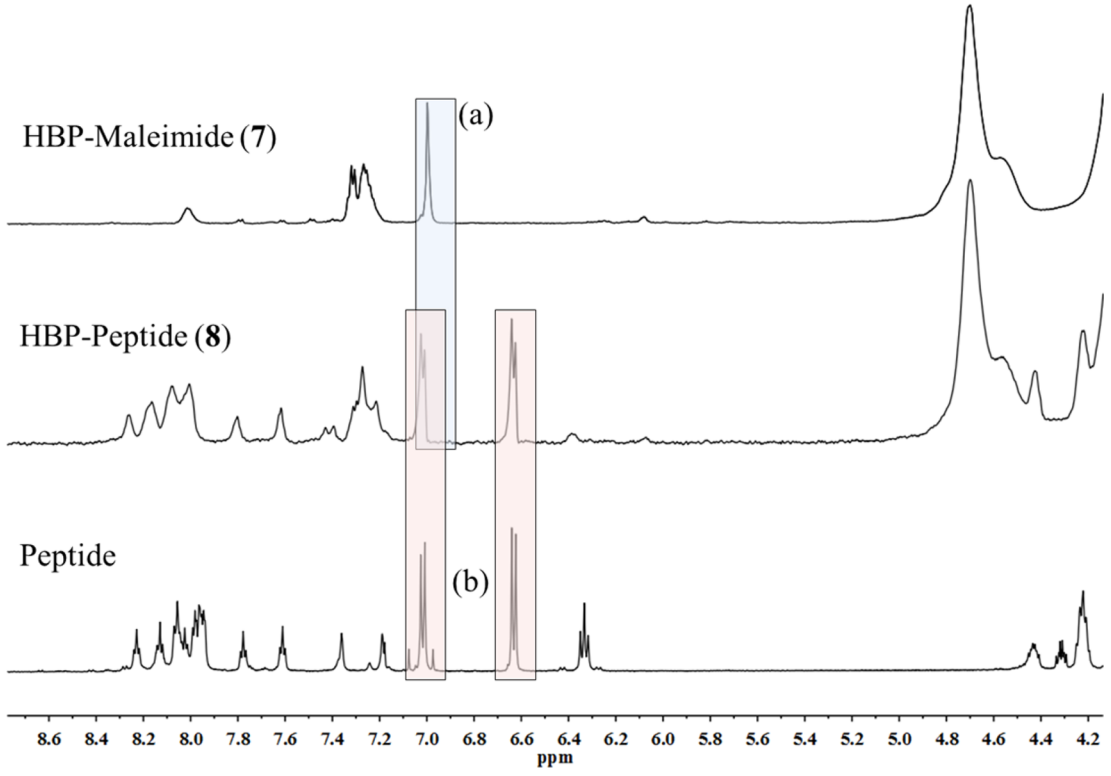

Figure 3. ^{1}H diffusion NMR spectra of HBP-maleimide and HBP-peptide compared against the ^{1}H NMR spectrum of the peptide alone. Highlighted regions show (a) the vinylic protons from the maleimide and (b) the aromatic tyrosine protons.

was characterized by SDS-PAGE and UV−vis spectroscopy because there was insufficient material to undertake NMR spectroscopy. Shown in Figure 1 is the ^{19}F NMR spectrum depicting the change in ^{19}F spectra between the CTA-PFP, HBP-PFP, and the HBP-control. There is a clear upfield shift in the ^{19}F resonances following polymerization (−153.3, −157.9, and −162.6 ppm), whereas an obvious band broadening also occurs due to the change in molecular mobility of the fluorine-containing species between the small molecule and the larger HBP. This is consistent with other studies investigating the

DOI: 10.1021/acs.biomac.5b00913
Biomacromolecules 2015, 16, 3235−3247

RAFT-synthesized PFP end-group functionality of linear polymers.[38] The broad signal at −72.3 ppm is due to the presence of the fluorinated monomer, TFEA, and is also seen in the ^{19}F spectrum of the HBP-control and is consistent with our recent reports.[34] The HBP-control was formed through the hydrolysis of the HBP-PFP to produce the deprotected acid. Deprotection was chosen to avoid any inadvertent coupling during subsequent analyses and was performed through hydrolysis of the PFP-ester functionality by dialysis. The HBP-control was dialyzed for 3 days whereupon no observable signal was present from the PFP moiety after this time (Figure S1). It was found that the hydrolysis of HBP-PFP proceeded with a 42.5 h half-life so that 95% hydrolysis was achieved after 264 h.

Coupling of Ligands to HPPs. The HBP-GluUrea was prepared through the conjugation of GluUrea (**3**) to HBP-PFP (**4**). The confirmation of successful conjugation is evidenced by the ^{1}H spectra of the HBP-PFP and HBP-GluUrea, performed in DMSO-d_6, where the appearance of both the ureido protons (assigned at 6.3 ppm) and the amino proton (assigned at 7.75 ppm) are observed in agreement with previously published work (Figure S2).[22] This is further supported in the stacked ^{13}C NMR spectra (Figure 2), where the three carbonyl signals from the glutamate (−173 to −175 ppm) become evident in the HBP-GluUrea spectrum (Figure 2; peak a). Importantly, disappearance of the carbonyl PFP-ester following amido-formation (disappearance of peak b) confirms amidation, while the carbonyl attributed to the urea-group also appears in the new conjugate (peak c). These three spectral signatures in the ^{13}C NMR suggest successful formation of HBP-GluUrea.

The HBP-peptide was obtained from a two-step ligation in which *N*-(2-aminoethyl)maleimide was first reacted with the PFP-active end-groups on the HBP-PFP to produce maleimide-functional end-groups. The HBP-peptide was then formed through the reaction of the maleimide end-groups with the C-terminal cysteine of the peptide via the well-known addition of sulfhydryl to a maleimide. Shown in Figure 3 are the ^{1}H diffusional spectra highlighting the disappearance of the vinylic protons at 6.98 ppm originating from the loss of the maleimide after reaction with the cysteine on the protein (Figure 3; peak a). After addition of the peptide, it can be seen that the proton spectrum develops signals owing to the peptide such as the aromatic tyrosine signals (7.00 and 6.62 ppm) highlighted in Figure 3 (peak b). Successful HBP-peptide formation is further supported by the ^{13}C NMR spectra (Figure S3) in which the vinylic carbons from the maleimide at 134.5 ppm disappears as they are converted to aliphatic carbons, whereas aromatic tyrosine peaks appear at 155.7, 130.0, 127.8, and 115.0 ppm.

The analysis of the HBP-J591 was performed using SDS-PAGE and UV−vis spectroscopy. UV−vis suggested 1.85 antibodies were bound per HBP and was calculated by the ratio of the antibody absorbance at 280 nm ($\varepsilon_{280\ nm}$ = 210 000 $M^{-1}cm^{-1}$) to that of the Cy5 present on the HBP-PFP ($\varepsilon_{647\ nm}$ = 177 200 M^{-1} cm^{-1}). UV−vis does not provide a means of determining if all antibodies are actually attached to a HBP, or associated loosely through physical interactions. Conversely, it is expected that there exists no free HPB-PFP as its removal was monitored by UV−vis measurements of the filtrate as the HBP-J591 was repeatedly passed through a 100 kDa centrifugal filtration column. In order to assess the conjugation reaction in a more quantitative manner, the HBP-J591 was run on a SDS-PAGE gel (Figure 4). The protein channel (Figure 4a) clearly shows the antibody and corresponding fragments after reduction using TCEP (lanes II and I, respectively). As expected, the HBP-control shows no protein signal (Figure 4a, lanes II and IV), whereas the HBP-J591 and reduced HBP-J591 give strong bands in lanes V and VI. The Cy5 fluorescence of the same gel (Figure 4b) shows no signal for the antibody (lanes I and II), whereas the HBP-control appears not to travel coherently through the gel. A strong, unretained band however can be seen (Figure 4b (iii)) showing the presence of either HBP-control (lanes III and IV), or as unreacted HBP (lanes V and VI). Importantly, the Cy5 signals highlighted with a red circle in Figure 4b (i) and (ii), indicate that the HBP is conjugated to the antibody, particularly the heavy chain in the reduced lane (Figure 4b; red circle (ii)). The light chain is not expected to be as strong in Cy5 signal (and therefore HBP) due to the relative size as compared to the heavy chain. It should be noted that due to the small working amounts of antibody and therefore HBP-J591, it was not possible to obtain NMR, GPC, or other data to verify the successful conjugation of the antibody to the HBP.

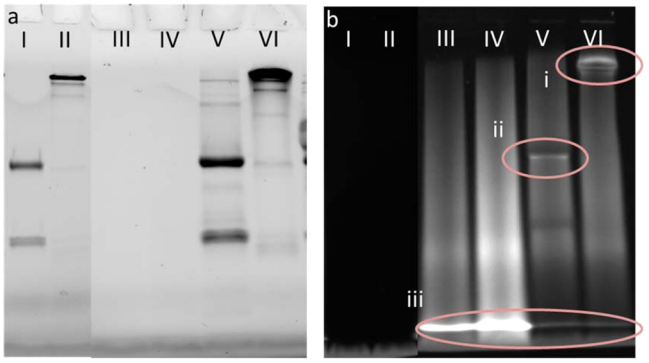

Figure 4. SDS-PAGE analysis of the HBP-J591 visualizing (a) proteins and (b) Cy5 fluorescence signals. Numbered lanes are (I) reduced antibody, (II) antibody, (III) HBP-control (2.7 μM), (IV) HBP-control (5.4 μM), (V) reduced HBP-J591, (VI) HBP-J591. Circled regions depict (i) fluorescent antibody, (ii) fluorescent heavy chain fragment, (iii) HBP not retained.

As a summary, Table 1 outlines the properties of all HBP materials that were synthesized. The molecular weight (M_n) of the HBP-PFP, as measured by GPC-MALLS, was 70200 Da ± 1.7%. The average chain size using both ^{1}H NMR and UV−vis measurements was calculated to be approximately 23 400 Da, and thus, the total number of PFP-activated end-groups available for functionalization on the initial HBP amounted to approximately 3. The calculation of the number of conjugated ligands was obtained by ^{1}H NMR (Figure 5). This was performed by taking the ratio of the integration of the five protons from the phenyl moiety of the CTA-PFP (7.15−7.35 ppm) (Figure 5a), with respect to either the two urea protons on the GluUrea (Figure 5b), the two vinylic protons on the maleimide (Figure 5c), or the four protons from the aromatic side-chain of the tyrosine fragment along the peptide (Figure 5d). It was determined that the conjugation of the maleimide, peptide, and GluUrea were all achieved in quantitative yield and therefore resulted in approximately three ligands per HBP. As described above, the number of antibodies per HBP was estimated by UV−vis spectroscopy and resulted in approximately 1.86 antibodies per HBP. This highlights the successful synthesis of the various HBP and the facile nature of the PFP-activated end-group ligation strategy. Furthermore, the attachment of either the maleimide or the GluUrea involved the

DOI: 10.1021/acs.biomac.5b00913
Biomacromolecules 2015, 16, 3235−3247

Table 1. Summary of the Various Properties of the HBP Constructs

	GPC MALLS (M_n, g/mol) (Đ, nm)	chain size (g/mol)		chains/HBP	ligands/RAFT end-group[a]	ligands/HBP	Cy5/HBP	D_h (nm)[b]
		^{1}H NMR	UV−vis					
HBP-PFP	70 200 ± 1.7% (1.83)	22 000	24 800	3.0	-	-	0.15	5.3
HBP-control	55 800 ± 6.8% (1.42)	27 100	30 100		-	-	0.14	4.3
HBP-GluUrea		24 800	23 200		1:1.1	3.3	0.18	6.1
HBP-maleimide		27 500	26 000		1:1	3	0.15	6.2
HBP-peptide		28 900	23 400		1:1.1	3	0.15	6.7
HBP-J591						1.86[c]		N/A

[a]Determined by ^{1}H NMR. [b]Determined in DMSO-d_6 using diffusion ordered spectroscopy and the Stokes−Einstein equation. [c]Determined by calculating the ratio of Cy5 (647 nm) per HBP-PFP to the antibody (280 nm).

reaction of a reactive amine nucleophile with the activated PFP-ester. This is known to cause aminolysis of RAFT CTAs;[37] however, this did not appear to occur to any measurable extent for the current system. This may be evidenced in Table 1 by the lack of significant average chain size increase as would occur if the trithiocarbonate end-group were to undergo aminolysis. Using both ^{1}H NMR and UV−vis spectroscopy of the HBP-Mal or HBP-GluUrea, in comparison to HBP-PFP, average chain size is calculated as 24 000 or 26 750 Da, respectively.

As expected, the hydrodynamic diameter (in DMSO-d_6, D_h) of 4.3 nm for the HBP-control (no end-group modification) increases up to 6.7 nm as the molar mass of the ligands increases. The Cy5 intensity remained relatively constant for all polymers throughout the modifications (0.14−0.18 Cy5 dyes per HBP).

The synthesis of all HBPs from the same core allowed the physicochemical properties of the nanomaterials to be the same, unless dictated by the targeting ligand. Thus, any differences between their ability to target the PSMA receptor is related predominantly to the ligand (not the carrier nanomaterial).

In Vitro and In Vivo Analysis. The binding of the various HBPs by PSMA was investigated using PC3-PIP (PSMA-proficient) and PC3-FLU (PSMA-deficient) cells across a range of concentrations and incubation durations. Flow cytometric analysis showed that PC3-PIP cells had significantly greater Cy5 uptake as compared to PC3-FLU cells following incubation with HBP-peptide under multiple conditions (Figure 6A (i) and (ii)). This was both in terms of the geometric MFI of Cy5 of the entire cell population (Figure 6Ai) and the percentage of cells positively stained (Figure 6A (ii)). Similar trends were observed when PC3-PIP and PC3-FLU cells were incubated with HBP-J591 under the same culture conditions (Figure 6B (i) and (ii)). These results suggest that HBP-peptide and HBP-J591 were bound to the cells via PSMA in a dose-dependent and time-dependent manner. In contrast, no difference in Cy5 signal was observed between the two cell lines incubated with HBP-GluUrea (Figure 6C (i) and (ii)) or HBP-control (Figure 6D (i) and (ii)).

To confirm these findings and to visualize intracellular Cy5, confocal microscopy was performed for each HBP. Consistent with the flow cytometry results, Cy5 accumulation could be seen within PC3-PIP cells but not PC3-FLU cells following incubation with HBP-peptide and HBP-J591 (Figure 7). Minimal Cy5 signal was detected following incubation with HBP-GluUrea or HBP-control, suggesting similar binding as that observed for the flow cytometry. To this point, we have provided in vitro evidence that following attachment of the peptide and J591 to our HBP backbone, their specificity for PSMA is preserved and can mediate endocytosis into prostate cancer cells. The lack of specificity for PSMA by HBP-GluUrea was surprising given that glutamate urea is showing promise in clinical trials as a PSMA-targeting agent for prostate cancer imaging.[2,3,42] In this study, we attribute the poor specificity and binding of the HBP-GluUrea to differences that might arise from the construct to which the glutamate urea is attached. The HBP used in this study contains predominantly hydrophilic PEGMA monomers with a 28% molar ratio of hydrophobic TFEA monomer (used to provide potential ^{19}F MR imaging capabilities). We hypothesize that this added hydrophobicity may affect the insertion into the pocket of the GCPII receptor through rearrangement of the polymer chains such that presentation of the ligand is not ideal for binding to the antigen. This effect will be studied in future work in which longer pegylated linkers can be attached to the polymer to investigate if this additional hydrophilicity improves binding of the small molecule substrate.

Because J591 is a well-characterized PSMA ligand that has also been evaluated in PCa patients as an imaging agent, we decided to further extend our study of the HBP-peptide with additional in vitro and in vivo experiments. To further confirm the specificity of HBP-peptide for PSMA, competitive binding experiments were performed in which PC3-PIP and PC3-FLU cells were incubated with a mixture of the HBP-peptide and free peptide at 10- to 160-fold molar excess. Flow cytometric analysis revealed that coincubation with free peptide inhibited binding of HBP-peptide to PC3-PIP cells under multiple polymer concentrations and time points (Figure 8A). As expected, no effect of the free peptide was seen on PC3-FLU cells (Figure 8B).

In order to validate the applicability of HPB-peptide in other prostate cancer cell lines, competitive binding assays were also performed on LNCaP and C42B cells (both PSMA-proficient) and DU145 cells (PSMA-deficient). Co-incubation with free peptide inhibited PSMA-mediated endocytosis in both LNCaP and C42B cells across multiple polymer concentrations, whereas it had no effect on DU145 cells (Figure 8C−E). The magnitude of HBP-peptide uptake (based on Cy5MFI) between the three PSMA-proficient cell lines tested varied, with PC3-PIP cells exhibiting the highest. This is attributed to variation between the cell lines such as PSMA abundance/expression level, post-translational modifications (e.g., glycosylation) of PSMA, and inherent endocytosis/metabolic rates.

Our in vitro data shows that both HBP-peptide and HBP-J591 show comparable PSMA-targeting potential in our study. Indeed, we previously showed that J591 conjugated to iron oxide magnetic nanoparticles homed to pre-established orthotopic LNCaP tumors in mice.[43] For this study, however, to further test the targeting efficiency and future utility of the

DOI: 10.1021/acs.biomac.5b00913
Biomacromolecules 2015, 16, 3235−3247

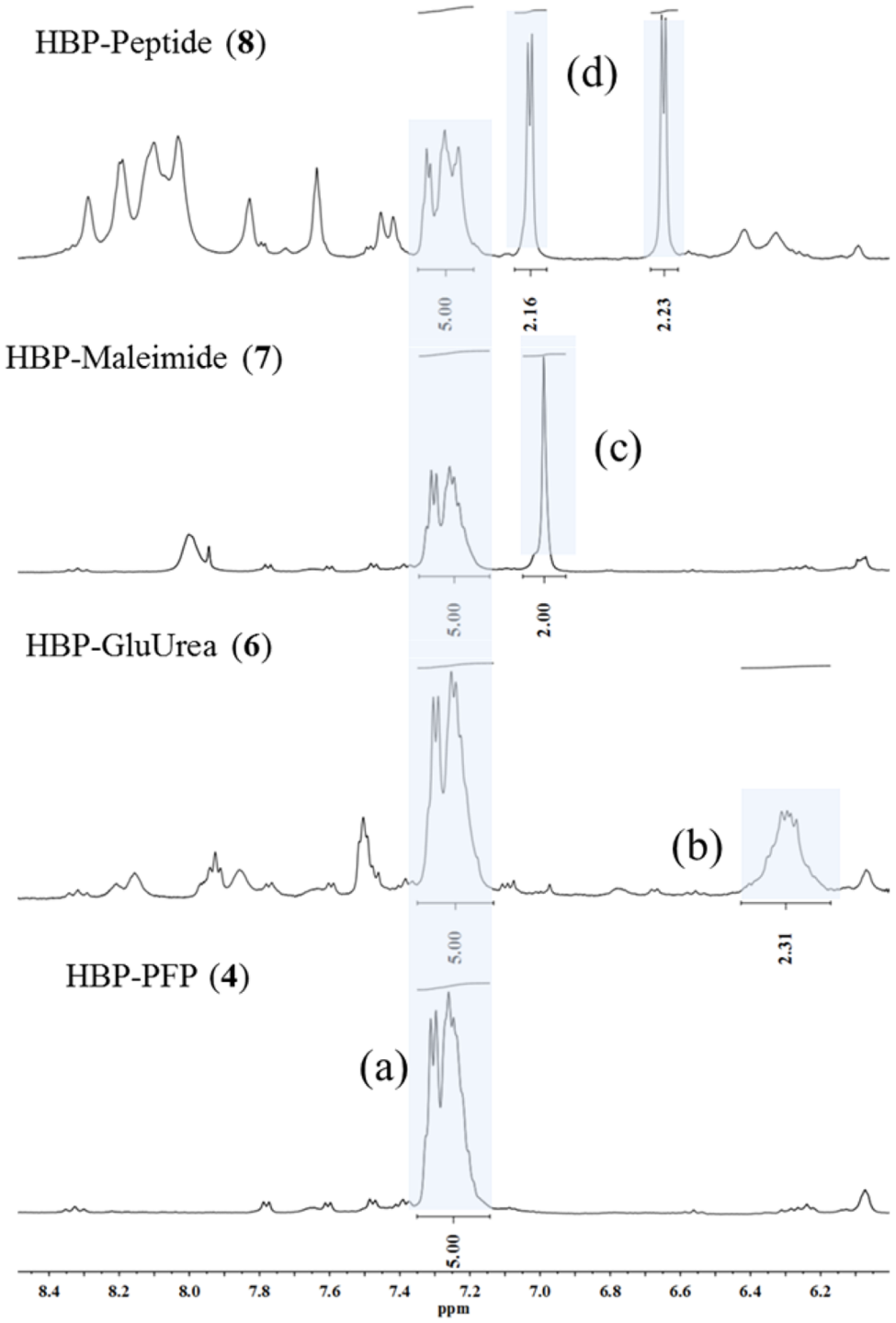

Figure 5. Integrated ^{1}H NMR spectra highlighting (a) the five protons from the phenyl moiety of the CTA-PFP (7.15−7.35 ppm), (b) the two urea protons on the GluUrea, (c) the two vinylic protons on the maleimide, and (d) the four protons from the aromatic side-chain of the tyrosine fragment along the peptide.

nanomedicine, we decided to focus and develop HBP-peptide further because it has been less well-characterized than the antibody, and as a smaller molecule, potentially has decreased effects on the overall biological behavior of the nanomedicines. Thus, the potential of HBP-peptide to target and detect PSMA-expressing prostate tumors was then assessed in vivo. A BALB/c nude mouse bearing subcutaneous PC3-PIP and PC3-FLU on opposite flanks was injected intravenously with HBP-peptide and imaged for Cy5 at various time points (24, 72, and 144 h) post injection (Figure 9A). The DsRed signal from the PC3 tumors clearly defines the two different tumors at the 72 h time point. At the 24 h time point, accumulation in both tumors is observed, as well as in the kidney and heart. The kidney is one potential route of excretion and is often observed for polymers of this size (∼10 nm),[32,33] whereas the additional signal in the upper region of the animal is likely blood in the heart from circulating polymer. This arises due to the enhanced circulation time afforded to the nanomedicine from the PEG. At 72 h, the

DOI: 10.1021/acs.biomac.5b00913
Biomacromolecules 2015, 16, 3235−3247

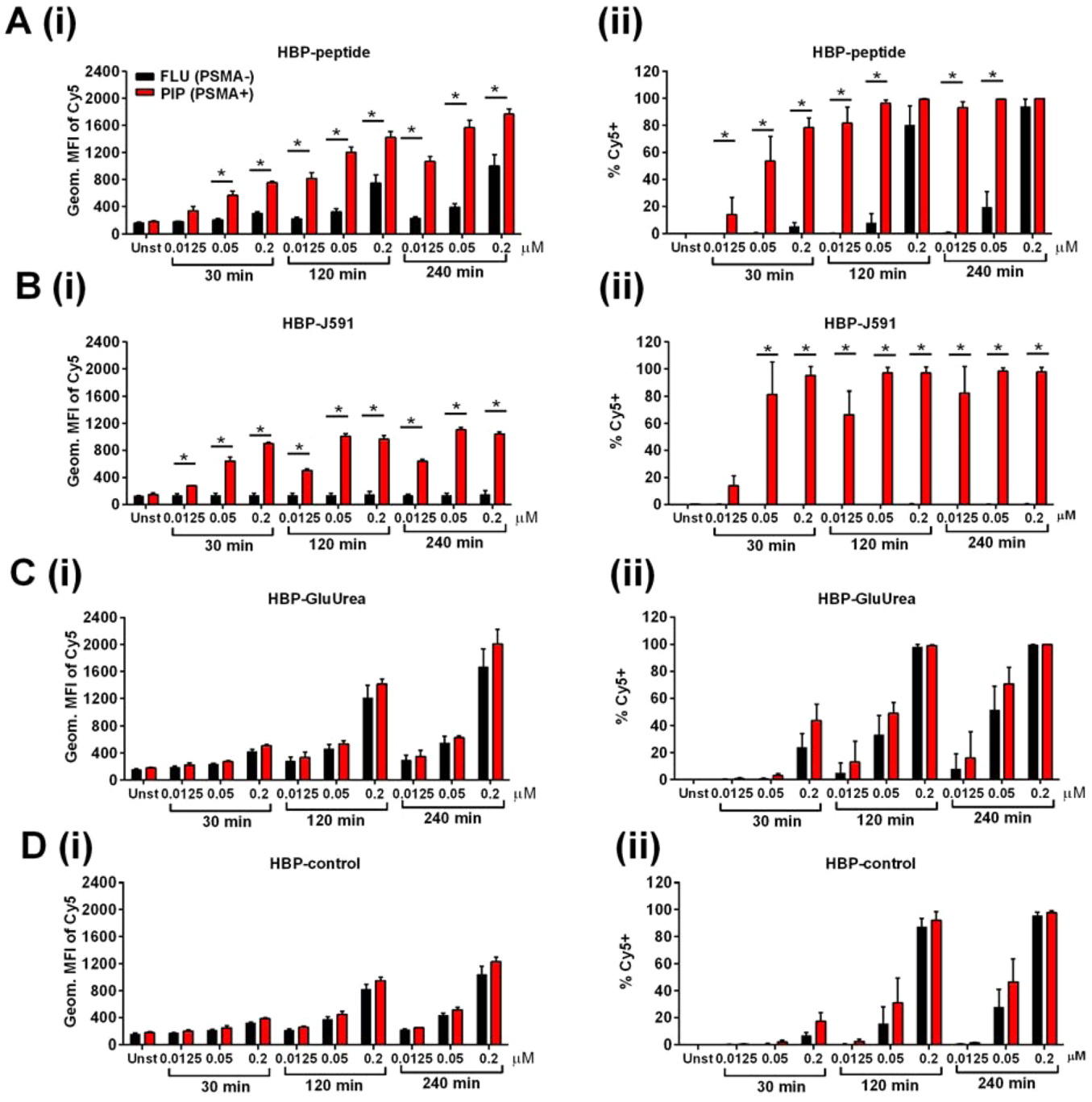

Figure 6. Flow cytometric analysis of PC3-FLU cells (PSMA-deficient; black bars) and PC3-PIP cells (PSMA-proficient; red bars) incubated with hyperbranched polymers; HBP-peptide (A), -J591 (B) -GluUrea (C) or -control (D), at 0.0125, 0.05, or 0.2 μM concentrations for 30, 120, or 240 min. Analysis was performed to assess Cy5 signal in cells given as the geometric mean fluorescence intensity (MFI) of Cy5 of the entire cell population, and the percentage of cells positively stained. Three independent experiments were performed (n = 3).

strong kidney signal is no longer observed (most material cleared form this organ), although significantly enhanced uptake in the PC3-PIP compared to the PC3-FLU is observed. Similarly, at 144 h postinjection, a significant signal is only observed in the PC3-PIP tumor highlighting the enhanced targeting of the nanomedicine to PSMA-expressing cells in the animal.

In order to investigate the relative uptake into PC3-PIP and PC3-FLU cells in the region of greatest accumulation (i.e., up to 48 h postinjection), an additional in vivo fluorescence study was conducted. BALB/c nude mice bearing subcutaneous PC3-PIP and PC3-FLU on opposite flanks were injected intravenously with either HBP-peptide (n = 4) or HBP-control (n = 1), and then imaged for Cy5 at various time points (2, 8, 24, and 48 h) post injection. Uptake of Cy5 by PC3-PIP tumors was apparent 2 h post injection, which increased progressively up to the 48 h time point (Figure S4). In contrast, minimal Cy5 was detected within PC3-FLU tumors at any time point up to 24 h. Moreover, injection of the control polymer (no ligand) showed minimal uptake in either tumor (Figure S5). This data supports our in vitro results and shows that the targeted HBP clearly showed greater accumulation in PSMA-expressing

DOI: 10.1021/acs.biomac.5b00913
Biomacromolecules 2015, 16, 3235−3247

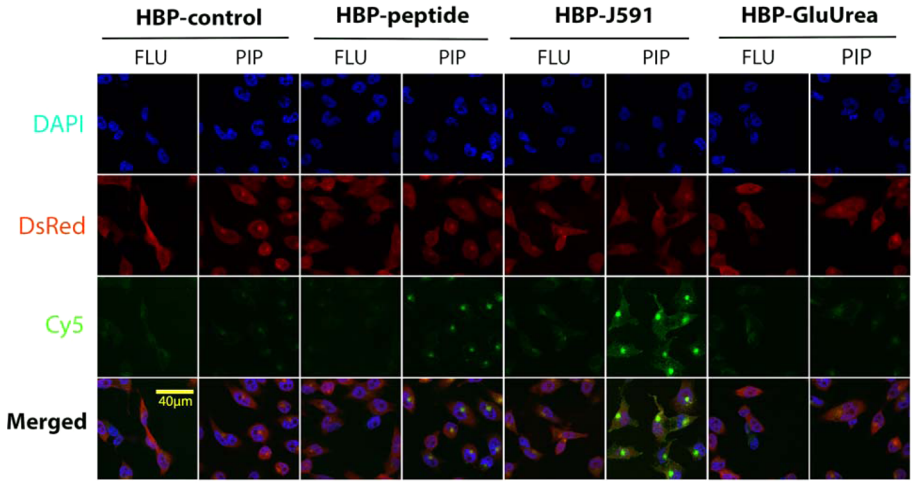

Figure 7. PSMA-mediated endocytosis of HBP-peptide and -J591 was confirmed by confocal microscopy. PC3-FLU and PC3-PIP cells were incubated with HBP-control, -peptide, -J591, or -GluUrea at 0.2 μM for 120 min. Confocal microscopy was performed to assess Cy5 signal in cells; DAPI (nuclear), DsRed (cytosolic), and Cy5 staining is shown.

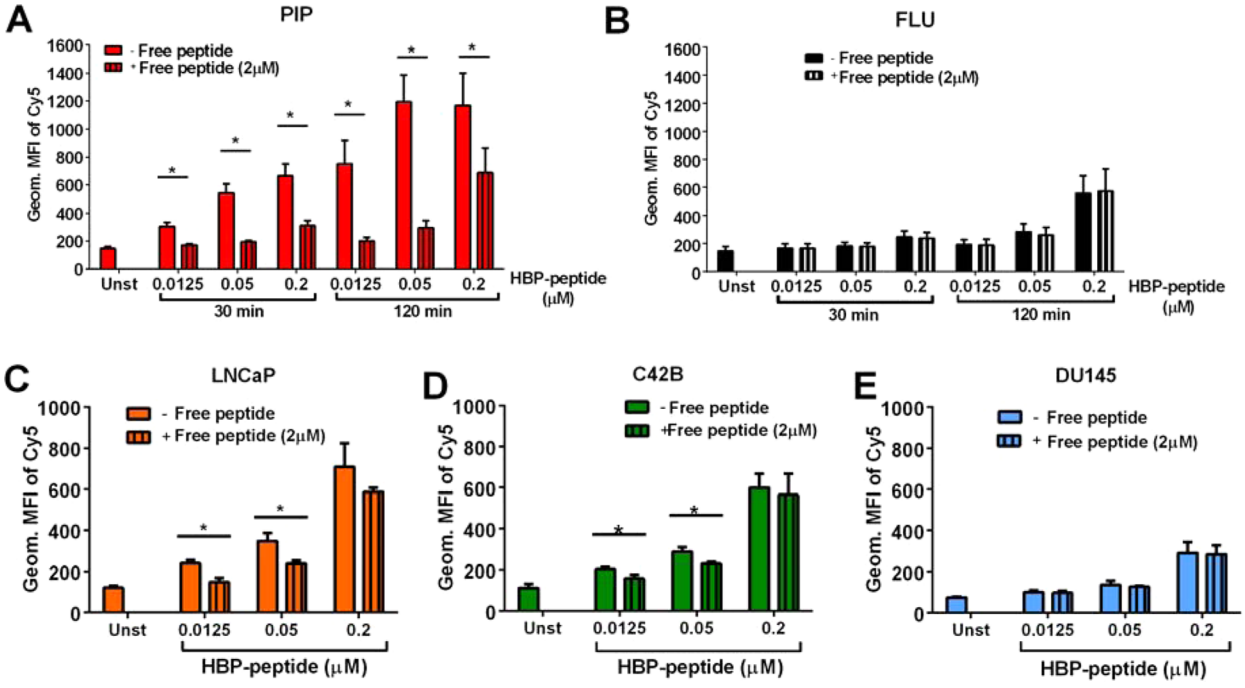

Figure 8. Competitive binding and internalization assays confirmed that endocytosis of HBP-peptide is PSMA-mediated. Geometric MFI of Cy5 is shown. PC3-PIP (A) and PC3-FLU cells (B) were incubated with HBP-peptide at 0.0125, 0.05, or 0.2 μM concentrations with or without free peptide (2 μM) for 30 or 120 min. Three independent experiments were performed. LNCaP (C) and C42B (D) (both PSMA-proficient) and DU145 cells (E) (PSMA-deficient) were incubated with HBP-peptide at 0.0125, 0.05, or 0.2 μM with or without free peptide (2 μM) for 120 min. Four independent experiments were performed (n = 4).

tumors at a very early stage following injection of the HPB-peptide.

In order to assess the anatomical distribution of HBP-peptide 48 h post injection, ex vivo imaging of the tumors and various organs was performed. Significantly greater accumulation of Cy5 in PC3-PIP tumors over PC3-FLU tumors was confirmed ex vivo (Figure 9B). A low but detectable accumulation of Cy5 within PC3-FLU tumors was observed, possibly through the enhanced permeability and retention (EPR) effect of tumors. HBP-peptide uptake by kidney, spleen, and liver was apparent, but relatively low, and indicates that these polymers do not exhibit extensive uptake by organs of the reticuloendothelial system (RES), as has been previously demonstrated for pegylated materials. Thus, HBP-peptide is endocytosed into prostate cancer cells via PSMA to a relatively high extent highlighting the potential of this targeted nanomedicine for future therapeutic and imaging applications.

CONCLUSION

In conclusion, targeting nanomedicines to PSMA holds promise for improving the clinical management of PCa. The ability to direct therapeutic payloads to locoregional lymph node metastases and bone metastases would have major implications in PCa treatment, whereas simultaneous imaging

DOI: 10.1021/acs.biomac.5b00913
Biomacromolecules 2015, 16, 3235−3247

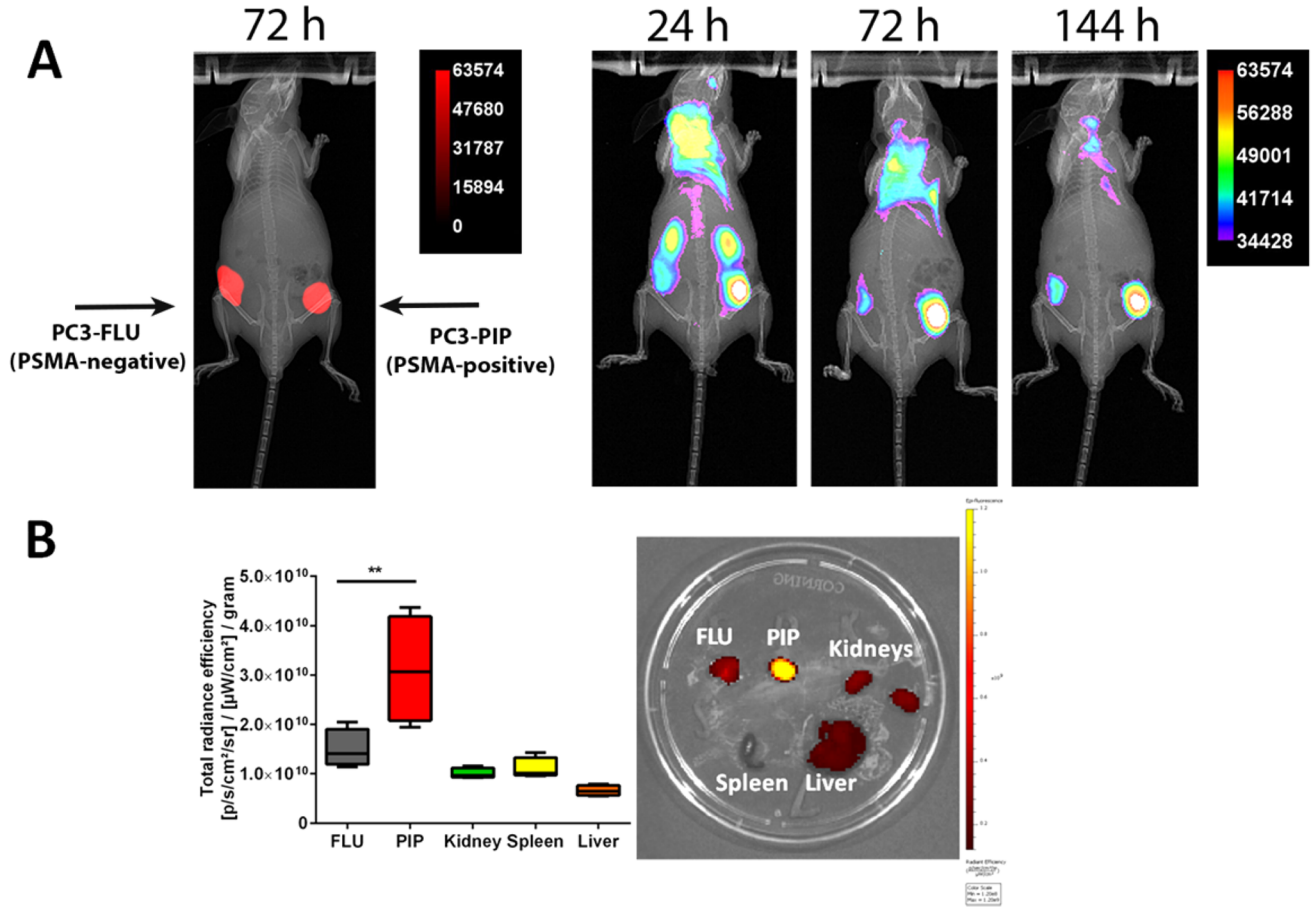

Figure 9. (A) Representative BALB/c nude mouse bearing subcutaneous PC3-FLU (left flank) and PC3-PIP (right flank) tumors injected intravenously with HBP-peptide and Cy5 localization imaged using the In-Vivo Xtreme at 1, 3, and 6 days post injection. (B) Box and whiskers plot (mean; min to max) of average radiance efficiency (Cy5) of various tissues/organs following excision 48 h postinjection with HBP-peptide (n = 4) with an accompanying representative fluorescence image.

would also assist in management decisions for patients on active surveillance or with a rise in prostate specific antigen levels, suggestive of disease recurrence. Importantly, nanomedicines offer the opportunity not only to deliver therapeutics to a particular site but also to monitor their release and subsequent response. In this project, we provide solid proof-of-concept data that hyperbranched polymers conjugated with PSMA ligands, in particular the peptide, have potential both as imaging agents and for targeted drug delivery, with the ability to monitor the response in real time for patients with PCa.

■ ASSOCIATED CONTENT

Supporting Information

The Supporting Information is available free of charge on the ACS Publications website at DOI: 10.1021/acs.biomac.5b00913.

NMR spectra of HBPs, flow cytometric analyses, and in vivo fluorescence images (PDF)

■ AUTHOR INFORMATION

Corresponding Authors

*E-mail: pamela.russell@qut.edu.au.
*E-mail: k.thurecht@uq.edu.au.

Author Contributions

●These authors contributed equally (A.V.F. and B.W.C.T.).

Notes

The authors declare no competing financial interest.

■ ACKNOWLEDGMENTS

We acknowledge funding from the National Health and Medical Research Council (APP1046831, (to P.J.R., K.J.T., A.K.W.)) and the Australian Research Council (FT110100284 (to K.J.T.), DP140100951 (to K.J.T.), DP110104299 (to A.K.W.)). This work was performed in part at the Queensland node of the Australian National Fabrication Facility (ANFF), a company established under the National Collaborative Research Infrastructure Strategy to provide nano- and microfabrication facilities for Australia's researchers. This research was conducted and funded by the ARC Centre of Excellence in Convergent Bio-Nano Science and Technology (CE140100036). P.J.R. is supported by the Australian Government Department of Health. We would like to thank Prof. Colleen C. Nelson from APCRC-Q for her support.

■ REFERENCES

(1) Jemal, A.; Bray, F.; Center, M. M.; Ferlay, J.; Ward, E.; Forman, D. *Ca-Cancer J. Clin.* **2011**, *61*, 69−90.
(2) Afshar-Oromieh, A.; Avtzi, E.; Giesel, F. L.; Holland-Letz, T.; Linhart, H. G.; Eder, M.; Eisenhut, M.; Boxler, S.; Hadaschik, B. A.; Kratochwil, C.; Weichert, W.; Kopka, K.; Debus, J.; Haberkorn, U. *Eur. J. Nucl. Med. Mol. Imaging* **2015**, *42*, 197−209.

DOI: 10.1021/acs.biomac.5b00913
Biomacromolecules 2015, 16, 3235−3247

(3) Afshar-Oromieh, A.; Haberkorn, U.; Schlemmer, H. P.; Fenchel, M.; Eder, M.; Eisenhut, M.; Hadaschik, B. A.; Kopp-Schneider, A.; Rothke, M. *Eur. J. Nucl. Med. Mol. Imaging* **2014**, *41*, 887−897.
(4) Eiber, M.; Maurer, T.; Souvatzoglou, M.; Beer, A. J.; Ruffani, A.; Haller, B.; Graner, F. P.; Kubler, H.; Haberhorn, U.; Eisenhut, M.; Wester, H. J.; Gschwend, J. E.; Schwaiger, M. *J. Nucl. Med.* **2015**, *56*, 668−674.
(5) Israeli, R. S.; Powell, C. T.; Fair, W. R.; Heston, W. D. *Cancer Res.* **1993**, *53*, 227−230.
(6) Chang, S. S.; O'Keefe, D. S.; Bacich, D. J.; Reuter, V. E.; Heston, W. D. W. *Clin. Cancer Res.* **1999**, *5*, 2674.
(7) Silver, D. A.; Pellicer, I.; Fair, W. R.; Heston, W. D.; Cordon-Cardo, C. *Clin. Cancer Res.* **1997**, *3*, 81−85.
(8) Wright, G. L., Jr.; Grob, B. M.; Haley, C.; Grossman, K.; Newhall, K.; Petrylak, D.; Troyer, J.; Konchuba, A.; Schellhammer, P. F.; Moriarty, R. *Urology* **1996**, *48*, 326−334.
(9) Ghosh, A.; Heston, W. D. *J. Cell. Biochem.* **2004**, *91*, 528−539.
(10) Wright, G. L., Jr.; Haley, C.; Beckett, M. L.; Schellhammer, P. F. *Urol. Oncol.* **1995**, *1*, 18−28.
(11) Rajasekaran, S. A.; Anilkumar, G.; Oshima, E.; Bowie, J. U.; Liu, H.; Heston, W.; Bander, N. H.; Rajasekaran, A. K. *Mol. Biol. Cell* **2003**, *14*, 4835−4845.
(12) Banerjee, S. R.; Pullambhatla, M.; Foss, C. A.; Nimmagadda, S.; Ferdani, R.; Anderson, C. J.; Mease, R. C.; Pomper, M. G. *J. Med. Chem.* **2014**, *57*, 2657−2669.
(13) Bander, N. H.; Carr, F. J.; Hamilton, A. *Modified mouse monoclonal antibodies specific to prostate-specific membrane antigen for diagnosis and treatment of prostatic disease or cancer*. Patent No. US20040120958A1, 2004.
(14) Murphy, G. P.; Boynton, A. L.; Holmes, E. H.; Tino, W. T. *Monoclonal antibodies specific for the extracellular domain of prostate-specific membrane antigen*. Patent No. US6150508A, 2000.
(15) Wu, X.; Ding, B.; Gao, J.; Wang, H.; Fan, W.; Wang, X.; Zhang, W.; Wang, X.; Ye, L.; Zhang, M.; et al. *Int. J. Nanomed.* **2011**, *6*, 1747−1756.
(16) Lupold, S. E.; Hicke, B. J.; Lin, Y.; Coffey, D. S. *Cancer Res.* **2002**, *62*, 4029−4033.
(17) Shen, D.; Xie, F.; Edwards, W. B. *PLoS One* **2013**, *8*, e68339.
(18) Huang, S. S.; Wang, X.; Zhang, Y.; Doke, A.; DiFilippo, F. P.; Heston, W. D. *Prostate* **2014**, *74*, 702−713.
(19) Heston, W. D. W.; Cramer, H. *Compounds which bind prostate-specific membrane antigen (PSMA), and therapeutic and diagnostic uses thereof*. Patent No. 2006-US7141, 2006.
(20) Humblet, V.; Misra, P.; Bhushan, K. R.; Nasr, K.; Ko, Y. S.; Tsukamoto, T.; Pannier, N.; Frangioni, J. V.; Maison, W. *J. Med. Chem.* **2009**, *52*, 544−550.
(21) Chen, Z.; Penet, M. F.; Nimmagadda, S.; Li, C.; Banerjee, S. R.; Winnard, P. T., Jr.; Artemov, D.; Glunde, K.; Pomper, M. G.; Bhujwalla, Z. M. *ACS Nano* **2012**, *6*, 7752−7762.
(22) Pearce, A. K.; Rolfe, B. E.; Russell, P. J.; Tse, B. W. C.; Whittaker, A. K.; Fuchs, A. V.; Thurecht, K. J. *Polym. Chem.* **2014**, *5*, 6932−6942.
(23) Kozikowski, A. P.; Nan, F.; Conti, P.; Zhang, J.; Ramadan, E.; Bzdega, T.; Wroblewska, B.; Neale, J. H.; Pshenichkin, S.; Wroblewski, J. T. *J. Med. Chem.* **2001**, *44*, 298−301.
(24) Wang, X.; Huang, S. S.; Heston, W. D. W.; Guo, H.; Wang, B.-C.; Basilion, J. P. *Mol. Cancer Ther.* **2014**, *13*, 2595−2606.
(25) Mesters, J. R.; Barinka, C.; Li, W.; Tsukamoto, T.; Majer, P.; Slusher, B. S.; Konvalinka, J.; Hilgenfeld, R. *EMBO J.* **2006**, *25*, 1375−1384.
(26) Hrkach, J.; Von Hoff, D.; Ali, M. M.; Andrianova, E.; Auer, J.; Campbell, T.; De Witt, D.; Figa, M.; Figueiredo, M.; Horhota, A.; et al. *Sci. Transl. Med.* **2012**, *4*, 128ra139.
(27) Horoszewicz, J. S.; Kawinski, E.; Murphy, G. P. *Anticancer Res.* **1987**, *7*, 927−935.
(28) Chang, S. S.; Heston, W. D. W. *Urol. Oncol. Semin. Ori.* **2002**, *7*, 7−12.
(29) Liu, H.; Moy, P.; Kim, S.; Xia, Y.; Rajasekaran, A.; Navarro, V.; Knudsen, B.; Bander, N. H. *Cancer Res.* **1997**, *57*, 3629−3634.
(30) Liu, H.; Rajasekaran, A. K.; Moy, P.; Xia, Y.; Kim, S.; Navarro, V.; Rahmati, R.; Bander, N. H. *Cancer Res.* **1998**, *58*, 4055−4060.
(31) Fuchs, A. V.; Gemmell, A. C.; Thurecht, K. J. *Polym. Chem.* **2015**, *6*, 868−880.
(32) Boase, N. R. B.; Blakey, I.; Rolfe, B. E.; Mardon, K.; Thurecht, K. J. *Polym. Chem.* **2014**, *5*, 4450−4458.
(33) Coles, D. J.; Rolfe, B. E.; Boase, N. R. B.; Veedu, R. N.; Thurecht, K. J. *Chem. Commun.* **2013**, *49*, 3836−3838.
(34) Rolfe, B. E.; Blakey, I.; Squires, O.; Peng, H.; Boase, N. R. B.; Alexander, C.; Parsons, P. G.; Boyle, G. M.; Whittaker, A. K.; Thurecht, K. J. *J. Am. Chem. Soc.* **2014**, *136*, 2413−2419.
(35) Thurecht, K. J.; Blakey, I.; Peng, H.; Squires, O.; Hsu, S.; Alexander, C.; Whittaker, A. K. *J. Am. Chem. Soc.* **2010**, *132*, 5336−5337.
(36) Huang, Y.; Wang, D.; Zhu, X.; Yan, D.; Chen, R. *Polym. Chem.* **2015**, *6*, 2794−2812.
(37) Moad, G.; Chong, Y. K.; Postma, A.; Rizzardo, E.; Thang, S. H. *Polymer* **2005**, *46*, 8458−8468.
(38) Roth, P. J.; Wiss, K. T.; Zentel, R.; Theato, P. *Macromolecules* **2008**, *41*, 8513−8519.
(39) Scarano, W.; Duong, H. T. T.; Lu, H.; De Souza, P. L.; Stenzel, M. H. *Biomacromolecules* **2013**, *14*, 962−975.
(40) Murelli, R. P.; Zhang, A. X.; Michel, J.; Jorgensen, W. L.; Spiegel, D. A. *J. Am. Chem. Soc.* **2009**, *131*, 17090−17092.
(41) Ardana, A.; Whittaker, A. K.; Thurecht, K. J. *Macromolecules* **2014**, *47*, 5211−5219.
(42) Bander, N. H.; Milowsky, M. I.; Nanus, D. M.; Kostakoglu, L.; Vallabhajosula, S.; Goldsmith, S. J. *J. Clin. Oncol.* **2005**, *23*, 4591−4601.
(43) Tse, B. W.; Cowin, G. J.; Soekmadji, C.; Jovanovic, L.; Vasireddy, R. S.; Ling, M. T.; Khatri, A.; Liu, T.; Thierry, B.; Russell, P. J. *Nanomedicine* **2015**, *10*, 375−386.

DOI: 10.1021/acs.biomac.5b00913
Biomacromolecules 2015, 16, 3235−3247

Polymer Chemistry

PAPER

View Article Online
View Journal

Cite this: DOI: 10.1039/c4py00999a

Development of a polymer theranostic for prostate cancer†

Amanda K. Pearce,[a,b] Barbara E. Rolfe,[a] Pamela J. Russell,[c] Brian W.-C. Tse,[c] Andrew K. Whittaker,[a,b,d] Adrian V. Fuchs[a,b] and Kristofer J. Thurecht*[a,b,d]

Received 22nd July 2014,
Accepted 21st August 2014

DOI: 10.1039/c4py00999a

www.rsc.org/polymers

Theranostics offers an improved treatment strategy for prostate cancer by facilitating simultaneous targeting of tumour cells with subsequent drug delivery and imaging. In this report we describe the synthesis of hyperbranched polymers that are biocompatible, can specifically target and be internalised by prostate cancer cells (through targeting of prostate-specific membrane antigen – PSMA) and ultimately facilitate controlled delivery of a model drug. The theranostic also incorporates a far-red fluorescent dye that allows tracking of the polymer *via* optical imaging. Controlled synthesis of the polymer is achieved *via* reversible addition fragmentation chain transfer polymerisation of polyethylene glycol monomethyl methacrylate, with ethylene glycol dimethacrylate as the branching agent. Incorporation of 20 mol% of an hydrazide-methacrylate monomer allows post-ligation of a model drug, fluorene-2-carboxaldehyde, through a hydrolytically-degradable hydrazone linkage. The rate of degradation of this particular linker was enhanced at endosomal pH (pH = 5.5) where ~95% of the model drug was released in 4 hours compared to less than 5% released over the same period at physiological pH. The theranostic showed high uptake into prostate cancer cells expressing prostate-specific membrane antigen, while minimal uptake was observed in PC3 cells negative for PSMA, highlighting the enhanced efficacy of the targeting ligand.

Introduction

The concept of theranostics – combining therapeutics and diagnostics – has gained great interest in recent years particularly in the area of cancer research. While the field is still in its infancy, significant research effort is focussed on developing theranostic devices capable of not only detecting and pinpointing disease at precise locations within the body, but also having the ability to deliver a therapeutic agent to the tumour tissue directly. The key to improving the prognosis of cancer sufferers lies in early detection. Specifically in the case of prostate cancer, early-stage disease sufferers have a 5-year prognosis of nearly 100% survival. However, patients with advanced, late-stage disease have a significantly reduced survival rate, dropping as low as 30% as metastases spread through the blood stream to organs such as bone and lymph nodes.[1–6] Theranostic approaches reported in the literature all share the same basic design: a targeting moiety, an imaging modality, a therapeutic payload and a mechanism to safely release the payload at a specific location.[7] The challenge in designing these complex systems lies in the introduction of multiple functionalities into a single particle, requiring complementary and facile synthetic methods.

It is well known that active targeting, such as through the use of an antibody, peptide or small molecule ligand, can significantly enhance the uptake of a polymeric device at the desired location.[8–11] Prostate Specific Membrane Antigen (PSMA) has been identified as a promising target for prostate cancer.[12–14] It is a highly prostate-restricted type II transmembrane glycoprotein, and multiple studies report that normal prostate tissue primarily expresses a splice variant that doesn't contain the transmembrane domain (PSM). Furthermore, PSMA expression is greatest (more than 10-fold higher than in normal prostate tissues) in high grade tumours and metastatic lesions in the lymph nodes and bones.[12,15–18] Most importantly, several studies have found that PSMA is not present on normal vasculature.[15,19,20] Based on this, PSMA has been suggested as a viable target for next-generation prostate cancer therapy.[21,22] Several small molecules have shown high affinity for PSMA, including 2-phosphonomethyl pentanedioic acid[23]

[a]Australian Institute for Bioengineering and Nanotechnology, The University of Queensland, St Lucia, QLD 4072, Australia. E-mail: k.thurecht@uq.edu.au; Fax: +61 7 3346 3973; Tel: +61 7 3346 3864
[b]Centre for Advanced Imaging, The University of Queensland, St Lucia, QLD 4072, Australia
[c]Australian Prostate Cancer Research Centre-Queensland, Institute of Health and Biomedical Innovation, Queensland University of Technology at, Translational Research Institute (TRI), 37 Kent St, Woolloongabba, Brisbane, QLD 4102, Australia
[d]ARC Centre of Excellence in Convergent Bio-Nano Science and Technology, The University of QLD, St Lucia, QLD, 4072, Australia
† Electronic supplementary information (ESI) available: Additional NMR characterisation, confocal microscopy and optical images. See DOI: 10.1039/c4py00999a

and the glutamate ureas.[24] Indeed, Murelli *et al.*[25] recently demonstrated the use of a small molecule containing glutamate urea as a targeting ligand for prostate cancer.[26–29] They also showed that varying the C2 position on the PSMA ligand had no significant effect on its targeting specificity, and thus could be used as a site for possible attachment to a carrier system. It has additionally been demonstrated for the small molecule ligands that the carbonyl of the urea linkage directly coordinates with the Zn^{2+} on the PSMA protein, while the three carboxylic acid moieties interact with amino acids at the active site of PSMA leaving the fourth acid group unbound and free for further modification.[30,31]

Another important aspect of a theranostic system is the ability to deliver a specific therapeutic in a controlled manner. The challenge lies in designing a system that allows controlled release of drug at the desired location, with minimal off-target release that may compromise healthy tissue. Tethering therapeutics to a theranostic fulfils this design requirement, while simultaneously solving another problem facing current treatments, namely that many chemotherapy drugs are poorly water-soluble, thus limiting their ability to reach and be internalised by target cells.[32] In addition, a significant advantage to covalently linking toxic therapeutics to a carrier system over conventional encapsulation approaches, is the ability to have better control over loading and release with higher stability and drug loading.[33,34] One *in vivo* stimulus that can trigger responsive release of drugs is the acidity of endosomal compartments in cells, and this can be exploited using a hydrazone linkage. Hydrazones respond to an acidic environment, but are superior over ester linkages in that they do not lead to localised acidosis upon degradation.[35–38] Thus, a theranostic device that enters a tumour cell *via* receptor mediated endocytosis can undergo rapid degradation of acid-sensitive linkages within the low pH (5.5) environment of the endosomal compartment, with consequent site-specific release of the therapeutic agent.[37–40]

Imaging plays an important role in the diagnosis of disease states in the clinic, and thus the final important aspect of a theranostic device is the inclusion of one or more imaging agents. Imaging methodologies can range from optical imaging with fluorescent dyes, to clinically-relevant methods such as Magnetic Resonance Imaging (MRI) and Positron Emission Tomography (PET).[27,28,41,42] While optical imaging is generally not directly applicable for use in the clinic, it is a useful technique for preliminary imaging studies *in vitro* and *in vivo* in small animal models. The incorporation of an optical imaging probe into a theranostic system allows facile characterisation of the behaviour of these nanoparticles, the specificity and efficiency of a targeting ligand, as well as the biodistribution of the resulting material.[43]

Of central importance to the development of theranostics is the design of a suitable carrier. Hyperbranched polymers offer a viable carrier platform for the development of a theranostic system for prostate cancer.[44,45] Similar to dendrimers, hyperbranched polymers have a highly branched architecture, but can be synthesised by facile controlled free radical polymerization methods and have simple purification steps. They have a highly branched structure with low polydispersity, which provides multiple 'arms' for functionalizing with diagnostic and therapeutic agents. Furthermore, through the use of macro-RAFT agents, hyperbranched polymers can be tailored to include a high degree of end-group functionality[46] that ultimately can be utilised for various biomedical applications including imaging[43] and drug delivery.[47–50]

Here we describe the development of a hyperbranched polymer carrier synthesised *via* reversible addition fragmentation chain transfer (RAFT) polymerisation. A new RAFT agent is synthesised in which the targeting ligand for PSMA is directly attached to the leaving group of the RAFT agent. Subsequent polymerisation results in half of the hyperbranched polymer end-groups expressing a targeting ligand directed towards prostate cancer cells. In addition, separate monomers containing an optical imaging dye and hydrazide functionality were incorporated directly into the polymerisation, producing a multimodal theranostic device designed to target PSMA+ cells, and with the capability of drug delivery through cleavage of the hydrazone linker at endosomal pH (Scheme 1).

Experimental

Materials

Unless otherwise stated, all reagents and solvents were purchased from Sigma Aldrich at the highest available purity and used as received. All monomers were passed through a short plug of basic alumina, immediately prior to use, to remove free radical inhibitors. Tetrahydrofuran and dimethylformamide were purified by a MB-SPS800 solvent purification system prior to use. Distilled water with a resistivity of 18.2 MΩ cm was obtained from an Elga ultra-pure water system.

Characterisation methods

All NMR experiments were undertaken on a Bruker Avance 500 high-resolution NMR spectrometer. ^{1}H NMR spectra were collected for 128 scans.

SEC-MALLS chromatographic system consisted of a 1515 isocratic pump (Waters), a 717 auto sampler (Waters), Styragel HT 6E and Styragel HT 3 columns (Waters), 2414 differential refractive index detector (Waters) and a Dawn Heleos laser light scattering detector (Wyatt). THF was used as the mobile phase with a flow rate of 1 mL min^{-1}. In order to minimise absorption or scatter from cy5-labelled polymers in the light scattering detector, the polymer was irradiated overnight at the excitation wavelength of the dye (640 nm) using a Horiba Fluoromax-4 instrument during which time the dye was fully quenched.

In vitro incorporation of Cy5-labelled polymers was analysed on an Accuri C6 Flow Cytometer (BD Bioscience, San Jose, CA) using the 640 nm laser collecting through the 675/25 filter.

In vitro microscopy images were acquired on a Carl Zeiss LSM 710 confocal laser scanning microscope.

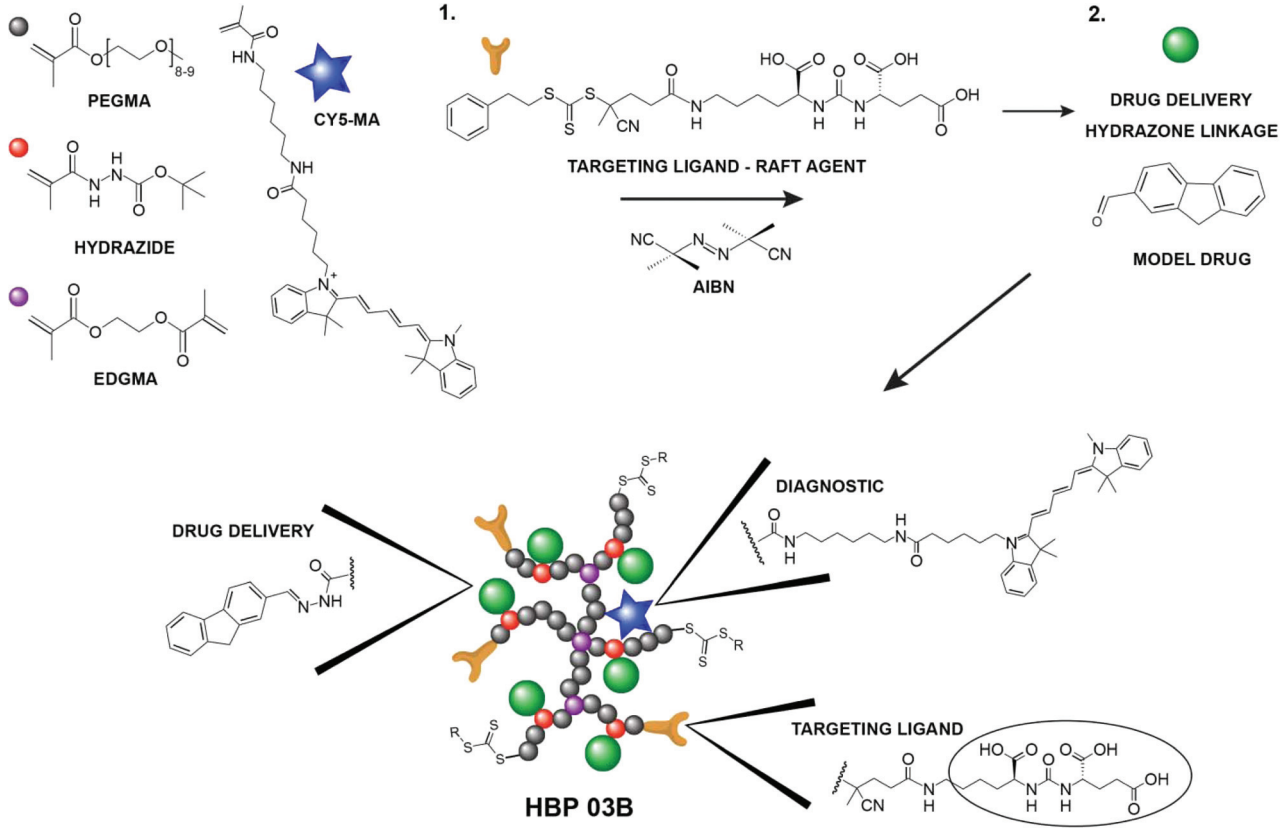

Scheme 1 The overall schematic of the hyperbranched polymer theranostic, highlighting the drug delivery, diagnostic and targeting elements in the final product. The polymers were first synthesised by controlled polymerisation using a RAFT agent that is designed to incorporate the targeting ligand (Step 1), followed by loading of the model drug (Step 2).

In vivo optical imaging experiments were performed on an In Vivo MS FX Pro instrument (now supplied by Bruker Corporation). Cy5 images were collected with a 640 ± 10 nm excitation and 700 nm ± 17.5 nm emission filter set (f-stop 2.80, 2 × 2 binning, 120 mm FOV, 10 s exposure time). DsRed fluorescence images were collected with a 550 ± 10 nm excitation and 600 nm ± 17.5 nm emission filter set (f-stop 2.80, 2 × 2 binning, 120 mm FOV, 20 s exposure time). To provide anatomical context, fluorescence images were co-registered with an X-ray image (f-stop 2.80, 0.2 mm aluminium filter, 120 mm FOV, 30 s acquisition time). All images were batch exported as 16 bit TIFF images and image processing was completed using Image-J (National Institutes of Health). Fluorescence images were false coloured and overlaid onto X-ray images.

Synthesis of polymeric theranostic

Synthesis of protected PSMA small molecule ligand. The PSMA ligand with protecting groups on the carboxylic acid groups was synthesised in two steps based on the method described by Murelli *et al.*:[25]

Synthesis of (9S,13S)-tri-tert-butyl 3,11-dioxo-1-phenyl-2-oxa-4,10,12-triazapentadecane-9,13,15-tricarboxylate – Step 1. Glu–O*t*Bu (O*t*Bu) HCl (5.59 g, 18.9 mmol) and triethylamine (TEA) (8.64 mL, 61.9 mmol) were stirred in dry DCM (120 mL) at −78 °C (dry ice/acetone) for 30 minutes. Triphosgene (1.86 g, 6.27 mmol) in DCM (40 mL) was added dropwise *via* a dry degassed syringe. The reaction was warmed to room temperature, purged with nitrogen and stirred for 30 minutes in an inert atmosphere. H–Lys(Z)–O*t*-Bu HCl (4.24 mg, 11.4 mmol) was added, followed by TEA (1.59 mL, 11.4 mmol). The reaction was allowed to stir overnight in an inert atmosphere at room temperature.

The reaction was diluted with dichloromethane (150 mL), and washed with water (2 × 250 mL), dried over anhydrous $MgSO_4$ and evaporated under reduced pressure leaving a colourless oil. The oil was purified by column chromatography (silica gel, hexane–ethyl acetate 60 : 40) to yield a colourless oil (5.9 g, 83% yield) (S1). ^{1}H NMR (500 MHz, DMSO-d6): 7.25–7.40 (m, Ph), 7.20 (t, OOCN*H*CH_2), 6.20–6.30 (dd, N*H*CON*H*), 4.99 (s, PhCH_2OOC), 3.85–4.10 (m, CH_2CHNH), 2.90–3.00 (m, NHCH_2CH_2), 2.10–2.30 (m, CH_2CH_2COO), 1.90–1.80 (m, $CH_2CH_2CH_2$), 1.58–1.70 (m, $CH_2CH_2CH_2$), 1.45–1.57 (m, $CH_2CH_2CH_2$), 1.44 (s, *t*Bu), 1.20–1.30 (m, $CH_2CH_2CH_2$). ESI-MS: calculated 621.36, actual 621.66.

Synthesis of (S)-di-tert-butyl 2-(3-((S)-6-amino-1-tert-butoxy-1-oxohexan-2-yl)ureido)pentanedioate – Step 2. S1 (5.0 g, 8.04 mmol) was dissolved in methanol (20 mL) and added dropwise into a vigorously stirred flask containing 10% Pd/C (0.2 g) which was flushed with hydrogen several times and the reaction stirred

overnight under a balloon of hydrogen at room temperature. After 20 hours no starting material was detected by TLC (10% MeOH/DCM). The reaction solution was filtered through a plug of celite and the solvent evaporated. The resulting oil was analysed by ^{1}H NMR to show complete removal of the benzyl protecting group. The product was used without purification (5.5 g, 93% yield) (S2). ^{1}H NMR (500 MHz, DMSO-d6): 6.20–6.40 ppm (m, N*H*), 3.85–4.10 (m, CH_2CHNH), 2.10–2.30 (m, $NHCH_2CH_2$), 1.80–1.90 (m, CH_2CH_2COO), 1.60 (m, $CH_2CH_2CH_2$), 1.50 (m, $CH_2CH_2CH_2$), 1.48 (m, $CH_2CH_2CH_2$), 1.44 (s, *t*Bu), 1.20–1.30 (m, $CH_2CH_2CH_2$). ESI-MS: calculated 487.33, actual 487.58.

Synthesis of PSMA ligand RAFT agent. (*S*)-4-Cyano-4-(((phenethylthio)carbonothioyl)thio)pentanoic acid (CPEPA) (2.72 g, 8.00 mmol) was dissolved in 20 mL DCM with pentafluorophenol (1.55 g, 8.42 mmol), stirring for 30 minutes at 0 °C. 1-Ethyl-3-(3-dimethylaminopropyl)carbodiimide (EDC, 1.44 g, 9.26 mmol) and dimethylaminopyridine (DMAP, 205 mg) in 2 mL DCM was added dropwise. The reaction was stirred for 2 hours at 0 °C, and then at room temperature overnight.

The reaction was washed with acidic water (20 mL), distilled water (20 mL) and brine (20 mL). The organic phase was dried with anhydrous $MgSO_4$ and the solvent removed by rotary evaporator to yield a yellow liquid. The product was purified by column chromatography using ethyl acetate as eluent, with the product eluting as the first fraction (S3).

PSMA ligand (S2) (965 mg, 1.98 mmol) was dissolved in 10 mL DMF. TEA (216 mg, 1.98 mmol) was slowly added, and the reaction stirred for 10 minutes. Then CPEPA-PFP (1 g, 1.98 mmol) was dissolved in 2 mL DMF and added dropwise to the PSMA ligand solution and stirred at room temperature overnight.

The product was purified by column chromatography (hexane–ethyl acetate 60 : 40) with the product eluting as the first fraction (1.15 g, 72% yield). ^{1}H NMR (500 MHz, DMSO-d6): 7.9 ppm (t, CON*H*), 7.2–7.4 ppm (m, Ph), 6.20–6.40 ppm (m, N*H*), 3.85–4.10 (m, CH_2CHNH), 3.7 ppm (CHC*H*S), 3.0 ppm (m, PhC*H*), 2.9 ppm (m, NHC*H*), 2.10–2.40 (m, $SCCH_2CH_2$), 1.80–1.90 (m, CH_2CH_2COO), 1.60 (m, $CH_2CH_2CH_2$), 1.50 (m, $CH_2CH_2CH_2$), 1.48 (m, $CH_2CH_2CH_2$), 1.44 (s, *t*Bu), 1.20–1.30 (m, $CH_2CH_2CH_2$). ESI-MS: calculated 808.36, actual 808.67.

Synthesis of Cy-5 methacrylamide monomer. Methacrylic acid (1.25 mL, 14.7 mmol), pentafluorophenol (2.85 g, 15 mmol) and DMAP (98.9 mg, 0.8 mmol) were dissolved in DCM (2 mL) on ice. The mixture was stirred for 30 minutes. EDC (2.56 g, 16.2 mmol) in DCM (1 mL) was added dropwise to the reaction, and stirred over ice for a further 2 hours. The reaction was then warmed to room temperature and stirred overnight.

The reaction was washed with 10% HCl (2 × 50 mL), distilled water (2 × 50 mL) and $NaHCO_3$ (2 × 50 mL). The organic phase was collected and dried with anhydrous $MgSO_4$ and concentrated on a rotary evaporator.

Cy5 amine (5 mg, 7.65×10^{-3} mmol) was dissolved in DMF (1 mL) and TEA (0.8 mg, 7.65×10^{-3} mmol) was slowly added. The solution was stirred for 10 minutes. Methacrylic acid-PFP (2.12 mg, 8.41×10^{-3} mmol) in DMF (500 μL) was added dropwise and stirred overnight at room temperature.

The monomer was purified by column chromatography (10% MeOH in DCM), with the monomer eluting as the second fraction (5 mg, 95% yield). ESI-MS: calculated 649.45, actual 649.76.

Synthesis and purification for PSMA-targeted hyperbranched polymers. All monomers were filtered through activated aluminium oxide before use to remove radical inhibitors. Polyethyleneglycol monomethylether methacrylate (PEGMA, avg M_n 475) (463 μL, 1.05 mmol), Boc-protected hydrazide methacrylate (TBMC) (53 mg, 2.63×10^{-1} mmol), ethylene glycol dimethacrylate (EGDMA) (24.8 μl, 1.32×10^{-1} mmol), azobis (isobutyronitrile) (AIBN) (4.3 mg, 2.63×10^{-2} mmol), PSMA ligand RAFT agent (106.4 mg, 1.32×10^{-1} mmol), Cy5 methacrylamide dye (2.5 mg, 8.85×10^{-3} mmol) and 900 μL dry tetrahydrofuran (THF) were placed in a 4 mL vial equipped with a magnetic stirrer bar. The vial was sealed with a silicon septum and reinforced with a cable tie, and the reaction mixture was flushed with argon gas for 30 minutes. The vial was placed in an oil bath and stirred at 72 °C for 24 hours. At the completion of the reaction, the polymer was precipitated dropwise into an excess of *n*-hexane three times to purify. Once the polymer had fully settled on the bottom of the beaker, the solvent was decanted from the top. The polymer was then dissolved in Milli Q water, and dialysed for 48 hours in a 3.5 kDa molecular weight cut-off pleated snakeskin tubing. Following the dialysis, the polymer was freeze dried for 24 hours and was labelled HBP02. ^{1}H NMR (500 MHz, DMSO-d6) δ: 0.5–2.00 ppm (m, CH_2, CH_3), 1.44 pm (s, *t*Bu), 3.25–3.75 ppm (m, CH_2CH_2O), 4.02 ppm (s, $COOCH_2$ PEGMA, $COOCH_2$ EGDMA), 4.18 ppm (m, CH_2CHNH), 6.25 ppm (m, NH), 7.10–7.45 ppm (m, Ph), 7.85 ppm, (s, NHCO).

HBP01 and HBP03 were synthesised as above, with the following modifications. HBP01 was synthesised using CPEPA RAFT agent (16.5 mg, 4.38×10^{-2} mmol) and was used as the untargeted control polymer. HBP03 was synthesised with an increased concentration of PSMA ligand RAFT agent (141.2 mg, 1.74×10^{-1} mmol), EGDMA (33.1 μL, 1.74×10^{-1} mmol) and AIBN (5.8 mg, 3.51×10^{-2} mmol) to provide an increased number of end-groups.

Formation of hydrazone bond with model drug

HBP-02 (100 mg, 3.33×10^{-3} mmol) was dissolved in 10% trifluoroacetic acid (TFA) in DCM (1 mL) and stirred overnight at room temperature. The polymer was precipitated into hexane three times to purify, followed by dialysis first in 10 mM NaCl solution, then pure water for 24 hours to remove any residual TFA. The polymer was dried on a freeze dryer for 24 hours and labelled HBP-02A.

The model drug chosen for this study was fluorene-2-carboxaldehyde. HBP-01A (80 mg, 5.71×10^{-3} mmol) and fluorene-2-carboxaldehyde (29 mg, 1.48×10^{-1} mmol) was dissolved in 10 mL anhydrous MeOH with a drop of glacial acetic acid. The reaction was stirred under reflux at 70 °C overnight. At the

completion of the reaction, the excess unreacted fluorene-2-carboxaldehyde was removed by precipitating the polymer into an excess of *n*-hexane three times. The solvent was decanted off and the polymer dried in a vacuum oven at 35 °C for 24 hours. The incorporation of fluorene-2-carboxaldehyde was characterised by NMR and UV-Vis spectroscopy. The resultant polymer was labelled HBP-02B.

In vitro analysis of targeting efficiency of glutamate-urea labelled theranostic

Studies were undertaken to quantify the targeting efficiency of the glutamate-urea functionalised polymers. Two human prostate cancer cell lines, PC3-PIP (PSMA-positive) and PC3-FLU (PSMA-negative), were received from Dr Warren Heston.[51] Both cell lines were seeded into 6 well plates, 0.25 million cells per well. The cells were incubated overnight with RPMI (Life Technologies, Mulgrave, Vic, Aust) containing 10% fetal bovine serum (FBS; Moregate, Brisbane, Aust). The targeted and non-targeted polymers were made to 5 μM in complete medium (RPMI + 10% FBS).

For uptake studies, the incubation medium was removed and 1 mL of polymer-containing medium was added to the appropriate well, and incubated with cells for 30 minutes. Following this the polymer solution was removed, the cells washed with RPMI twice. Cells were detached from the wells using trypsin-EDTA, which were transferred to Eppendorf tubes with 1 drop of FBS. After centrifugation, cell pellets were resuspended in 200 μL of PBS for FACS analysis.

For confocal microscopy, cells were seeded into a 24 well plate on coverslips and incubated with polymer solutions (20 μM in complete medium). Following incubation, the cells were washed twice with PBS, then cells fixed in 4% paraformaldehyde (PFA) solution (0.5 mL) for 10 minutes. The PFA was then removed and the cells washed twice with PBS. Nuclei were stained by incubation of fixed cells with Hoechst Dye (33342; Invitrogen) (10 mg mL^{-1} diluted 1 : 5000 in PBA) for 10 minutes. After washing twice with PBS to remove free polymer, coverslips were mounted onto glass microscope slides for examination under a confocal microscope.

In vivo analysis of targeting efficiency of glutamate-urea labelled theranostic

All studies were in accordance with guidelines of the Animal Ethics Committee of The University of Queensland (UQ), and Australian Code for the Care and Use of Animals for Scientific Purposes. Studies were undertaken to quantify the targeting efficiency of the glutamate-urea labelled polymer *in vivo*. Nu/nu mice were implanted with both PSMA positive and negative cell lines on opposite flanks. Each mouse was injected subcutaneously with 2×10^6 PC3-PIP cells (left flank) and 2×10^6 PC3-FLU (right flank). The imaging experiments were performed 8 days after tumour cell injections. HBP-03A (targeted) and HBP-01 (control) were diluted in PBS to 20 mg mL^{-1}. 100 μL of HBP-03A and HBP-01 were injected *via* the tail vein into Mouse 1 and 2, respectively. Fluorescence and XRay images were acquired using an In Vivo MS FX Pro imaging station. Mice were anaesthetised with 2% isoflurane during all procedures.

In vitro analysis of drug release at physiological pH

Standards of fluorene-2-carboxaldehyde were measured at seven concentrations, and plotted as concentration *vs*. fluorescence intensity. The emission and excitation were 330 nm and 410 nm respectively. The entrance and exit slit widths were set to 4 nm. Experiments for determining the kinetics of degradation of the hydrazone bond were carried out on a Horiba Fluoromax-4. Measurements were taken every 3 minutes for 8 hours. The cuvettes were fitted with a stirrer bar and were stirred during all measurements.

Results and discussion

Synthesis of polymeric theranostic

In order to produce the final theranostic material for targeting prostate cancer, it was first necessary to synthesise a novel RAFT agent containing the targeting ligand for PSMA, as well as a polymerisable optical dye based on Cy5-methacrylamide.

The RAFT agent was developed by first synthesising the small molecule targeting ligand for PSMA. As shown in Fig. 1, a lys–glu peptide was synthesised with protection of both the free amine and acid group of lysine and the acid groups on the glutamic acid. In the second step, the benzyl protecting group was selectively removed from the lysine and subsequently reacted with the carboxylic acid functional group of the RAFT agent that had been previously activated with pentafluorophenol (S3). This activated-ester efficiently reacted with the amine group of the targeting ligand molecule (Fig. 1), to yield the required RAFT agent. The targeted RAFT agent was readily purified using column chromatography in high yield, demonstrating a facile synthetic route to a targeting agent that can be polymerised directly into the theranostic device. This approach is advantageous as it removes the necessity for post-modification of the polymer with targeting ligand, with good control over the number and density of ligand on the polymeric nanoparticle.

The synthesis of a monomeric Cy-5 methacrylamide occurred *via* amide-formation through reaction of pentafluorophenol-activated methacrylic acid and amine-functional Cy-5. The product was formed in high yield. ^{1}H NMR and mass spectroscopy analysis (MW 649.8 Da) confirmed the presence of a single methacrylamide species with no unreacted Cy-5 amine remaining in the solution (ESI Fig. S5†). The hyperbranched polymers were synthesised by RAFT polymerisation, with the addition of a bifunctional vinyl monomer at low concentration (8 mol%) to form branching points in the macromolecule.[44,52] The synthetic yield of these polymers was high, with typical monomer conversions in the range of 97–99%. The resultant hyperbranched polymers are unimolecular with well-defined end-groups and the molecular structure was characterised by ^{1}H NMR (Fig. 2, HBP03A) and SEC-MALLS. Each polymer is comprised of multiple 'arms', terminated by the RAFT end-

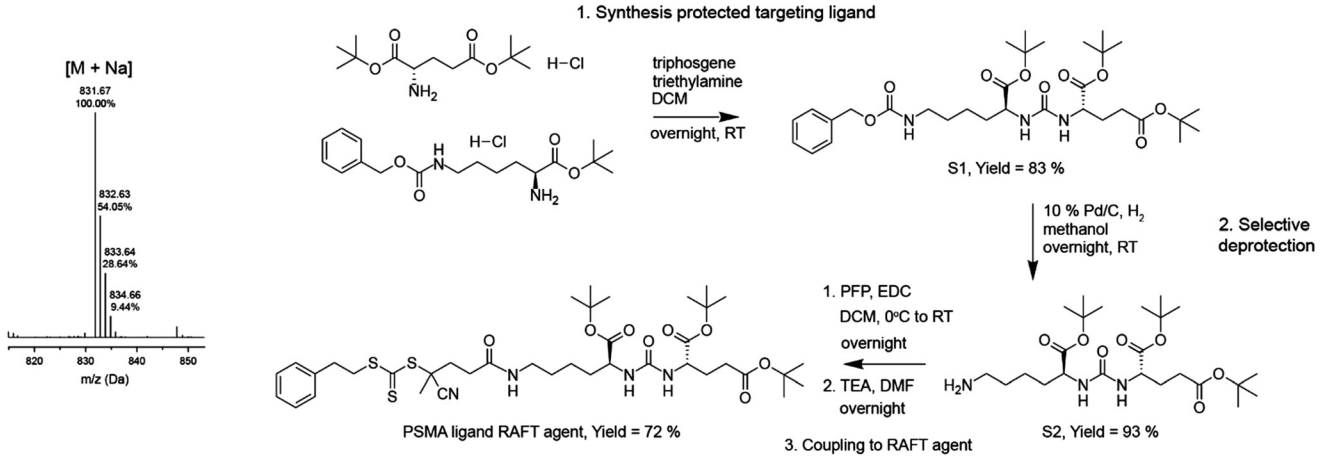

Fig. 1 The synthetic scheme leading to the final PSMA-targeting RAFT agent. Mass spectroscopy confirms a single molecular weight species at 831 Da $[M + Na]^+$. (^{1}H NMR, Fig. S4, ESI†).

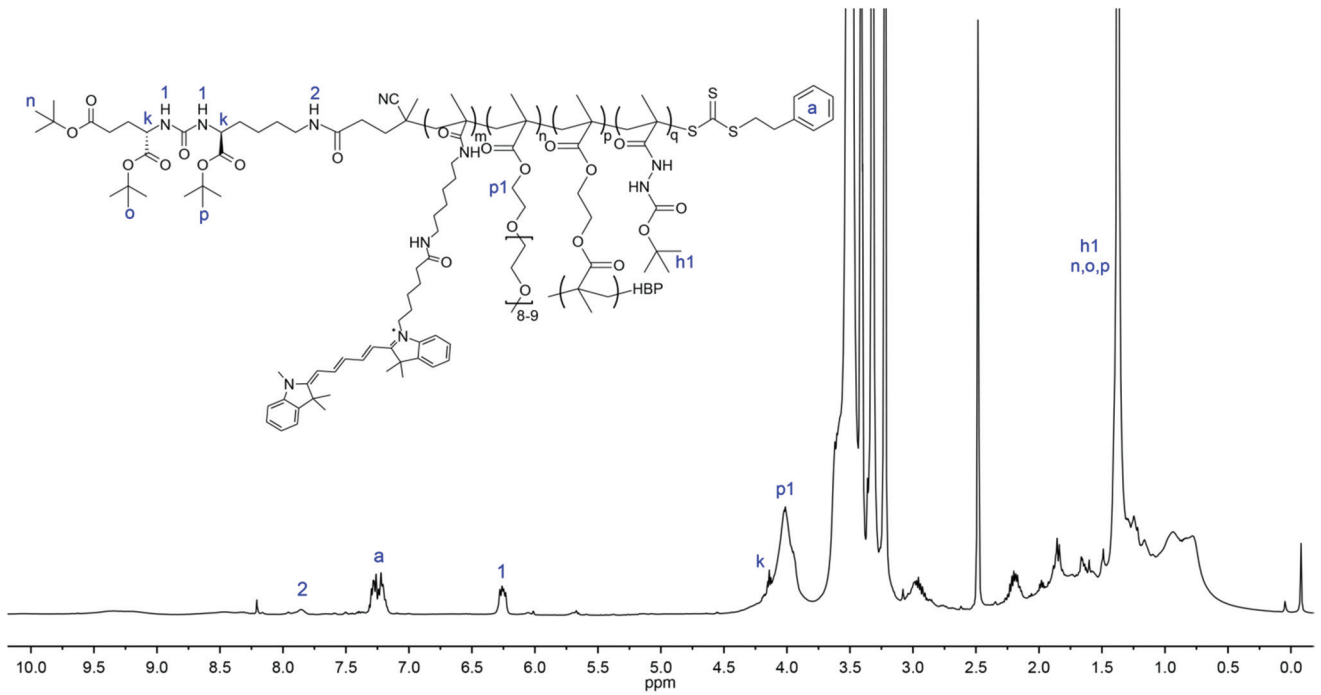

Fig. 2 Representative ^{1}H NMR spectra of hyperbranched polymer: HBP03A. The diagnostic resonances for molecular weight characterisation have been highlighted.

groups. By comparing the ^{1}H NMR signals of the RAFT end-groups and the polymeric repeat unit signals the molecular weight of each arm could be calculated. The resonance of the benzyl group on the RAFT agent (Fig. 2, resonance a, 7.3 ppm) and the methylene group adjacent to the carbonyl groups on the PEGMA repeat units (Fig. 2, resonance p1, 4.1 ppm) were used to estimate the molecular weight of arms. Additionally, the resonance of the methyl groups of the *t*-butyl protecting group on both the TMBC repeat units and the targeting group on the RAFT agent (Fig. 2, resonance (h1,n,o,p), 1.4 ppm) were used to approximate the number of TBMC units in each arm. The integrations of these peaks showed a ratio of 1 : 14 : 4.5, RAFT–PEGMA–TMBC, from which it was determined that for this particular polymer, each arm had a molecular weight of approximately 8.5 kDa, with 22 mol% TMBC incorporation.

The absolute molecular weight of the polymers was measured by SEC-MALLS. From the ratio of M_n (SEC-MALLS) to M_n (NMR), the number of chains within each hyperbranched polymer particle was determined. The physical properties of the hyperbranched polymers synthesised in this study are summarised in Table 1, where three different polymers were synthesised with varying comonomer concentrations.

The rationale for attaching the targeting ligand through the R group of the RAFT agent was to both decrease the variability

Table 1 Summary of physical and chemical properties of the control and PSMA-targeted hyperbranched polymers

	Monomer conversion	M_n (D_M) SEC-MALLS	M_n ^{1}H NMR	# End groups	# Branch points	D_h	# Cy5 dyes	Experimental TBMC–PEGMA
HBP 01	98%	39 kDa (1.6)	12 kDa	3.5	2.5	5.1 nm	0.1	19 : 81
HBP 02	99%	35 kDa (1.4)	15 kDa	2.3	1.3	6.2 nm	0.1	22 : 78
HBP 03	98%	39 kDa (1.7)	8.5 kDa	4.6	3.6	5.5 nm	0.1	22 : 78

in the number of targeting ligands present on each polymer particle (since post-modification is typically lower yielding), and to increase the amount of targeting ligands that could be attached compared to standard post-polymerisation methods. A further advantage of this method is that the number of targeting ligands is then able to be tuned by varying the concentrations of RAFT agent, branching agent and initiator to monomer.[53] With this in mind, HBP02 was synthesised with a ratio of monomer–RAFT–brancher–AIBN 100 : 5 : 5 : 1, which resulted in a lightly branched polymer having 2–3 randomly coupled chains. The feed ratio of monomers in HBP03 was modified to 100 : 10 : 10 : 2, and resulted in a polymer with approximately half the arm molecular weight of HBP02, increasing the number of targeting ligands to 4–5. Thus, the control over the chemistry imparted by the RAFT agent allows for investigation into the efficiency of targeting by increasing the number of targeting ligands present on the particle. The incorporation of the monomeric dye into the polymer was characterised by UV-Vis spectroscopy where the molar extinction coefficient of Cy5 was used to estimate the number of dye molecules per polymer. Typically, one in every sixteen polymer particles contained a Cy5 molecule for both the PSMA-targeted and control polymers. This was approximately 50% less than expected based on feed ratios, and is most likely due to different reactivity of the dye-methacrylamide as compared to the other monomer. Nonetheless, the amount of dye incorporated into each polymer was sufficient for all *in vitro* and *in vivo* analyses.

Removal of the *t*-butyl protecting groups on HBP02 and HBP03 was quantitatively achieved through reaction with TFA. Importantly, UV-Vis analysis showed that the deprotection reaction did not have a significant effect on the Cy5 moieties on the polymer (83% of the dye groups remained).

In vitro analysis of targeting efficiency of glutamate-urea labelled theranostic

Previous studies have shown that small molecules based on the glutamate ureas can successfully target PSMA.[24–27] It is also known that this targeting agent can be readily attached to a carrier system with minimal loss in targeting efficiency. In this study, the hyperbranched polymers were functionalised with the glutamate urea by incorporation into the RAFT agent. This resulted in polymers with a defined number of targeting ligand end-groups, HBP02A with 2.3 and HBP03A with 4.6 (here, the A postscript refers to polymers with active targeting ligand attached). Additionally, a control hyperbranched polymer was synthesised having no glutamate urea functionality. It was expected that the glutamate urea functionalised polymers would show specific uptake into the PSMA-positive cells (PC3-PIP), whereas there would be minimal uptake of the control polymer through a receptor-mediated mechanism.[13,14,20,27–29] It was further expected that the PSMA-negative cell line (PC3-FLU) would likewise show minimal uptake of any of the polymer samples. To validate this hypothesis, the PSMA-targeted polymers (HBP02A and HBP03A), control polymer (HBP01), and an additional control (HBP03; glutamate urea functionalised with the protecting groups intact) were incubated with PC3-PIP and PC3-FLU cells. Cells were incubated for 30 minutes with one of the 4 different polymer solutions, each at a concentration of 5 μM for flow cytometry and 20 μM for confocal microscopy.

Flow cytometric analysis showed significant and specific uptake of the glutamate urea targeted polymers, but not control polymers by the PSMA+ cells. In addition, all samples showed minimal uptake into PSMA– cells (Fig. 3). Confocal microscopic images confirmed these observations, with the glutamate urea targeted polymer showing significant uptake into the PSMA+ PC3-PIP cells, with fluorescence detected through the Cy5 channel (650 nm), but no Cy5 fluorescence observed in any other samples (Fig. 3, 1A–D).

The combined confocal and flow cytometry data suggest that the hyperbranched polymers functionalised with a PSMA targeting ligand using the RAFT approach, show selectively enhanced uptake into cells that positively express PSMA, making them good candidates for further theranostic development.

In vivo analysis of targeting efficiency of glutamate-urea labelled theranostic

Based on the success of the *in vitro* targeting studies, a preliminary investigation of the efficiency of the glutamate urea-conjugated polymers was undertaken *in vivo* in nude mice carrying PC3-PIP (PSMA+) and PC3-FLU (PSMA–) tumours on opposite flanks. To aid in visualisation, both tumour cell lines were transfected to express dsRed. Mouse 1 was intravenously injected with HBP-03A (targeted experiment), and Mouse 2 with the control (HBP-01). Fluorescence images were taken of both mice at 4 and 24 hours post-injection. After 4 hours, significant signal is observed at the PSMA+ tumour site (Mouse 1), correlating with the position of the tumour through co-registration of the signal arising from dsRed. Conversely, no Cy5 signal is observed at the location of the PSMA– tumour, confirming specificity of the glutamate-urea ligand for PSMA. While the results suggest receptor-mediated uptake of HBP-03A into PC3-PIP cells *in vivo*, Cy5 signal could also be detected in the kidneys, the expected excretion route for nano-

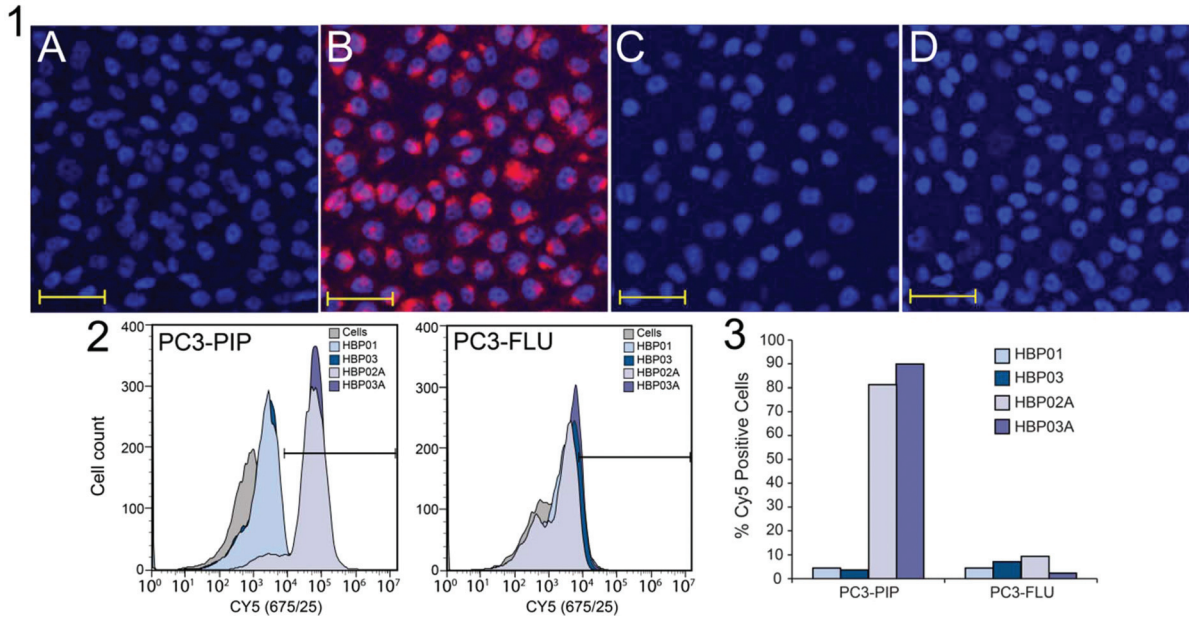

Fig. 3 1. Confocal microsope images showing uptake of Cy5-labelled (red) polymers following incubation of (A) HBP01 (control) with PC3-PIP cells, (B) HBP03A (targeted) with PC3-PIP cells, (C) HBP01 (control) with PC3-FLU cells and (D) HBP03A (targeted) with PC3-FLU cells. The cell nuclei (stained with Hoechst 33342; blue) show the position of the cells. The scale bar represents 50 μm. 2. FACS plots show Cy5 fluorescence for PC3-PIP and PC3-FLU cells incubated with medium alone, HBP01, HBP03, HBP02A or HBP03A for 30 mins. 3. %Cy5 positive cells from FACS data showing significant uptake of targeted samples by PC3-PIP cells only. Additional confocal microscope images Fig. S8, ESI.†

materials of this size. After 24 hours, significant signal was still detected in the PSMA+ tumour in Mouse 1, indicating that the theranostic was still localised within the tumour tissue. In contrast, the images of Mouse 2 obtained 4 and 24 hours post-injection show that no Cy5 signal is observed within the animal (Fig. S9, ESI†) indicating rapid excretion. This suggests that the theranostic is cleared within 4 hours if it does not interact with cellular proteins *via* the glutamate urea moiety.

Ex vivo analyses (24 hours) confirms that the glutamate urea targeted polymer was internalised by PSMA+ tumours in Mouse 1. It is interesting to note that the signal is primarily observed around the periphery of the tumour, with no signal appearing from the centre of the tumour, which may be attributed to poor vascularisation, and possibly necrosis, in the inner regions of the tumour mass.[54,55] Furthermore, a small amount of Cy5 signal was also detected on the PSMA− tumour. This accumulation could be attributed to the enhanced permeability and retention (EPR)[56] effect where leaky blood vessels around the tumour lead to accumulation of a small amount of the circulating polymer in the tumour tissue. While the kidneys still show the presence of some polymer when the organs are excised, all other organs and the blood show minimal fluorescence signal confirming that if polymer is not taken up by tumour cells it is cleared *via* the renal system. Interestingly, Mouse 2 shows the presence of a small amount of signal in the liver when the organs are excised, but not in any other organs in the animal. This confirms that the majority of the polymer has been cleared from the animal with a small amount sequestered into the liver most likely through phagocytosis (Fig. S9, ESI†). After fluorescence images had been acquired, flow cytometric analysis of excised tumours, liver and kidneys was performed to further validate the imaging data (Fig. 4C). This showed that 36.4% of cells in the PSMA+ tumour from Mouse 1 had taken up the targeted polymer. In contrast, uptake in the PSMA− tumour was less than 10%.

In vitro analysis of drug release at physiological pH

Following validation of the targeting efficiency of the glutamate urea small molecule targeting ligand, the next step was to investigate the drug delivery aspect of the theranostic. The polymer HBP03 was chosen for this investigation as it has the highest number of targeting ligands and showed good targeting to prostate cancer cells. The removal of the Boc- protecting group to yield the hydrazide-containing monomer unit (TBMC) and subsequent attachment of the model drug fluorene-2-carboxaldehyde was characterised by ^{1}H NMR (HBP03B; Fig. S10, ESI†). Quantitative removal of the protecting groups was confirmed by complete removal of the *t*-butyl peak in the NMR spectrum at 1.4 ppm following the reaction.

Subsequent formation of the hydrazone bond through reaction of hydrazide with an aldehyde group on the model drug occurred in 65% yield. For HBP03B, a total of three fluorene-2-carboxaldehyde groups were incorporated into each polymer particle as confirmed by ^{1}H NMR. UV-Vis analysis was also used for secondary validation and also suggested that approximately three fluorene-2-carboxaldehyde units were incorporated into each polymer (calculated extinction coefficient of 3.32×10^4 cm^{-1} M^{-1} at 330 nm). A possible explanation for the lower than expected yield of hydrazone formation could be

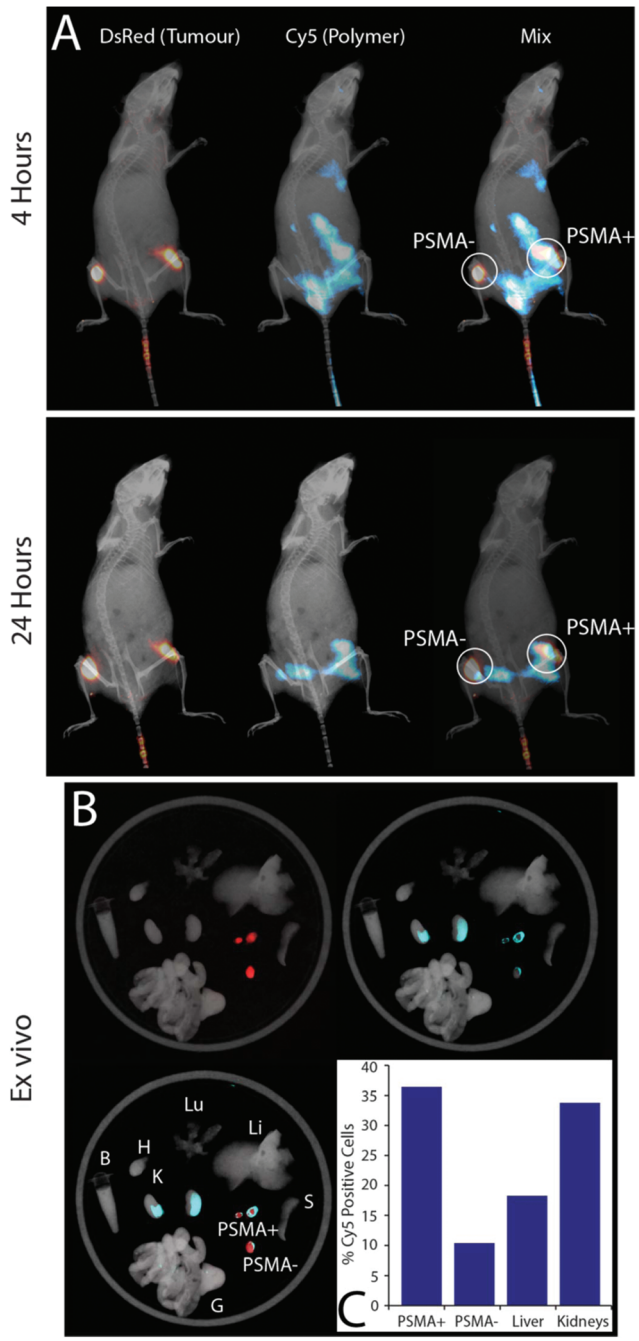

Fig. 4 Nu/nu mouse (Mouse 1) with subcutaneous PSMA+ and PSMA– tumours on contralateral flanks. (A) Fluorescence image four hours and 24 hours post injection with HBP-03A (targeted). The images show successful uptake of the targeted polymer into the PSMA+ tumour cells. (B) The excised organs of the same mouse after 24 hours confirming the presence of the polymer in the PSMA+ tumour site and (C) flow cytometric analysis of Cy5 positive cells in excised organs. (B: blood, H: heart, Lu: lungs, Li: liver, K: kidneys, S: spleen, G: gut).

attributed to hydrolysis of some of the TBMC repeat units into methacrylic acid during the TFA deprotection step, thereby limiting the number of hydrazide groups available for conjugation. Nonetheless, a yield of 65% for conjugation of model drug was sufficient for analysis of the degradation kinetics.

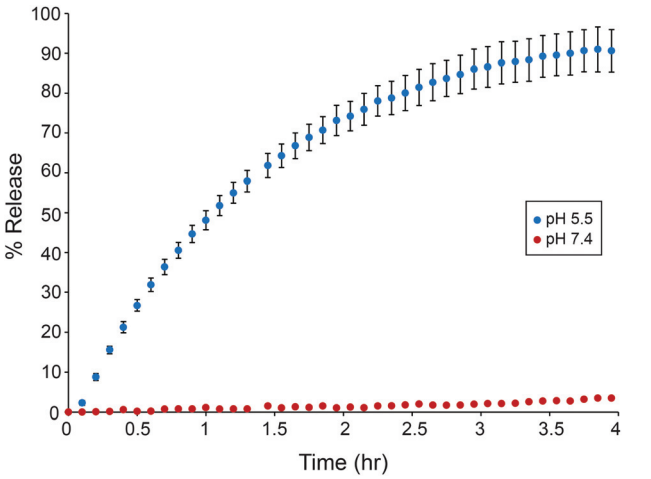

Fig. 5 The release profile of the model drug fluorene-2-carboxaldehyde from the hyperbranched polymer system. The curve in blue shows the release of the drug in pH 5.5.

The degradation of the hydrazone bond in this particular system was readily quantified by fluorescence spectroscopy, as the fluorescent signal of the model drug is quenched when the molecule is bound to the polymer through the hydrazone linkage due to intramolecular photoinduced electron transfer.[57] Upon hydrolysis, the model drug is released and shows a marked increase in fluorescence intensity. This increase in intensity was recorded over a 4 hour period, and following calibration with known standards of the model drug, the fluorescence intensity could be expressed as concentration of the free molecule in solution. This could be further compared to the total known concentration originally present in the sample to yield a quantitative profile of hydrazone bond degradation over time. This is depicted in Fig. 5. The experiment was conducted at pH 7.4 (serum pH) and at pH 5.5 (endosomal pH) to compare the release in these two biologically relevant environments. Over a 4 hour period, approximately 90% of the bound model drug is released in a controlled manner. Importantly, this release falls within an acceptable therapeutic timeframe based on the imaging results shown in Fig. 4. It can also be seen that under conditions that mimic the pH of blood (pH 7.4), minimal release of the model drug is observed (<5%) indicating remarkable stability of the system at this pH. It can therefore be concluded that this is a viable system for controlled release of a chemotherapeutic.

Conclusions

In this report we have demonstrated the synthesis of a theranostic hyperbranched polymer for prostate cancer. The hyperbranched polymers were constructed through facile synthetic methods utilising RAFT polymerisation. Targeting of the particles was achieved through the use of a glutamate-urea based small molecule targeting ligand, which was attached to the R-group of the RAFT agent prior to polymerisation. *In vitro* cell

assays with PSMA+ and PSMA− cells showed that the small molecule targeting ligand had high specificity for PSMA+ cells, with minimal uptake observed for control polymers that exhibit no targeting towards PSMA. There was also minimal uptake of any polymer in PSMA− cells. *In vivo* experiments in mice further confirmed the specificity of the targeting ligand for PSMA, with the targeted polymer showing four times higher uptake in tumours that overexpressed PSMA than those that don't express the protein.

In order to demonstrate applicability of this system as a theranostic, a model drug was attached to the polymer through the use of a hydrolytically-degradable hydrazone linkage. The rationale was that this linkage could be cleaved at acidic pH, such as that within the endosome, while remaining stable at a physiological pH. *In vitro* experiments showed 90% release of the model drug in an acidic (pH 5.5) environment over 4 hours, which covers a therapeutically relevant timeframe. Over the same timeframe at physiological pH 7.4, the polymers demonstrated significant stability, with less than 5% release. This synthetic approach shows promise as a theranostic platform for treating prostate cancer.

Acknowledgements

The researchers would like to thank Warren D. Heston (Department of Cancer Biology, Cleveland Clinic, Cleveland, USA) for the PC3 cells used in this study, Yiming Ma for her assistance with the *in vitro* cell culture experiments, and Karine Mardon for her assistance with the *in vivo* injections. The PC3 cells were modified to express DsRed using a plasmid supplied by Dr Brett Hollier (Queensland University of Technology, Brisbane, Australia). This work was performed in part at the Queensland node of the Australian National Fabrication Facility, a company established under the National Collaborative Research Infrastructure Strategy to provide nano- and microfabrication facilities for Australia's researchers. We acknowledge funding from the National Health and Medical Research Council (APP1046831, PJR, KJT, AKW), the Australian Research Council (FT110100284 (KJT), DP140100951 (KJT), DP110104299 (AKW)), and the Australian Commonwealth Government Australian Postgraduate Award (AKP). This research was conducted and funded by the ARC Centre of Excellence in Convergent Bio-Nano Science and Technology (CE140100036).

Notes and references

1 J. Ferlay, P. Autier, M. Boniol, M. Heanue, M. Colombet and P. Boyle, *Ann. Oncol.*, 2007, **18**, 581.
2 S. K. Pal, P. Twardowski and O. Sartor, *Clin. Interv. Aging*, 2010, **5**, 395.
3 V. Kundra, P. M. Silverman, S. F. Matin and H. Choi, *Am. J. Roentgenol.*, 2007, **189**, 830.
4 E. D. Crawford, M. A. Eisenberger, D. G. McLeod, J. T. Spaulding, R. Benson, F. A. Dorr, B. A. Blumenstein, M. A. Davis and P. J. Goodman, *N. Engl. J. Med.*, 1989, **321**, 419.
5 M. A. Eisenberger, B. A. Blumenstein, E. D. Crawford, G. Miller, D. G. McLeod, P. J. Loehrer, G. Wilding, K. Sears, D. J. Culkin, I. M. Thompson Jr., A. J. Bueschen and B. A. Lowe, *N. Engl. J. Med.*, 1998, **339**, 1036.
6 D. P. Petrylak, C. M. Tangen, M. H. Hussain, P. N. Lara Jr., J. A. Jones, M. E. Taplin, P. A. Burch, D. Berry, C. Moinpour, M. Kohli, M. C. Benson, E. J. Small, D. Raghavan and E. D. Crawford, *N. Engl. J. Med.*, 2004, **351**, 1513.
7 C. Fang and M. Zhang, *J. Controlled Release*, 2010, **146**, 2.
8 L. Li, Q. Yang, Z. Zhou, J. Zhong and Y. Huang, *Biomaterials*, 2014, **35**, 5171.
9 M. Talelli, C. J. F. Rijcken, S. Oliveira, R. van der Meel, P. M. P. van Bergen en Henegouwen, T. Lammers, C. F. van Nostrum, G. Storm and W. E. Hennink, *J. Controlled Release*, 2011, **151**, 183.
10 Y. Yang, Z. Zhou, S. He, T. Fan, Y. Jin, X. Zhu, C. Chen, Z.-r. Zhang and Y. Huang, *Biomaterials*, 2012, **33**, 2260.
11 N. Yonenaga, E. Kenjo, T. Asai, A. Tsuruta, K. Shimizu, T. Dewa, M. Nango and N. Oku, *J. Controlled Release*, 2012, **160**, 177.
12 J. S. Horoszewicz, E. Kawinski and G. Murphy, *Anticancer Res.*, 1987, **7**, 927.
13 S. S. Chang, D. S. O'Keefe, D. J. Bacich, V. E. Reuter, W. D. W. Heston and P. B. Gaudin, *Clin. Cancer Res.*, 1999, **5**, 2674.
14 A. Ghosh and W. D. W. Heston, *J. Cell. Biochem.*, 2004, **91**, 528.
15 D. A. Silver, I. Pellicer, W. R. Fair, W. Heston and C. Cordon-Cardo, *Clin. Cancer Res.*, 1997, **3**, 81.
16 S. D. Sweat, A. Pacelli, G. P. Murphy and D. G. Bostwick, *Urology*, 1998, **52**, 637.
17 R. G. Lapidus, C. W. Tiffany, J. T. Isaacs and B. S. Slusher, *Prostate*, 2000, **45**, 350.
18 S. L. Su, I. P. Huang, W. R. Fair, C. T. Powell and W. D. Heston, *Cancer Res.*, 1995, **55**, 1441.
19 H. Liu, P. Moy, S. Kim, Y. Xia, A. Rajasekaran, V. Navarro, B. Knudsen and N. H. Bander, *Cancer Res.*, 1997, **57**, 3629.
20 S. S. Chang, V. E. Reuter, W. D. Heston, N. H. Bander, L. S. Grauer and P. B. Gaudin, *Cancer Res.*, 1999, **59**, 3192.
21 L. M. Freeman, B. R. Krynyckyi, Y. Li, G. Korupulu, K. Saleemi, M. K. Haseman and D. Kahn, *Q. J. Nucl. Med.*, 2002, **46**, 131.
22 M. K. Haseman, S. A. Rosenthal and T. J. Polascik, *Cancer Biother. Radiopharm.*, 2000, **15**, 131.
23 B. S. Slusher, J. J. Vornov, A. G. Thomas, P. D. Hurn, I. Harukuni, A. Bhardwaj, R. J. Traystman, M. B. Robinson, P. Britton, X. C. Lu, F. C. Tortella, K. M. Wozniak, M. Yudkoff, B. M. Potter and P. F. Jackson, *Nat. Med.*, 1999, **5**, 1396.
24 A. P. Kozikowski, J. Zhang, F. Nan, P. A. Petukhov, E. Grajkowska, J. T. Wroblewski, T. Yamamoto, T. Bzdega, B. Wroblewska and J. H. Neale, *J. Med. Chem.*, 2004, **47**, 1729.

25 R. P. Murelli, A. X. Zhang, J. Michel, W. L. Jorgensen and D. A. Spiegel, *J. Am. Chem. Soc.*, 2009, **131**, 17090.
26 Z. Chen, M.-F. Penet, S. Nimmagadda, C. Li, S. R. Banerjee, P. T. Winnard, D. Artemov, K. Glunde, M. G. Pomper and Z. M. Bhujwalla, *ACS Nano*, 2012, **6**, 7752.
27 S. R. Banerjee, M. Pullambhatla, C. A. Foss, S. Nimmagadda, R. Ferdani, C. J. Anderson, R. C. Mease and M. G. Pomper, *J. Med. Chem.*, 2014, **57**, 2657.
28 H. M. Shallal, I. Minn, S. R. Banerjee, A. Lisok, R. C. Mease and M. G. Pomper, *Bioconjugate Chem.*, 2014, **25**, 393.
29 C. A. Foss, R. C. Mease, H. Fan, Y. Wang, H. T. Ravert, R. F. Dannals, R. T. Olszewski, W. D. Heston, A. P. Kozikowski and M. G. Pomper, *Clin. Cancer Res.*, 2005, **11**, 4022.
30 S. A. Kularatne, Z. Zhou, J. Yang, C. B. Post and P. S. Low, *Mol. Pharm.*, 2009, **6**, 790.
31 S. A. Kularatne, K. Wang, H.-K. R. Santhapuram and P. S. Low, *Mol. Pharm.*, 2009, **6**, 780.
32 B. Seruga, A. Ocana and I. F. Tannock, *Nat. Rev. Clin. Oncol.*, 2011, **8**, 12.
33 J. Lim, A. Chouai, S.-T. Lo, W. Liu, X. Sun and E. E. Simanek, *Bioconjugate Chem.*, 2009, **20**, 2154.
34 F. Kratz, U. Beyer and M. T. Schutte, *Crit. Rev. Ther. Drug Carrier Syst.*, 1999, **16**, 245.
35 S. D. Khaja, S. Lee and N. Murthy, *Biomacromolecules*, 2007, **8**, 1391.
36 J.-K. Kim, V. K. Garripelli, U.-H. Jeong, J.-S. Park, M. A. Repka and S. Jo, *Int. J. Pharm.*, 2010, **401**, 79.
37 S. Binauld, W. Scarano and M. H. Stenzel, *Macromolecules*, 2012, **45**, 6989.
38 T. Etrych, M. Sirova, L. Starovoytova, B. Rihova and K. Ulbrich, *Mol. Pharm.*, 2010, **7**, 1015.
39 T. Etrych, M. Jelinkova, B. Rihova and K. Ulbrich, *J. Controlled Release*, 2001, **73**, 89.
40 B. Rihova, T. Etrych, M. Pechar, M. Jelinkova, M. Stastny, O. Hovorka, M. Kovar and K. Ulbrich, *J. Controlled Release*, 2001, **74**, 225.
41 B. E. Rolfe, I. Blakey, O. Squires, H. Peng, N. R. B. Boase, C. Alexander, P. G. Parsons, G. M. Boyle, A. K. Whittaker and K. J. Thurecht, *J. Am. Chem. Soc.*, 2014, **136**, 2413.
42 N. R. B. Boase, I. Blakey and K. J. Thurecht, *Polym. Chem.*, 2012, **3**, 1384.
43 K. J. Thurecht, I. Blakey, H. Peng, O. Squires, S. Hsu, C. Alexander and A. K. Whittaker, *J. Am. Chem. Soc.*, 2010, **132**, 5336.
44 B. Liu, A. Kazlauciunas, J. T. Guthrie and S. Perrier, *Macromolecules*, 2005, **38**, 2131.
45 D. Konkolewicz, A. Gray-Weale and S. Perrier, *Macromol. Theory Simul.*, 2010, **19**, 219.
46 W. Scarano, H. T. Duong, H. Lu, P. L. De Souza and M. H. Stenzel, *Biomacromolecules*, 2013, **14**, 962.
47 J. H. Tan, N. A. J. McMillan, E. Payne, C. Alexander, F. Heath, A. K. Whittaker and K. J. Thurecht, *J. Polym. Sci., Part A: Polym. Chem.*, 2012, **50**, 2585.
48 M. Elsabahy, R. Shrestha, C. Clark, S. Taylor, J. Leonard and K. L. Wooley, *Nano Lett.*, 2013, **13**, 2172.
49 J. Zou, F. Zhang, S. Zhang, S. F. Pollack, M. Elsabahy, J. Fan and K. L. Wooley, *Adv. Healthcare Mater.*, 2014, **3**, 441.
50 H. P. Luehmann, E. D. Pressly, L. Detering, C. Wang, R. Pierce, P. K. Woodard, R. J. Gropler, C. J. Hawker and Y. Liu, *J. Nucl. Med.*, 2014, **55**, 629.
51 T. Nakajima, M. Mitsunaga, N. H. Bander, W. D. Heston, P. L. Choyke and H. Kobayashi, *Bioconjugate Chem.*, 2011, **22**, 1700.
52 S. Perrier, P. Takolpuckdee and C. A. Mars, *Macromolecules*, 2005, **38**, 2033.
53 N. R. B. Boase, I. Blakey, B. E. Rolfe, K. Mardon and K. J. Thurecht, *Polym. Chem.*, 2014, **5**, 4450.
54 R. K. Jain, *Cancer Res.*, 1987, **47**, 3039.
55 R. K. Jain, *Cancer Metastasis Rev.*, 1990, **9**, 253.
56 H. Maeda, G. Y. Bharate and J. Daruwalla, *Eur. J. Pharm. Biopharm.*, 2009, **71**, 409.
57 S. p. Dufresne, L. Callaghan and W. G. Skene, *J. Phys. Chem. B*, 2009, **113**, 15541.

Biographical Sketch

NAME THOMAS KRYZA (PI)	POSITION TITLE POST-DOCTORAL FELLOW, AUSTRALIAN PROSTATE CANCER RESEARCH CENTRE – QUEENSLAND (APCRC-Q), INSTITUTE OF HEALTH AND BIOMEDICAL INNOVATION (IHBI), FACULTY OF SCIENCE & TECHNOLOGY, QUEENSLAND UNIVERSITY OF TECHNOLOGY (QUT)		
EDUCATION/TRAINING			
INSTITUTION AND LOCATION	DEGREE (IF APPLICABLE)	YEAR(S)	FIELD OF STUDY
University of Lille 1 Lille, France	**Bachelor of Biology**	2006-07	Cellular Biology and Physiology
University of Lille 1 Lille, France	**Master of Biology and Biotechnology** *Obtained with honours*	2007-09	Biology and Health
François Rabelais University Tours, France	**Doctor of Philosophy (PhD)** *Obtained with the grade honours and congratulation of Jury*	2010-13	Life and Health Sciences

RESEARCH AND PROFESSIONAL EXPERIENCE:

- Sep 2008 – Jun 2009: **Master student research training**
INSERM Unit U908, Lille, France
"Study of secretome modification associated with cancerogenesis by 2D electrophoresis"

- Oct 2010 – Sep 2013: **PhD student**
Centre d'Etude des Pathologies Respiratoires, INSERM Unit U1100/EA6305, Tours, France
"Role of kallikrein-12 in the tissue remodeling associated with pulmonary diseases"

- Oct 2011 – Sep 2013: **University teaching Assistant**
Plant Physiology department of University François-Rabelais, Tours, France
Theorical teaching of "Experimental Approaches" and "Personal and Professional Project" for BSc students

- Oct 2013 – Jan 2014: **Research Assistant**
Centre d'Etude des Pathologies Respiratoires, INSERM Unit U1100/EA6305, Tours, France
"Impact of kallikrein-12 in extracellular matrix proteolysis and cancer progression"

- Jun 2014 – Jul 2014: **Invited Researcher**
Jacob University, SPP 1629, Dr K. Brix group, Bremen, Germany
"Using molecular probes to visualize protease activity"

- Aug 2014 – Present: **Post-doctoral fellow**
APCRC-Q, QUT, Translational Research Institute (TRI) Brisbane, Australia
1) Involvement of kallikrein-4 in stromal cell activation and initiation of prostate cancer
2) Modification of proteases expression in prostate cancer cells during progression of prostate cancer

- Mar 2016 – June 2016: **Demonstrator in "Cellular biology"** for The School of Biomedical Sciences, Queensland University of Technology.

- Mar 2017 – present: **Demonstrator in "Cellular biology"** for The School of Biomedical Sciences, Queensland University of Technology.

AWARDS / PRIZES:

2012: **Best Oral Communication Award** of 25th colloque BioTechno Centre, Seillac, France

2012: **Best Poster Communication Award** (Cancer session) of "Journées de Recherches Respiratoire", Lille, France

2013**: Travel Grant Award** from Cancéropôle Grand-Ouest, Nantes, France

2015: **Best Poster Communication Award** (ECR category) of "TRI Symposium 2015", Brisbane, Australia

2015: **Travel Grant Award** from International Society of Proteolysis, Penang, Malaysia

2015: **Travel Grant Award** from The School of Biomedical Sciences, Brisbane, Australia

2016: **Travel Grant Award** from The School of Biomedical Sciences, Brisbane, Australia

2016 :**Best Science Poster** (ECR category) of "TRI Symposium 2016", Brisbane, Australia

OTHERS RELATED ACTIVITIES:

Sept 2010 – Feb 2014: **ADOCT organising committee** (PhD student association)

Jan 2014 – Jun 2014: **Primary supervisor of 2 Technical students** (6 months), Centre d'Etude des Pathologies Respiratoires, INSERM Unit U1100/EA6305, Tours, France

2014-Present: **Fire warden**; QUT, Translational Research Institute (TRI) Brisbane, Australia

2015-Present: **Responsible of PC2 laboratory** ; QUT, Translational Research Institute (TRI) Brisbane, Australia

Sept 2016 – Present: **Associate supervisor of a PhD student** (Ms. Samaneh Farashi) working on association study of miRNA-regulatory SNPs with prostate cancer risk, prognosis and progression

PROFESSIONAL MEMBERSHIPS

- Australian Society for Medical Research (ASMR)
- International Proteolysis Society (IPS)

Peer-Reviewed Publications

1. **Kryza T,** Achard C, Parent C, Marchand-Adam S, Guillon-Munos A, Iochmann S, Korkmaz B, Respaud R, Courty Y, Heuzé-Vourc'h N. Angiogenesis stimulated by human kallikrein-related peptidase 12 acting via a platelet-derived growth factor B-dependent paracrine pathway. FASEB J. 2014 Feb;28(2):740-51. doi: 10.1096/fj.13-237503. Epub 2013 Nov 13. (Cited 6)

2. **Kryza T**, Lalmanach G, Lavergne M, Lecaille F, Reverdiau P, Courty Y, Heuzé-Vourc'h N. Pro-angiogenic effect of human kallikrein-related peptidase 12 (KLK12) in lung endothelial cells does not depend on kinin-mediated activation of B2 receptor. Biol Chem. 2013 Mar;394(3):385-91. doi: 10.1515/hsz-2012-0291. (PMID:23152405) (Cited 3)

3. Brellier F, Martina E, Degen M, Heuzé-Vourc'h N, Petit A, **Kryza T**, Courty Y, Terracciano L, Ruiz C, Chiquet-Ehrismann R. Tenascin-W is a better cancer biomarker than tenascin-C for most human solid tumors. BMC Clin Pathol. 2012 Sep 4;12:14. doi: 10.1186/1472-6890-12-14. (PMID:22947174) (Cited 12)

4. **Kryza T**, Silva Munasinghage L, Loessner D, Heuzé-Vourc'h N and Clements JA. The kallikrein-related peptidase family: dysregulation and functions during cancer progression. Biochimie, 2015, September 1st doi:10.1016/j.biochi.2015.09.002 (Cited 1)

5. Dalloneau E, Baroukh N, Mavridis K, Maillet A, Gueugnon F, Courty Y, Petit A , **Kryza T**, Del Rio M, Guyetant S, Cadena-Castadena DC , Dhommée C, Arnoult C, Scorilas A, Gouilleux-Gruart V and Heuzé-Vourc'h N. Down regulation of the neonatal Fc receptor expression in Non-Small-Cell lung cancer tissues is associated with a poor prognosis. Oncotarget, 2015, June 15, 2016, DOI: 10.18632/oncotarget.10074

Manuscripts in submission process

6. **Kryza T,** Furhman-Luck R, Stephens C, Loessner D, Hooper J, Risbridger G. and Clements J. Kallikrein-related peptidase 4 induces cancer-associated fibroblast features in prostate-derived stromal cells. *(Molecular Oncology, in reviewing)*

7. Munasinghage Silva L., Stoll T, Hoogland C., Dong Y., Kryza T., Stephens CR., Lachlan Hastie M., Kleifeld O., Gorman JJ., Clements AC. Integration of two in-depth quantitative proteomics approaches determines the kallikrein-related peptidase 7 (KLK7) degradome in ovarian cancer cell secretomes *(Molecular & Cellular Proteomic, in reviewing)*

8. **Kryza T,** Parent C, Marchand-Adam S, Korkmaz B, Courty Y, Clements J, Heuzé-Vourc'h N. Impact of the kallikrein-related peptidase 12 on super-fibronectin formation and migration of endothelial cells could be inhibited using newly generated monoclonal antibody. (*Ready to submit*)

Manuscripts soon to be submitted / in preparation

9. **Kryza T**, Tevz G, Mc-Pherson S, Lehman M, Stephens C, Nelson C and Clements J. Deregulation of proteases in prostate cancer cells following androgen targeted therapies. (*Manuscript in preparation)*

10. **Kryza T**, Mc-Pherson S, Lehman M, Stephens C, Lesner A, Nelson C and Clements J. Role of the kallikrein-related peptidase 14 in progression of prostate cancer cells to androgen resistance. (*Manuscript in preparation)*

11. Bock N, Shokoohmand A, **Kryza T**, …,Nelson C, Clements J and Hutmacher D. A new 3D live osteoblasts-derived matrix to studied interaction prostate cancer cells and bone microenvironment. (*Manuscript in preparation)*

12. Furhman-Luck R, …. **Kryza T**, …, Clements J. Deciphering substrate repertoire of the kallikrein-related peptidase-4 by combining cutting-edge proteomic approaches. *(Manuscript in preparation)*

CONFERENCE PARTICIPATION

Oral communications:

- 4th International Symposium on Kallikreins and Kallikrein-Related Peptidases (September, 2-4 2011 ; Rhodes, Greece) « Is human kallikrein related peptidase 12, a novel kininogenase ? »

- 3rd International Symposium on Vasoactive and Inflammatory Mediators (June, 21-23 2012 ; Paris, France) « The kallikrein related peptisade 12 (KLK12) is implicated in lung angiogenesis »

- 25ème colloque BioTechno Centre (October, 11-12 2012 ; Domaine de Seillac, France) « Involvement of kallikrein-related peptidase 12 in lung angiogenesis »

- 5ème journée Recherche Tours-Poitier (November, 30 2012 ; Tours, France) « Function of kallikrein-12 in lung cancer associated angiogenesis»

- 5th International Symposium on Kallikreins and Kallikrein-Related Peptidases (September 28 – October 1 2013 ; Toronto, Canada) « KLK12 stimulates angiogenesis through PDGFB dependent paracrine pathway »

- Journées de Recherches Respiratoire (October, 11-12 2013 ; Montpellier, France) «Pro-angiogeneic effect of kallikrein-related peptidase 12 is mediated through modulation of bioavailability of PDGF-B»

- 31th Protease Winter School (February 26 – March 2 2014 ; Tiers, Italy) "KLK12 proangiogenic effect depends of PDGF-B pathway"

- DAAD Work shop 2014: German-Australian Network on Personalized Cancer Medicine (July 3-4 2014, Munich, Germany) "The impact of kallikrein-related peptidase 12 (KLK12) on extracellular matrix proteins"

- DAAD Work shop 2015: German-Australian Network on Personalized Cancer Medicine (July 3-4 2014, Munich, Germany) "Dysregulation of proteolytic network in prostate cancer cells after androgen deprivation/ androgen targeting therapies"

- 6th International Symposium on Kallikreins and Kallikrein-Related Peptidases (September 28 – October 1 2015 ; Brisbane, Australia) « KLK4 involvement in initiation of prostate cancer: impact on stromal cells»

- International Proteolysis Society Early Career Workshop 2015 (October, 4-8th 2015, Penang, Malaysia) "Involvement of KLK4 in interaction between prostate cancer cells and stromal cells"

- TRI Symposium 2016 (October, 25th 2016, Brisbane, Australia) "Kallikrein-related peptidase 14 is upregulated after androgen targeting therapies and involved in aggressive prostate cancer"

Poster Communications:

- Journées de Recherches Respiratoire (October, 15-16 2010 ; Nantes, France) « Extracellular matrice remodelling mediated by kallikrein-related peptidase: Involvement in lung carcinogenesis.»

- Journées du Cancéropôle Grand Ouest (October, 18-19 2010 ; Tours, France) « Impact of extracellular matrice remodelling mediated by kallikreins on lung cancer progression. »

- Journée Recherche de la Faculté de Médecine (November, 18 2010 ; Tours, France) « Involvement of kallikrein-related peptidases in extracellular matrix remodelling and lung cancer. »

- Forum de l'Ecole Doctorale (June, 23 2011 ; Tours, France) « Human kallikrein-related peptidase 12: a new kininogenase? »

- 24ème colloque BioTechno Centre (October, 13-14 2011 ; Domaine de Seillac, France) « Involvement of KLK12 in kinin generation »

- Journée Recherche Tours-Poitier (December, 2 2011 ; Poitier, France) « Impact of kallikrein-related peptidase 12 in fibronectin matrice formation by endothelial cells »

- 25ème colloque BioTechno Centre (October, 11-12 2012 ; Domaine de Seillac, France) « Involvement of KLK12 in lung neoangiogenesis »

- Journées de Recherches Respiratoire (October, 19-20 2012 ; Lille, France) « Involvement of kallikrein-related peptidase 12 in lung cancer associated angiogenesis »

- OzMRS-CTx Metastasis Symposium (December, 1 2014 ; Melbourn, Australia) « Modulation of protease expression in prostate cancer cells after androgen deprivation »

- Prostate cancer world congress 2015 (August, 17-21 2015, Cairns, Australia) "Modulation of protease expression in prostate cancer cells after androgen deprivation »

- TRI Symposium 2015 (September, 17th 2015, Brisbane, Australia) "KLK4 is involved in establishment of CAF phenotype during initiation of prostate cancer"

- TRI Symposium 2015 (September, 17th 2015, Brisbane, Australia) "Dysregulation of the proteolytic network in prostate cancer cells after androgen deprivation and androgen-targeting therapies"

- 6th International Symposium on Kallikreins and Kallikrein-Related Peptidases (September 28 – October 1 2015 ; Brisbane, Australia) « Dysregulation of the proteolytic network in prostate cancer cells after androgen deprivation and androgen-targeting therapies »

- International Proteolysis Society Conference 2015 (October, 4-8th 2015, Penang, Malaysia) "Dysregulation of the proteolytic network in prostate cancer cells after androgen deprivation and androgen-targeting therapies"

- Prostate Cancer Collaborative Research 2015 (November, 26-29 2015, Brisbane Australia) "KLK4 is involved in establishment of CAF phenotype during initiation of prostate cancer"

- Prostate Cancer Collaborative Research 2015 (November, 26-29 2015, Brisbane Australia) "Dysregulation of the proteolytic network in prostate cancer cells after androgen deprivation and androgen-targeting therapies"

- 17th Asia-Pacific Prostate Cancer Conference (August, 31st – September 3rd 2016, Melbourne, Australia) "Kallikrein-related peptidase 4 induces cancer-associated fibroblast features in prostate derived fibroblasts"

- TRI Symposium 2016 (October, 25th 2016, Brisbane, Australia) "Kallikrein-related peptidase 4 induces cancer-associated fibroblast features in prostate derived fibroblasts" (Poster prize, ECR category)